Mechanisms for Concentrating Impurities at Line Contact Tube Support Crevices in PWR SG's

Heated Crevice Seminar

Argonne

October 8-11, 2002

Peter Millett

Dennis Hussey

iSagacity

Outline of Presentation

- **Introduction**

- **Line Contact Designs in Use**

- **Experimental and Field Observations regarding Line Contact Designs**

- **Approaches to Quantitative modeling**

  - **-3 step process**
  - **-review packed crevice model**
  - **-extrapolation to line contact crevices**

- **Summary**

iSagacity

Introduction

- Corrosion of SG tubing at supports continues to be an industry problem
- New plants and replacement SG's use support plate design with a line contact at the tube
- Line contact designs are less susceptible to fouling and dryout….but they are not immune to the precursor to accumulation of aggressive chemicals
- Most of the industry R&D efforts over the past 20+ years regarding crevice concentration and corrosion mechanisms has been focused on fouled drilled hole support plates

3

iSagacity

Introduction

- An improved quantitative analysis of line contact crevices can lead to improved operational and maintenance practices for the current generation of SG's

- How can we best extrapolate from drilled hole operating experience?

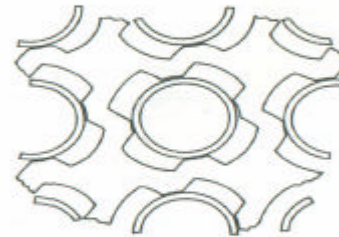- Is our mechanistic understanding of these types of crevices sufficient ?

4

iSagacity

Line Contact Designs
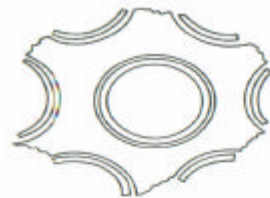
(a) Drilled, without flow holes
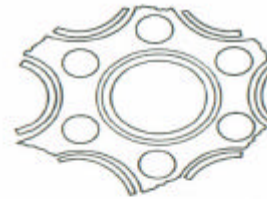
(b) Drilled, with flow holes

(c) Broach-trefoil

(d) Broach-quatrefoil

(e) Eggcrate

iSagacity

Fleet Statistics for Support Structure Design Features

- Source: EPRI SG Degradation Database (September 2002)

- Includes design data for 237 plants world-wide

- 42% of the plants were originally designed with drilled hole support plates

  - 60% of those plants have replaced their SG's

    - 27% of replacements use grid/egg-crate design

    - 73% of replacements use broached design

- All replaced SG's were original drilled hole designs

6

iSagacity

Review of Some Key Experimental Programs and Analytical Models

1. Curlee and Baum, Westinghouse, "Single-Tube Thermal and Hydraulic Tube Support Test," EPRI NP 2046, September 1981

2. Bankoff, et.al., Northwestern University, " Boiling Heat Transfer in a Narrow Eccentric Annulus," EPRI NP 2610, September 1982

3. Merte, et.al, University of Michigan, "Boiling in Narrow Crevices in SG's," EPRI NP-2638, November 1982

4. Cassell and Vroom, CE, "T-H Tests of SG Tube Support Plate Crevices," EPRI NP-2838, January 1983

5. Curlee and Baum, Westinghouse, "Tube Support Plate T-H Testing," EPRI NP-3052, May 1983

6. Krupowicz and Rentler, CE, "Corrosion Performance of Alternative SG Materials and Designs," EPRI NP-3044, July 1983

iSagacity

Objectives of EPRI Support Structure Design R&D Programs

- To better understand the T-H characteristics of alternative SG designs

- To characterize the onset and extent of dryout at the SG tube/support contact for alternative designs

- To provide a basis for the prediction of the onset of dryout

- To compare the susceptibility of different designs to fouling and accumulation of non-volatile chemicals

iSagacity

Experimental Findings (Dryout)

- Dryout as measured by increased wall superheat is a necessary condition for the concentration of chemicals

- Dryout occurs at or near the contact between the tube and support

- Dryout depends strongly on the primary/secondary temperature difference and shows no clear dependence on local quality, flow rate and pressure

- Drilled holes and Concave designs show dryout under prototypical SG conditions. Flat lands and Convex do not (non-fouled)

9

iSagacity

Experimental Findings (Fouling)

- Sludge deposits at or near the contact point first

- Fouling increases the superheat away from the contact point , enhances superheat at the contact point, and expands the dryout region

- Concave & Flat lands have a propensity to confine or entrap the outer precipitating oxide and sludge deposits

- All designs demonstrated dryout (to different degrees) after sludge was added to the experimental device

iSagacity

Corrosion in Trefoil Designs (NP3044)
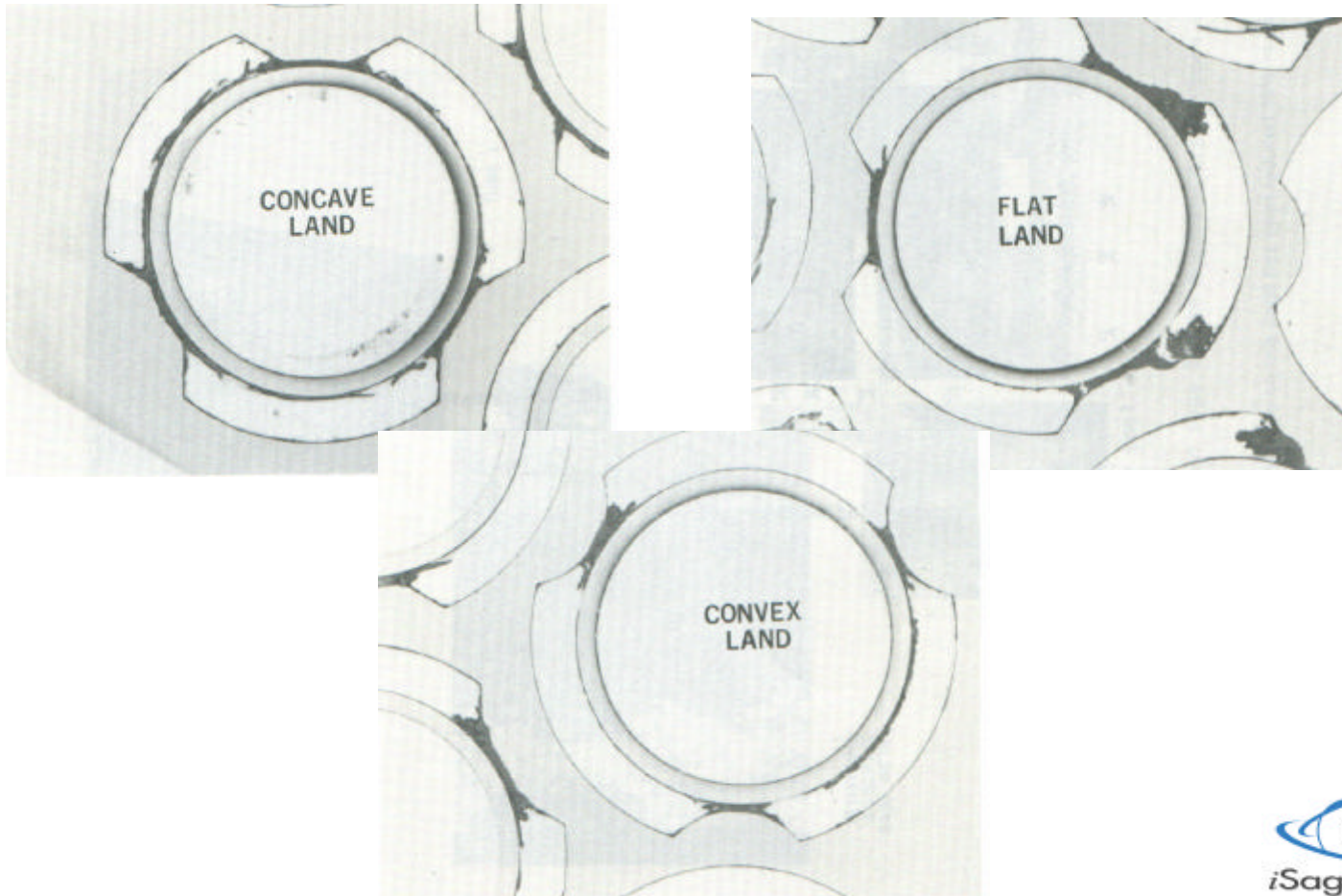
Effect of Heat Flux on Superheat (NP2046)
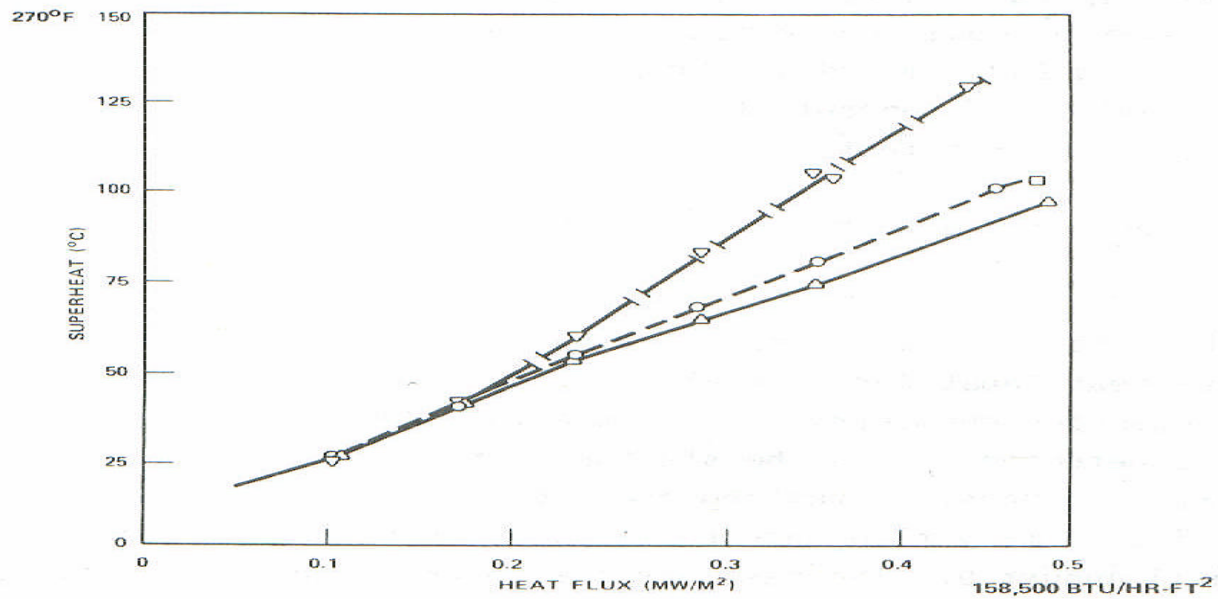
| SYMBOL	DESIGN	MASS VELOCITY (KG/S-M^2)	QUALITY
▽	CYLINDRICAL HOLE	109	13.9%
○	CONCAVE QUAT	109	12.5%
△	NUCLEATE BOILING FLAT QUAT CONVEX QUAT	112 109	12.8% 16.2%

12

459

Dryout in Various Designs (NP2838)

Figure S-1. Tubewall Excursion Onset Conditions
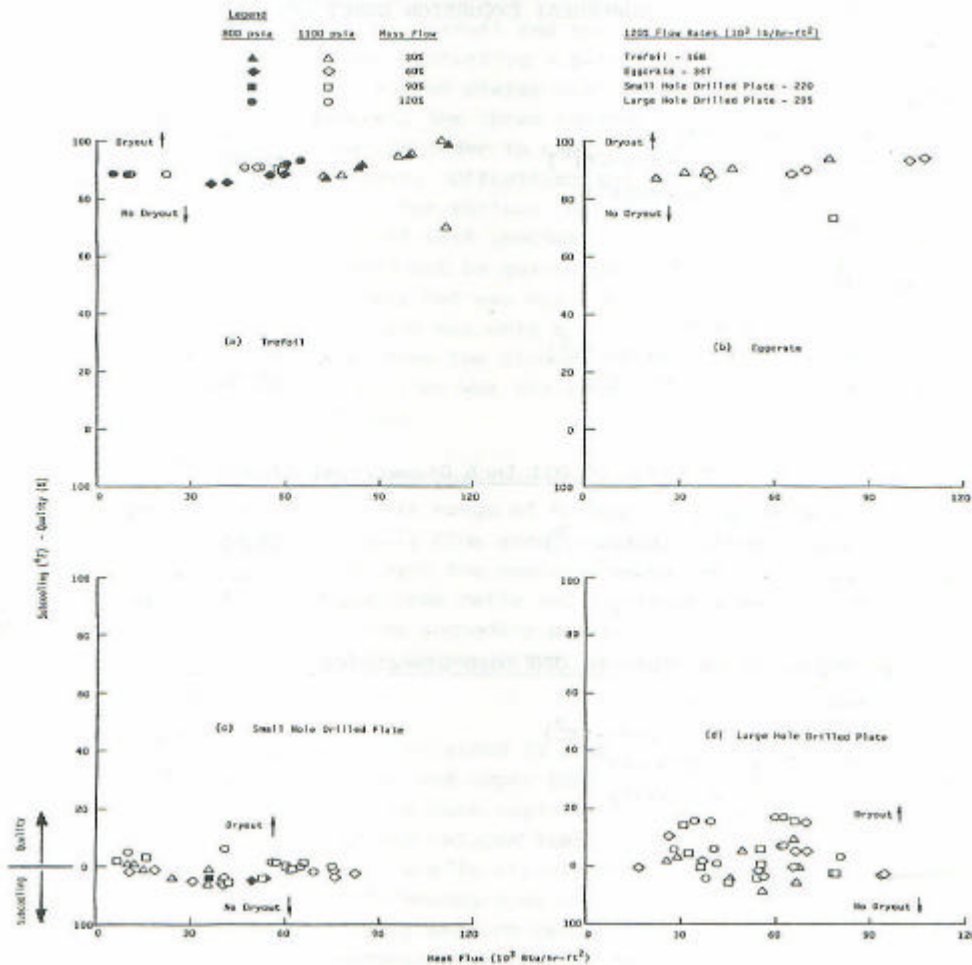
Analytical Model Development & Observations

- SG crevice T-H models have been developed to describe boiling in the absence of fouling
- Early models focused on an eccentric drilled hole support. Approach was to solve heat/mass/mom. equations in the complex geometry
- Boiling in narrow gaps consists of three regimes:
  - isolated bubble regime
  - coalesced bubble regime
  - dryout regime
- Analytical models predict transition from one regime to the next and extent of dryout patch

14

461

Visual Appearance of Crevice Boiling Phenomena (NP2610)

15

462
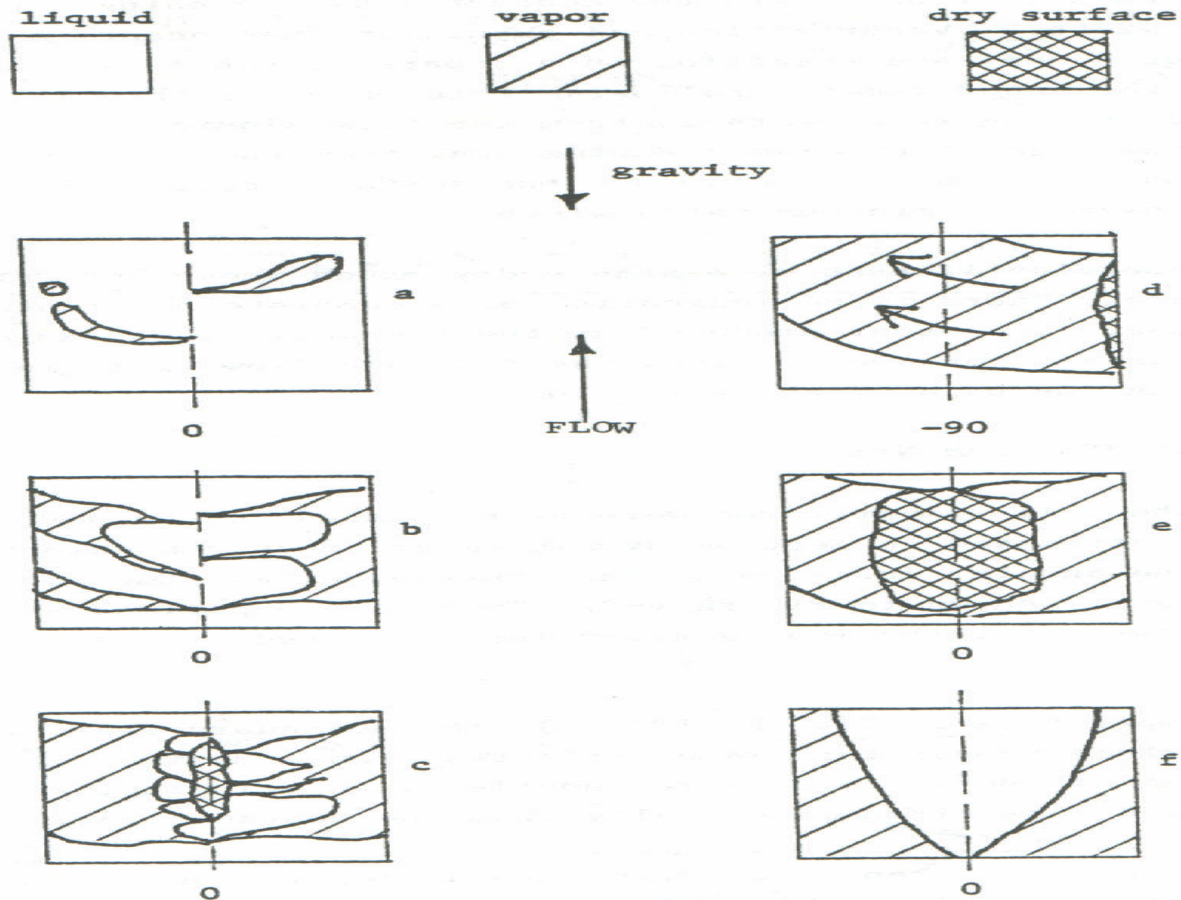
Limitations of Early Work to Present Concerns

- Emphasis is either on behavior of crevices in the absence of fouling/impurities or with excessive levels of fouling/impurities

- Modern SG's operate with low levels of both soluble and insoluble impurities

- We may be most interested in the mild fouling condition and the long term behavior
  - transition to dryout
  - extent and location of concentration zone

16

463

Towards a quantitative basis for predicting current plant conditions

- Working assumption: Overall process can be adequately described by three mechanisms occurring in series

    Step 1.- Dryout occurs at tube/line contact. Local T-H processes dictate location and extent

    Step 2.- Local deposition of corrosion products from the feedwater at and near the dryout zone. Fouling increases size and location of the dryout zone

    Step 3.- Non-volatile chemicals accumulate in the fouled crevice region through well-established T-H mechanism

iSagacity

Step 1: Predictive Modeling

- References 1,2,3 and others (notably, Ishabashi) can be used to guide further development if needed. Goal is to describe presence of and extent of dryout patch

- Much advanced CFD can be used to improve predictive capabilities

- Models can be benchmarked against T-H data from References 1-6.

iSagacity

Step 2: Predictive Modeling

- **Numerous Boiling Deposition models have been published in the literature (e.g. Beal-Westinghouse, Turner/Lister-AECL)**

- **For example:**

$$dW/dt = P\frac{Q}{L}C - KW$$

W=weight of crud deposit at time t, g/cm2
C=crud concentration in reactor water, g/kg
P= probability of deposition, dimensionless
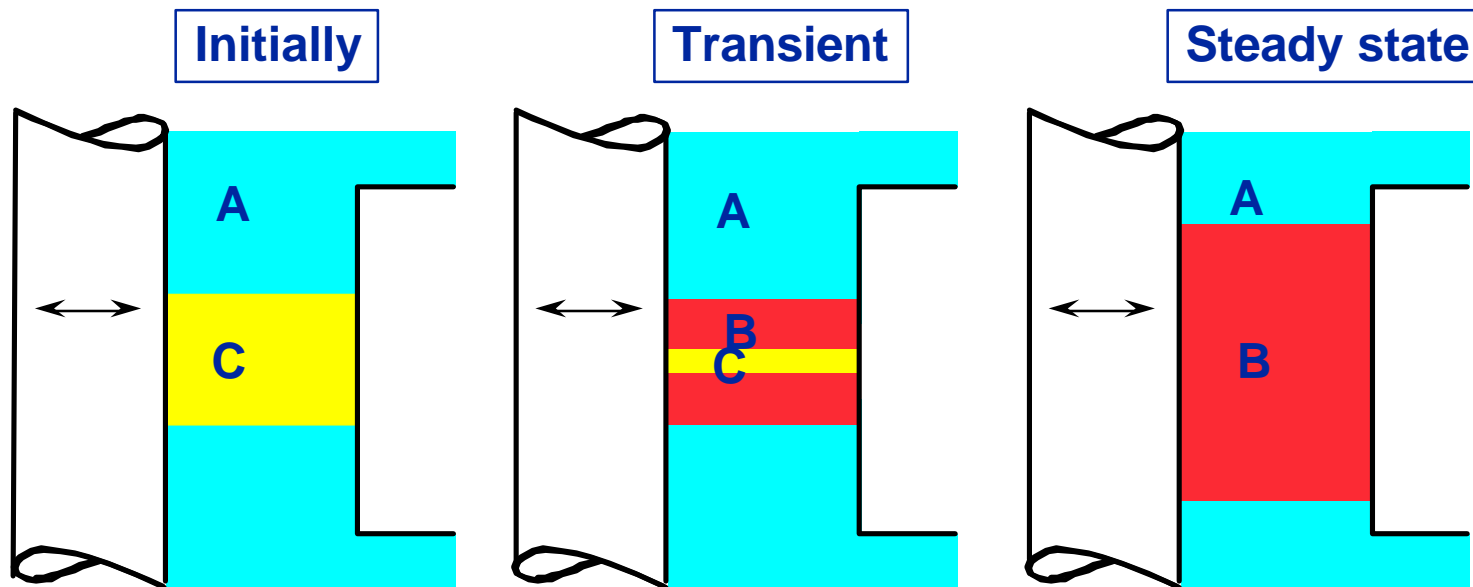**Q=heat flux on the fuel surface, kcal/cm2/day**
L=latent heat of vaporization of water, kcal/kg
t=time, day
K=release constant, day^{-1}

- **Deposition models require empirical constants**
- **Limitation will be lack of experimental data for geometries and chemistries of interest**

19

iSagacity

Step 3: Predictive Modeling

Initially　　**Transient**　　**Steady state**

A : Bulk Water　　　B : Impurities Concentrated　　　C : Blanketed Region

If sufficient liquid cannot be drawn into the porous media to maintain
nucleate boiling, a steam blanketed region will exist initially below the
nucleate boiling region. As time evolves, impurities fill the crevice.

20

Packed Crevice Model

- One dimensional model : axial direction only
- Symmetry at the middle of the support plate assumed
- Single chemical specie
- Based on the conservation of mass momentum and energy
- The model predicts the factor of concentration of a species (concentration in the crevice / concentration in the bulk) as a function of the axial dimension
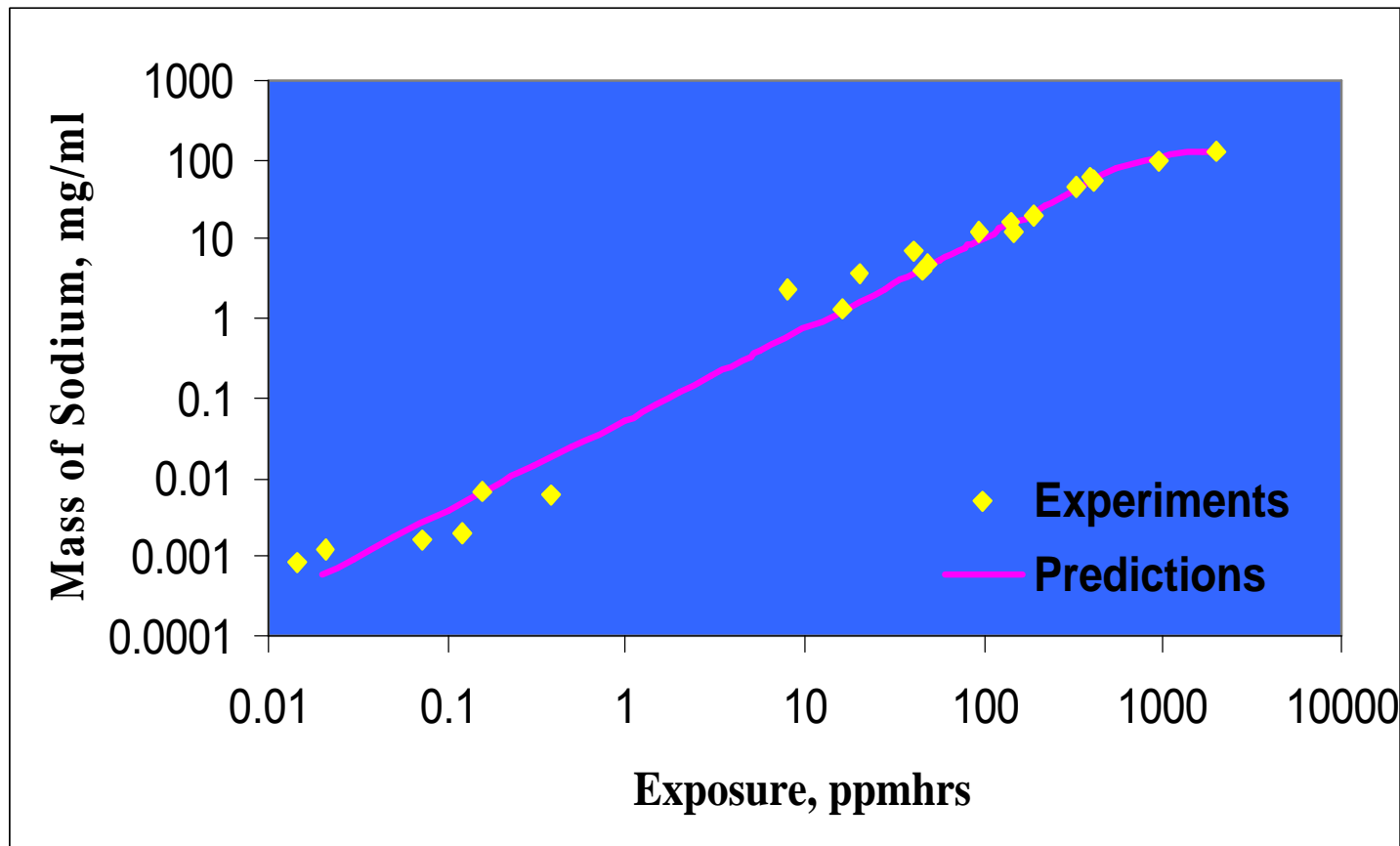
iSagacity

Crevice Chemistry

- **Conservation of Species (e.g. Na)**

$$e\, S\, [\, \dot{N} a\,] \;=\; -\,(\, v_l\, [\, Na\,]\,)' \;+\; k_{vl}\, (\, v_l\, [\, Na\,]\,)' \;-\; (\, DS\, [\, Na\,]'\,)'$$

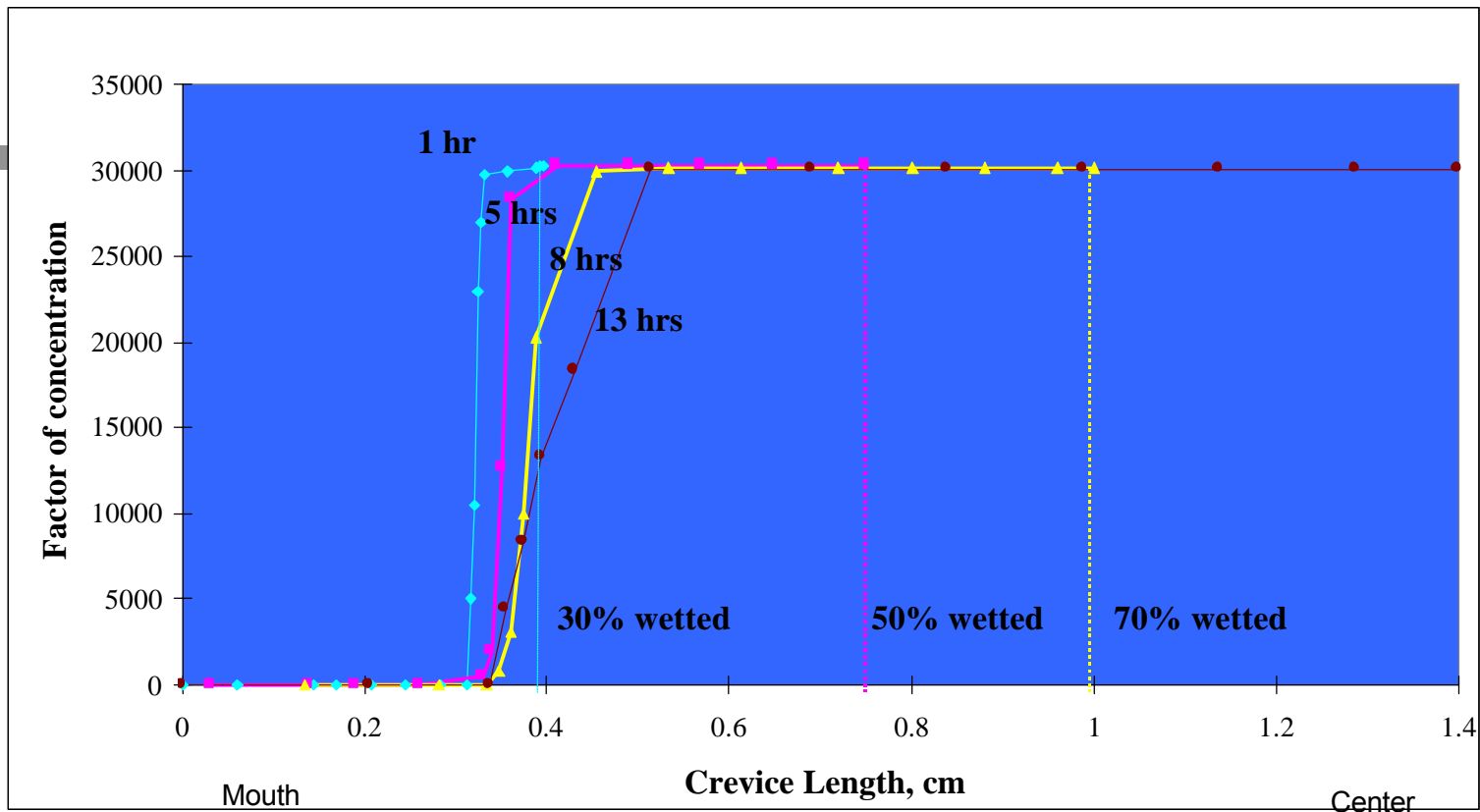**Rate of accumulation of Sodium** = **Convection** - **Volatilization** - **Diffusion**

- **Multi-component chemical equilibrium defines species interactions (e.g. MULTEQ-REDOX)**

22

Boiling Crevice Model Benchmarking

Crevice Concentration Profile
Crevice exposed to 20ppm sodium

The crevice slowly fills with a concentrated solution. The wetted length increases.

Summary

- Line contact designs are less susceptible to fouling and dryout….but they are not immune to the precursor to accumulation of aggressive chemicals

- An improved quantitative analysis of line contact crevices can lead to improved operational and maintenance practices for the current generation of SG's

- Early laboratory testing and field observations would be useful in benchmarking new models

- Deposition modeling may be the most challenging

25

Hideout and Hideout Return in PWR Steam Generators: Predictions of Crevice Chemistry

S. G. Sawochka

NWT Corporation

Argonne National Laboratory

October 2002
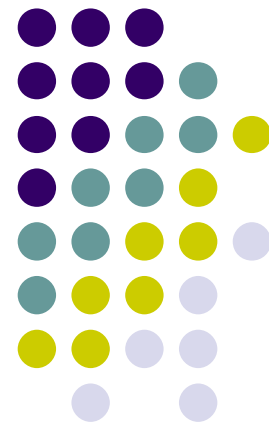
Hideout During Normal Operation

- Species concentrate and may precipitate in flow restricted boiling regions

- Crevice concentration factors can exceed 10^8 at BPE limit

- Hideout on free surfaces also can be significant but concentration factors much lower

- Hideout and hideout return studies can provide valuable insights relative to local region chemistry

Hideout During Normal Operation

- Mass balance approach to hideout estimation not possible on a routine basis due to analytical sensitivity limitations

- However, hideout has been measured during normal operation

  - Inject chemical impurities at known rate into feedwater

  - Quantify blowdown removal

  - Recycle of impurities transported by steam eliminates need for steam data

Estimation of Hideout Rate Constant

$$\frac{d(MC_{SG})}{dt} = W_I C_I - W_{BD} C_{SG} - W_{HO} C_{SG}$$

Where:

C_{SG} = Contaminant concentration increase in the steam generator blowdown above level prior to injection, ppb

C_I = Contaminant concentration in the injection solution, ppb

W_I = Injection flowrate, kg/h

W_{BD} = Blowdown flowrate, kg/h

M = Mass of liquid in the steam generator, kg

t = Time, h

W_{HO} = Hideout rate constant, kg/h

- Hideout assumed to be governed by evaporation rate in crevice

Sodium and Potassium Hideout at 95% Power (W-51)
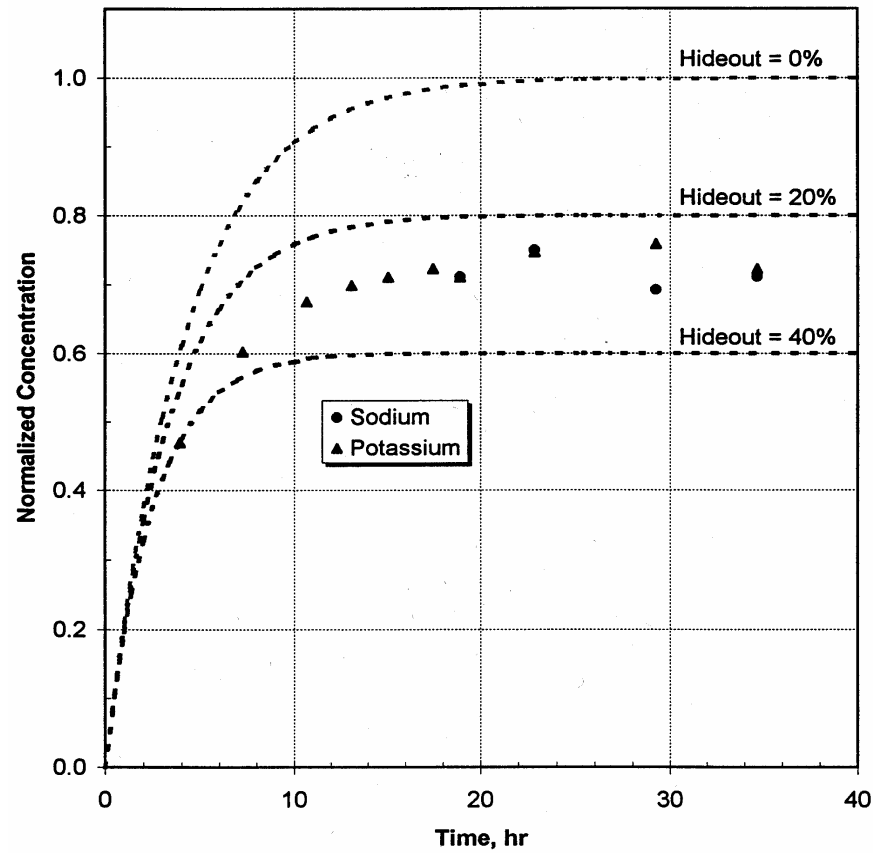
Potassium and Chloride Hideout at 95% Power (W-51)
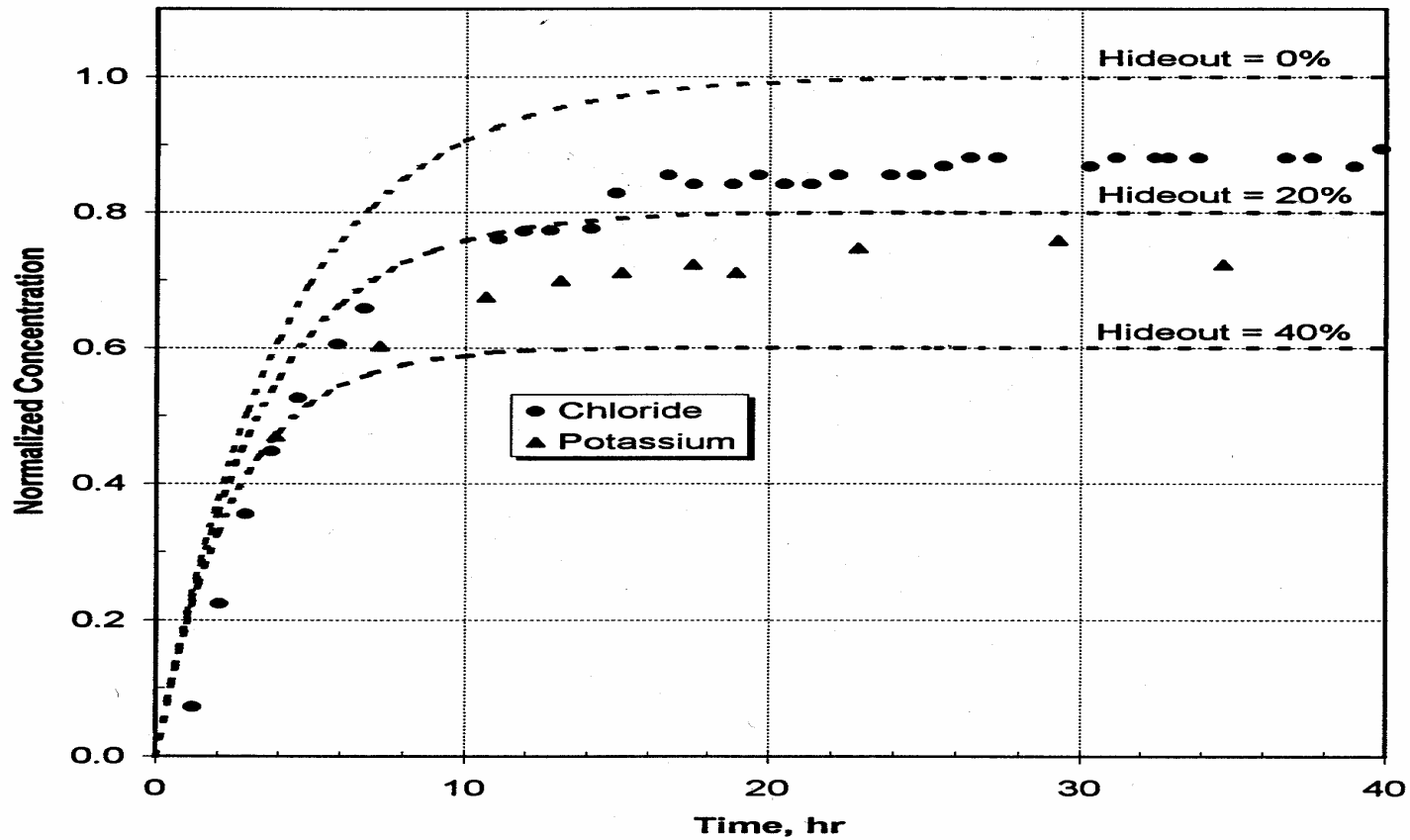
Injection Test Results

- Conformance of data to model supported validity of model for sodium, potassium and chloride

- Hideout rate constants varied with species

- Technique to estimate crevice impurity inventory on real time basis appeared present

- Differences lead to crevice chemistry prediction uncertainties if reliance placed on contaminant ingress ratios or bulk water concentration ratios

Conclusions: NaCl Ingress

- Assuming equal hideout fractions, a near neutral crevice pH is expected

- Basing crevice concentration ratios on bulk water concentrations yields an acidic crevice prediction

- Basing crevice concentration ratios on hideout rate data, a caustic crevice is predicted

- Mode of attack predictions vary:

  - Neutral pH – Minimal attack

  - Acid crevice – Denting/Pitting/Possible IGSCC

  - Caustic – IGA/IGSCC

Conclusions

- Recognition of difference in hideout fractions critical to crevice chemistry predictions

- Problem further complicated by non-conformance of sulfate hideout to model

Chloride and Sulfate Hideout at 95% Power (W-51)

482
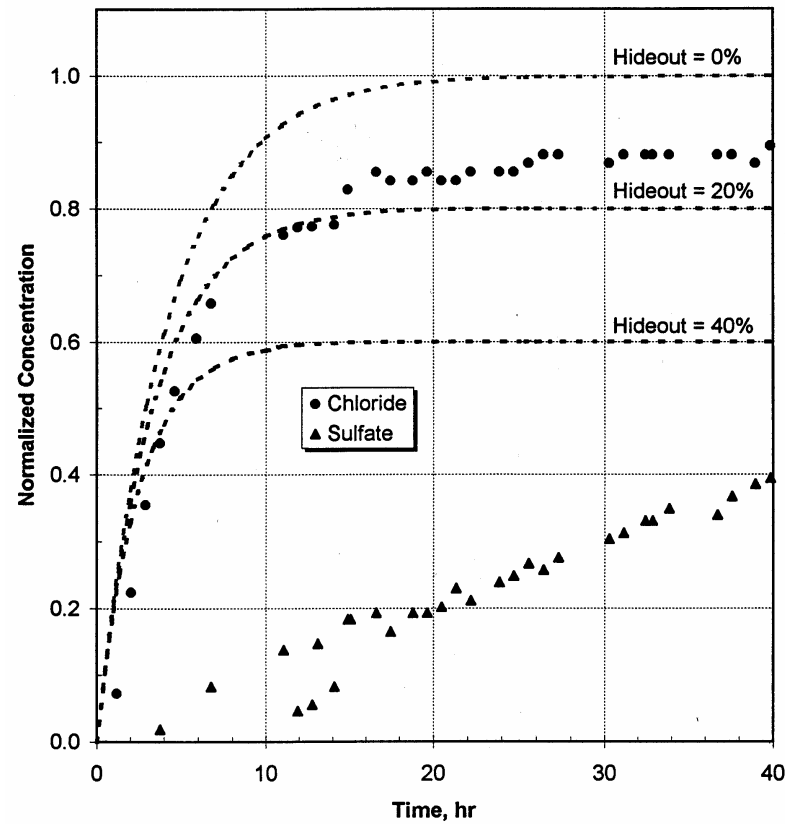
Sulfate Behavior

- Initial model inadequately described process

- Adsorption process initially governs hideout

$$C_o = KC_b$$

Where

C_o = Surface concentration, kg/kg oxide

C_b = Concentration in the bulk, kg/kg water

K   = adsorption coefficient (kg/kg oxide)/(kg/kg water)

- Evaporation mechanism governs once surface adsorption capacity satisfied

Results of Single Phase Adsorption Tests

- Sulfate adsorption quantified at low sulfate concentrations

- Desorption of sulfate by pure water occured over several days

- Results consistent with hypothesis developed from plant data

- No significant Cl, Na or Ca adsorption

- Phosphate adsorption significant (as expected)

- Magnesium "adsorption" also significant (not expected)

Summary of RSG Hideout Evaluations

- Hideout of sodium, chloride and potassium governed by a boiling process in flow restricted regions

- Sulfate hideout initially governed by surface adsorption; after adsorptive limit is reached, hideout by evaporative processes governs

- Calcium and magnesium hideout rate constants much higher than highly soluble species

- Hideout rate constants markedly impacted by steam generator design and cleanliness

- Decreased hideout at reduced power

Bases for Inventory Calculation

	Hideout Rate Constant (W_{HO}), lb/h		
	Sodium	Potassium	Chloride
Westinghouse			
Plant A (D4 SG)	18,000	21,000	11,000
Plant B (51A SG)	12,000	30,000	2,000
Plant C (51 SG)	3,500	6,000	2,900
Plant D (D5 SG)	0	700	300
Combustion Engineering			
Plant E (67 SG)	25,000	35,000	15,000

CREV-SIM

- Method of estimating impurity accumulation rates in crevices based on hideout rate constant

$$\text{Hideout Rate} = W_{HO} \, C_{BD}, \text{ e. g.,}$$

$$= (1000) \, (1) \, (10^{-9}) = 10^{-6} \text{ lbs/h Na}$$

- Results provide reasonable basis for real time crevice chemistry tracking using CREV-SIM code

- Correlations of CREV-SIM crevice inventory predictions and hideout return data attempted but not particularly successful

CREV-SIM Application Problems

- Hideout rate constant varies with plant design, power, operating history, etc.

- Hideout rate depends on crevice chemistry, e.g., chloride volatility will vary with pH

- Relation of hideout rate to blowdown concentration may not be linear; data available only at ~3 to 10 ppb

- Blowdown concentrations approaching LLD values at time of evaluation

- Incomplete return of hideout species expected

CREV-SIM Application Problems

- Resolution requires intermittent determination of hideout rate constants

    - Blowdown flowrate variation

    - Cycle mass balance – a simple approach

- Use of code has been minimal to author's knowledge; emphasis placed on hideout return technique for EOC crevice chemistry prediction

Hideout Return in PWR Steam Generators

- Crevice and surface deposit impurities return to bulk liquid during shutdowns

  - Void collapse/rewetting

  - Diffusion to bulk

  Hideout Return (HOR) = Inventory Increase + Blowdown Removal – Feedwater Input

- Approach based on assumption that species ratios reflect crevice ratios

- MULTEQ or Molar Ratio Index approaches used to assess chemistry

Hideout Return Data Applications

- Predictions of chemistry and corrosion tendencies in local regions

- Source term assessments

- Molar ratio control program assessments

- CREV-SIM updating

HOR Assessment

- Emphasis on hideout return immediately after shutdown for crevice chemistry predictions

  - Highly soluble species return rapidly

  - Precipitate return is delayed

- Data for total shutdown evolution used for source term assessments and confirmation of crevice chemistry inferences

- EPRI hideout return code available

Inferences from Concentration and Return Data

- Species that return <u>promptly</u> on shutdown (before cooldown) probably present as solubles or highly soluble precipitates on tubing surfaces and in crevices

- Species that return preferentially during cooldown probably exist as precipitates during normal operation <u>or</u> are returning from very difficult to access regions

  - Many precipitates exhibit retrograde solubility

  - Simultaneous return of two species during cooldown infers their association as a compound

- Quantitative source breakdown not possible – reliance is on ratio similarity assumption

Predictions of Chemistry in Local Regions

- Highly Soluble Species
  - Sodium
  - Chloride
  - Potassium
- Adsorbed Species
  - Silica
  - Sulfate
- Precipitated Species
  - Calcium
  - Magnesium
  - Aluminum
  - Sulfate
  - Silica
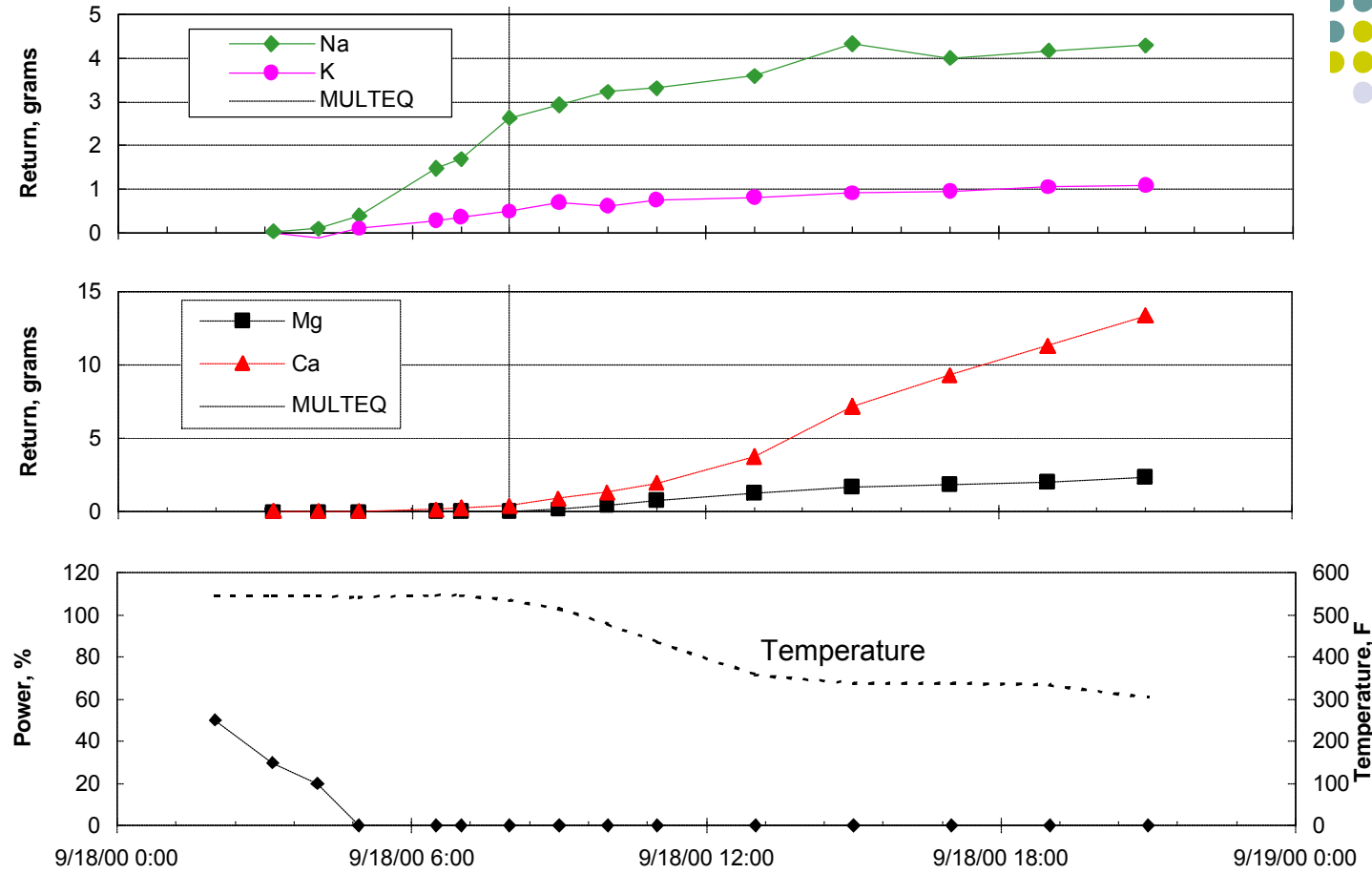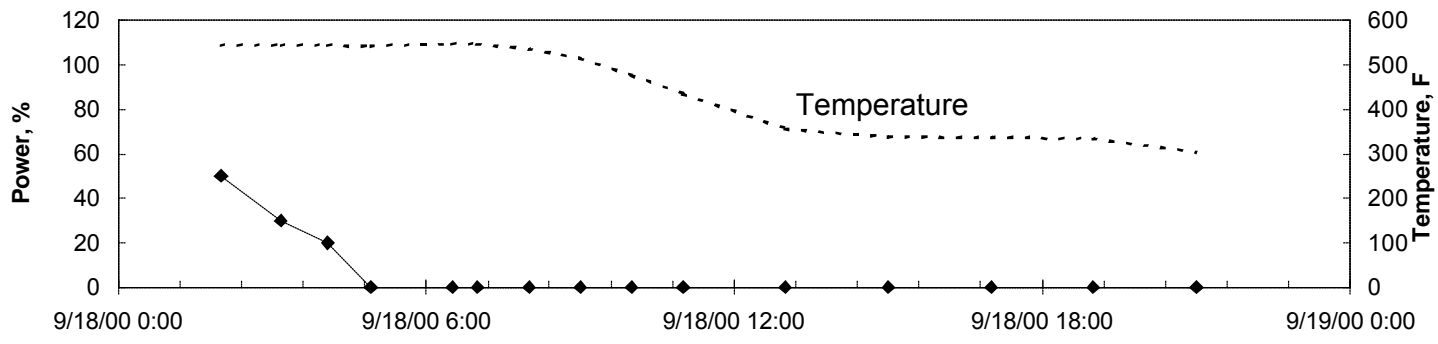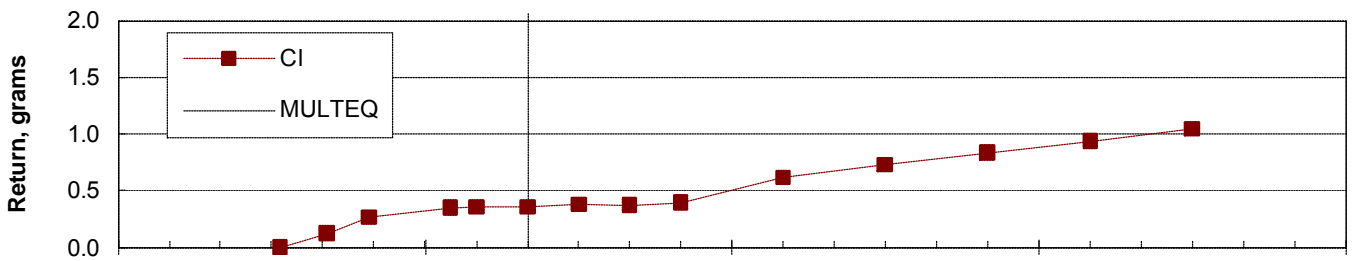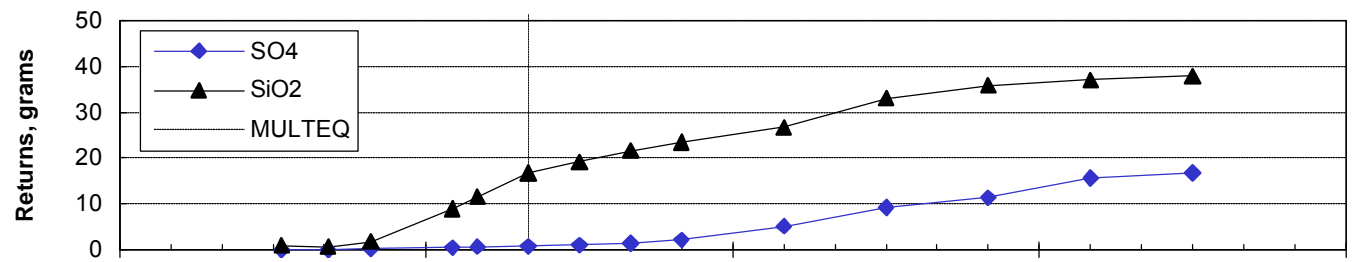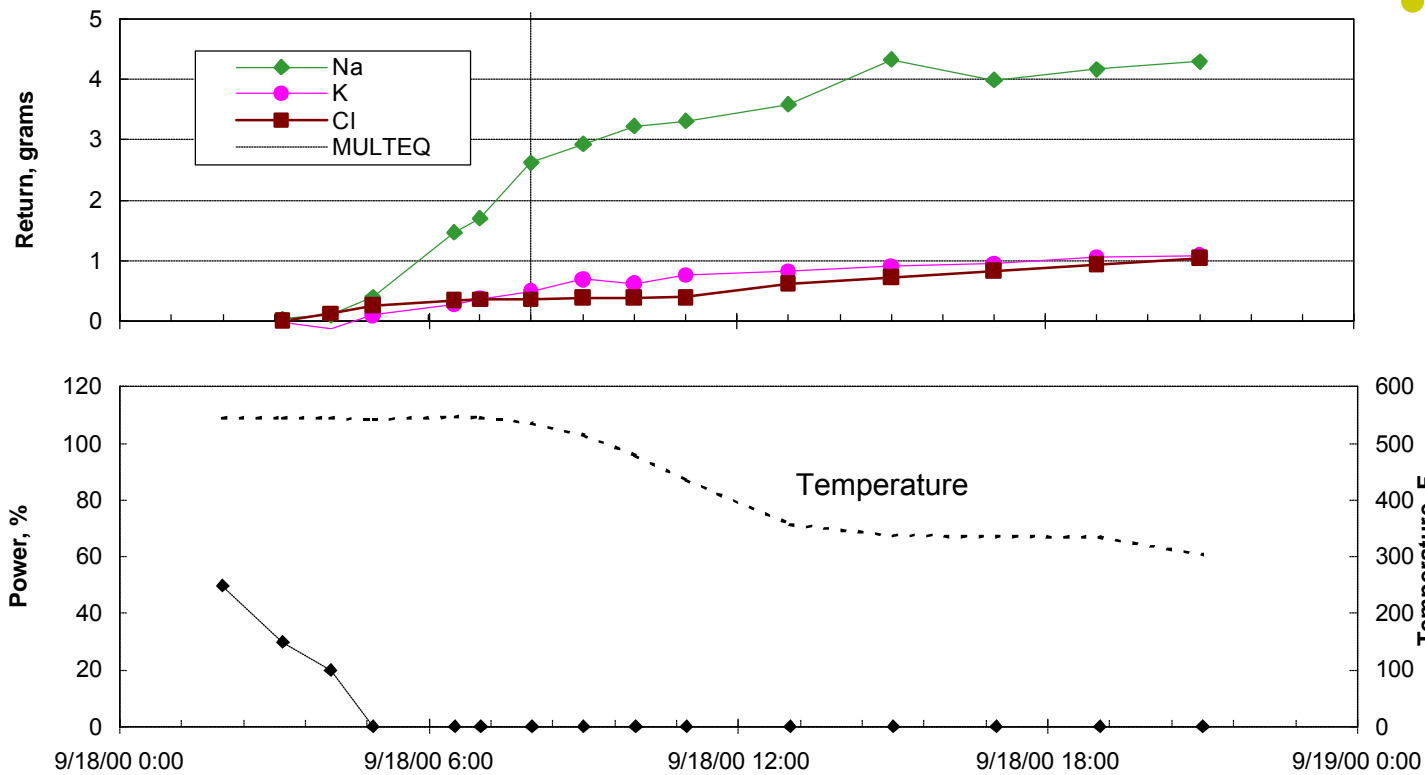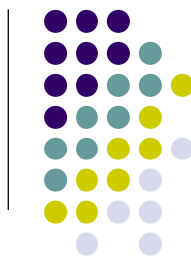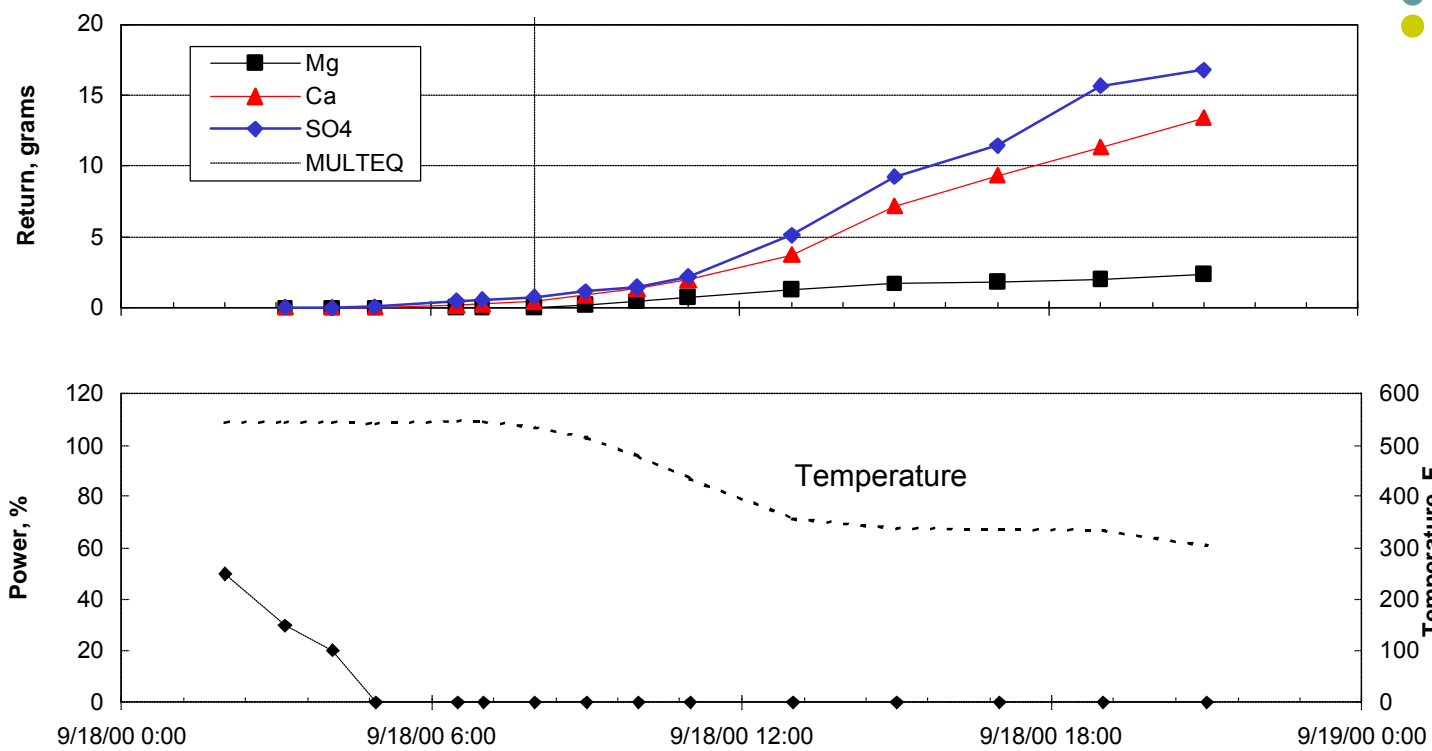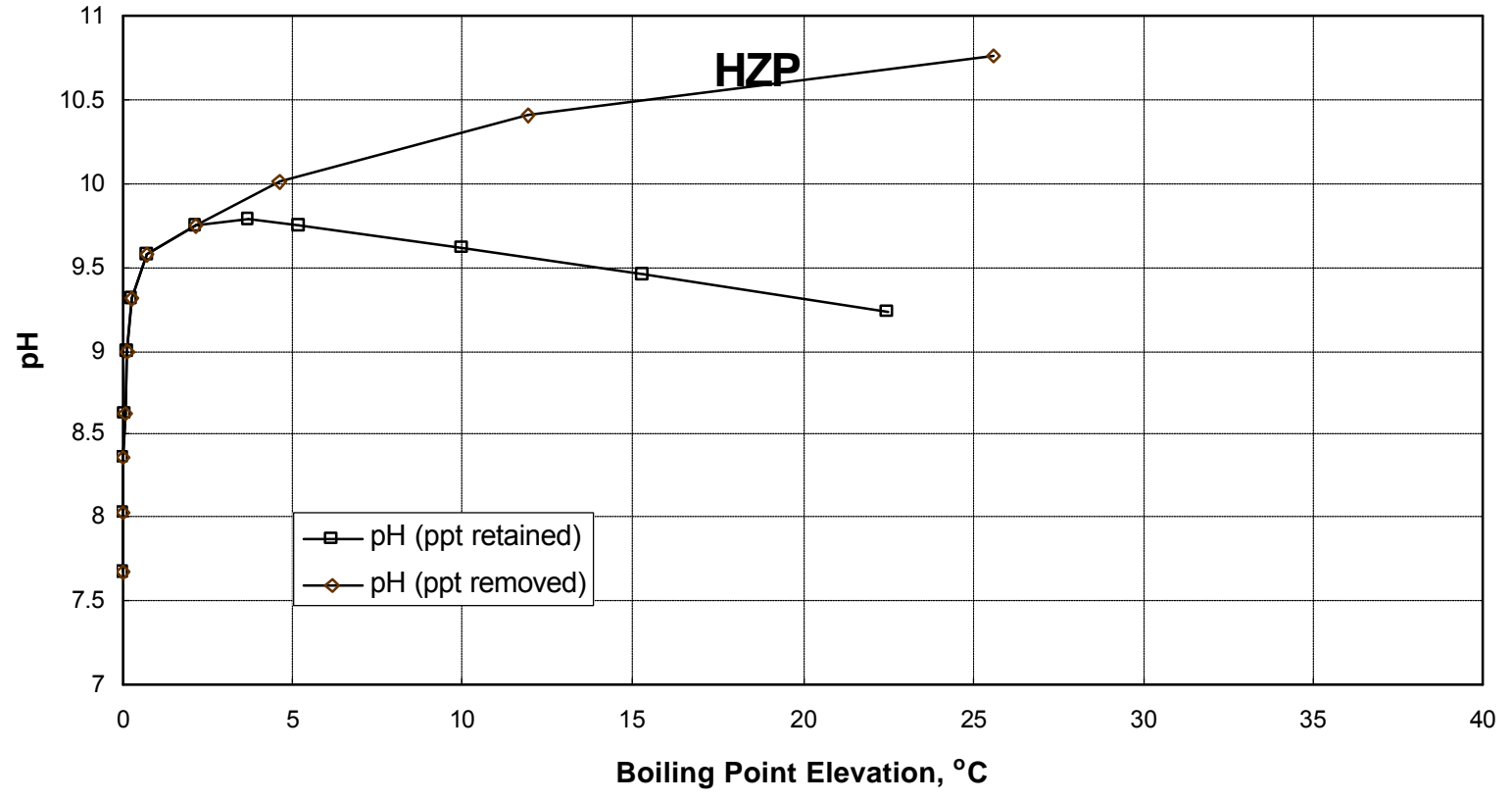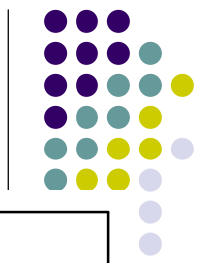
Crevice Chemistry Predictions for Plant X

- MULTEQ Basis (precipitates retained)

- Caustic solution predicted, $pH_T \sim 9.2$ (precipitates retained)

- Precipitates

Na_2SO_4 $CaSiO_3$ SiO_2 $Ca_2Mg_5Si_8O_{22}(OH)_2$

$Na_2Si_2O_5$ K_2SO_4 CaF_2
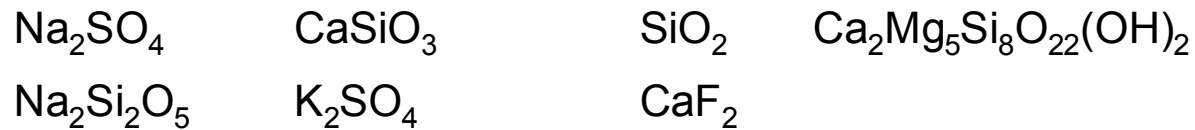
- Solution at BPE of 22°C

  - 3.1 MOLAL Na
  - 0.01 MOLAL Ca
  - 5.5 MOLAL K
  - 5.7 MOLAL Cl

  - 0.5 MOLAL SO_4
  - $5 (10^{-10})$ MOLAL H^-
  - 0.2 MOLAL OH^-

Crevice Chemistry Predictions for Plant X

- Solution is not a concentrated acid or base

- Neutral salts are major ionics

- Laboratory corrosion data on which to base prediction of long term corrosion tendencies not available

HOR Variations

Plant	Cumulative Return						
	Na	Cl	K	Ca	Mg	SiO_2	SO_4
A	18	18	3	8	0.5	90	3.6
B	3	2	1.5	0.9	0.1	100	5
C	0.11	0.01	0.04	2.2	0.3	28	0.05
D	0.4	0.7	0.1	0.3	0.05	140	
E	0.15	0.12	0.04	0.20	0.03	35	0.35
F	0.2	0.1	0.3	0.6	0.1	600	18
G	2.5	0.35	0.5	0.4	0.07	16	0.8
H	0.6	0.8		2.5	1.0	21	2
I	0.3	0.8	0.25	28	0.6	30	0.9

Relation of HOR and Blowdown Chemistry

	MIHAMA-3	OHI-2[a]	MIHAMA-2[a]	Plant Y (U.S.)
Blowdown, ppb				
Na	<0.1	<0.1	3	0.4
Cl	0.64	0.23	2.2	0.3
SO_4	0.71	0.23	1.7	0.9
HOR, g/SG				
Na	0.35	0.59	3.71	2.5
K	0.07	0.21	1.16	0.5
Cl	0.79	0.34	1.82	0.35
SO_4	4.26	2.61	41.22	0.8
Mg	3.41	2.71	4.59	0.4
Ca	2.57	3.82	8.03	0.4

a) Takamatsu, et al, Airlie, 1995

Hideout Return Data Overview

- Total returns for highly soluble species are in the range of 0.1 to 5 grams per SG (current generation clean units)

- Major variations between plants related to design and cleanliness

- Silica return generally exceeds return of other species, i.e., 20 to 500 grams (? adsorption)

- Hardness element and sulfate returns vary markedly with impurity sources

- Predicted crevice solutions normally are concentrated NaCl/KCl not concentrated acids or basis

Hideout Return Data Overview

- pH_T of 4 to 9.5 common but acidic and caustic cases do occur

- Limiting pH approached at low BPE

- Recent HOR data becoming difficult to assess due to low returns, effects of makeup water inputs, and presence of other species (Al)

- Soluble return compromises value of crevice artifact examination for solution matrix information, i.e., known highly soluble species infrequently observed on fracture faces

Hideout Return Evaluation Schematic

HOR DATA
POWER, TEMP, %NR, BD FLOW, CONCENTRATIONS

CUMULATIVE RETURNS, grams

PROMPT RETURN, grams
PR + HZP, HZP ONLY

| MULTEQ | RATE CONSTANT APPROACH | MRI |

pH,
CHEMISTRY,
MRC ASSESSMENT

CREVICE INVENTORY, grams

MRC BASIS

MULTEQ

MRI
$$\frac{Na + K}{Cl + ExSO4}$$

pH,
CHEMISTRY

506
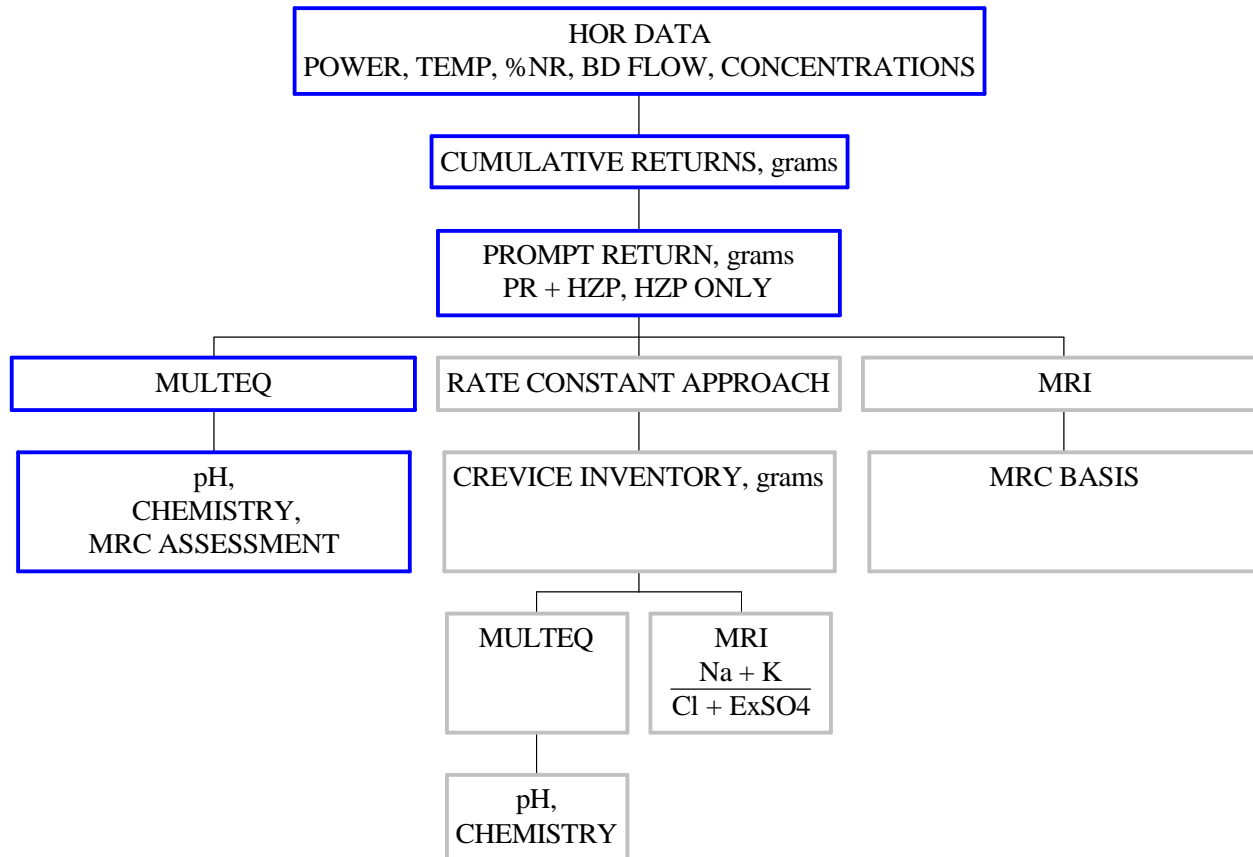
Molar Ratio (Crevice Chemistry) Control

- Perform hideout return studies during each shutdown

- Perform MULTEQ/MRI calculations of crevice chemistry based on hideout return data

- Assess impact of changes in impurity ratios such as Na/Cl on crevice chemistry, i.e., MRC approach evaluation

- If appropriate, adjust ratio to improve crevice pH by:

  - Source reduction/elimination

  - Chloride injection

    - NH_4Cl

  - Other

507

Molar Ratio Index (MRI)
An Alternative Approach to Crevice Chemistry Prediction/Control

- Define the MRI

$$MRI = \frac{[Na]+[K]}{[Cl]+[ExSO_4]}$$

  - Where
    - All returns are in equivalents/liter
    - ExSO4 = [SO4] – [Ca] (+ values only)

- Not a quantification but an indicator of crevice pH range
  - MRI <1 indicates acidic to mildly caustic crevices
  - MRI >1 indicates near neutral to caustic crevices
  - For neutral crevice, adjust blowdown chemistry to yield HOR MRI =1

MRI Graph

Precipitates Retained

Molar Ratio Index (Na + K / Cl + ExSO$_4$), eq/eq

509
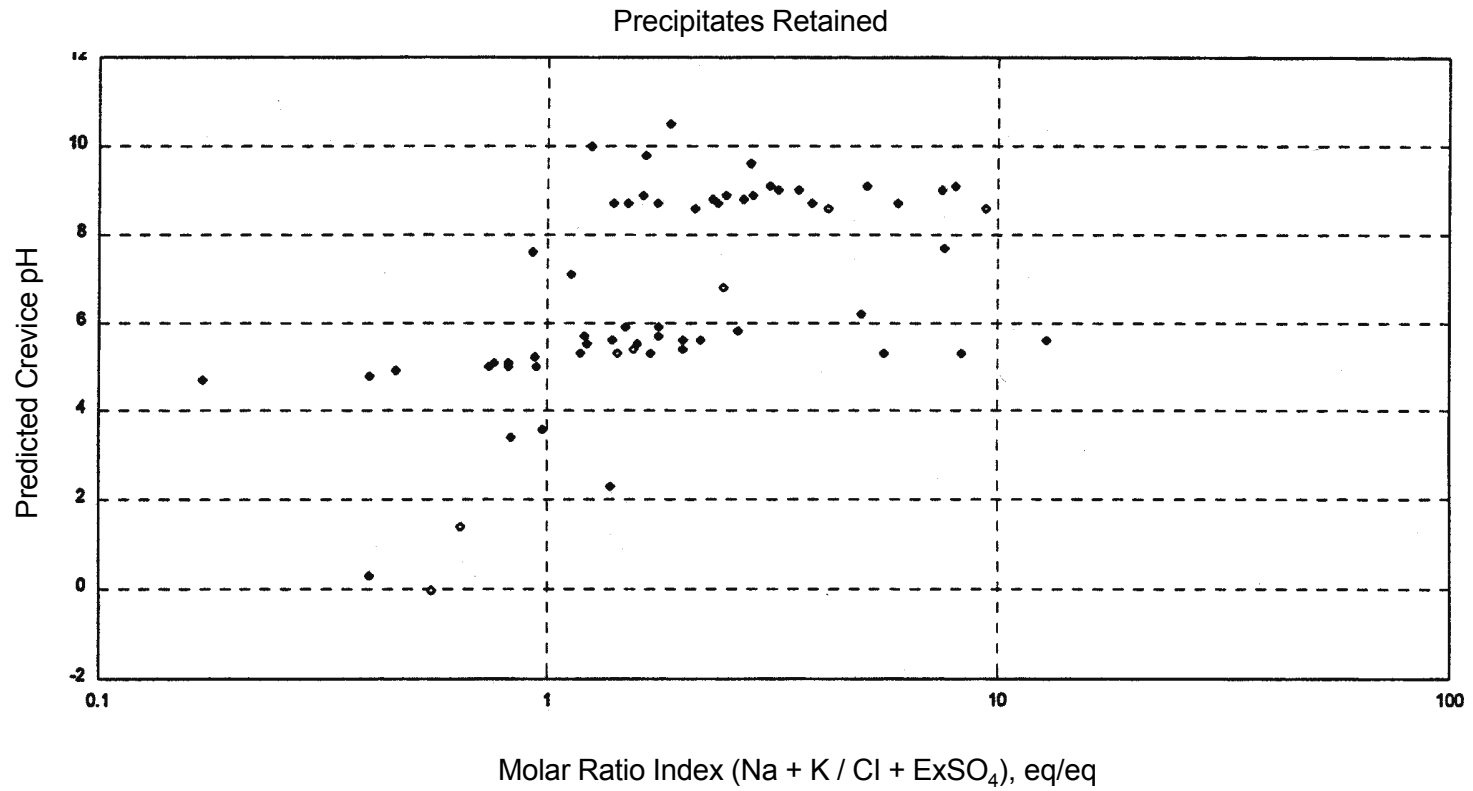
HOR Mechanistic Considerations

- Return during power reduction probably from SG surfaces

  - More return from CE and fouled open structure W units

  - Return increases with fouling

  - Upper portions of bundle probably govern

- Subsequent Return Rate = $K_1 (C_{crevice} - C_{bulk})$

  - Linear: Solubilization Continuous

  - Exponential: All soluble initially (Rate Constant Approach)

  - Inconsistency of rate constants for monovalent species suggests mixed mode, i.e., accuracy of exponential predictive tool questionable

A Perspective

- Consider 10 grams of soluble species, e.g., NaCl

- Assume 140,000 line contact "crevices" in an RSG

  - 0.07 mg NaCl per crevice

  - For a 10 molal solution (BPE limit), this corresponds to ~2 (10^{-4}) ml of solution which covers several percent of the tube surface

- Even at low hideout rates, impurity accumulation in crevices can be significant from corrosion perspective

Tube Area, % covered

10 grams @ 1 molal

10 grams @ 10 molal

Solution Volume in Line Contact
(0.875" Dia. Line Contact; 1" Tube Support)
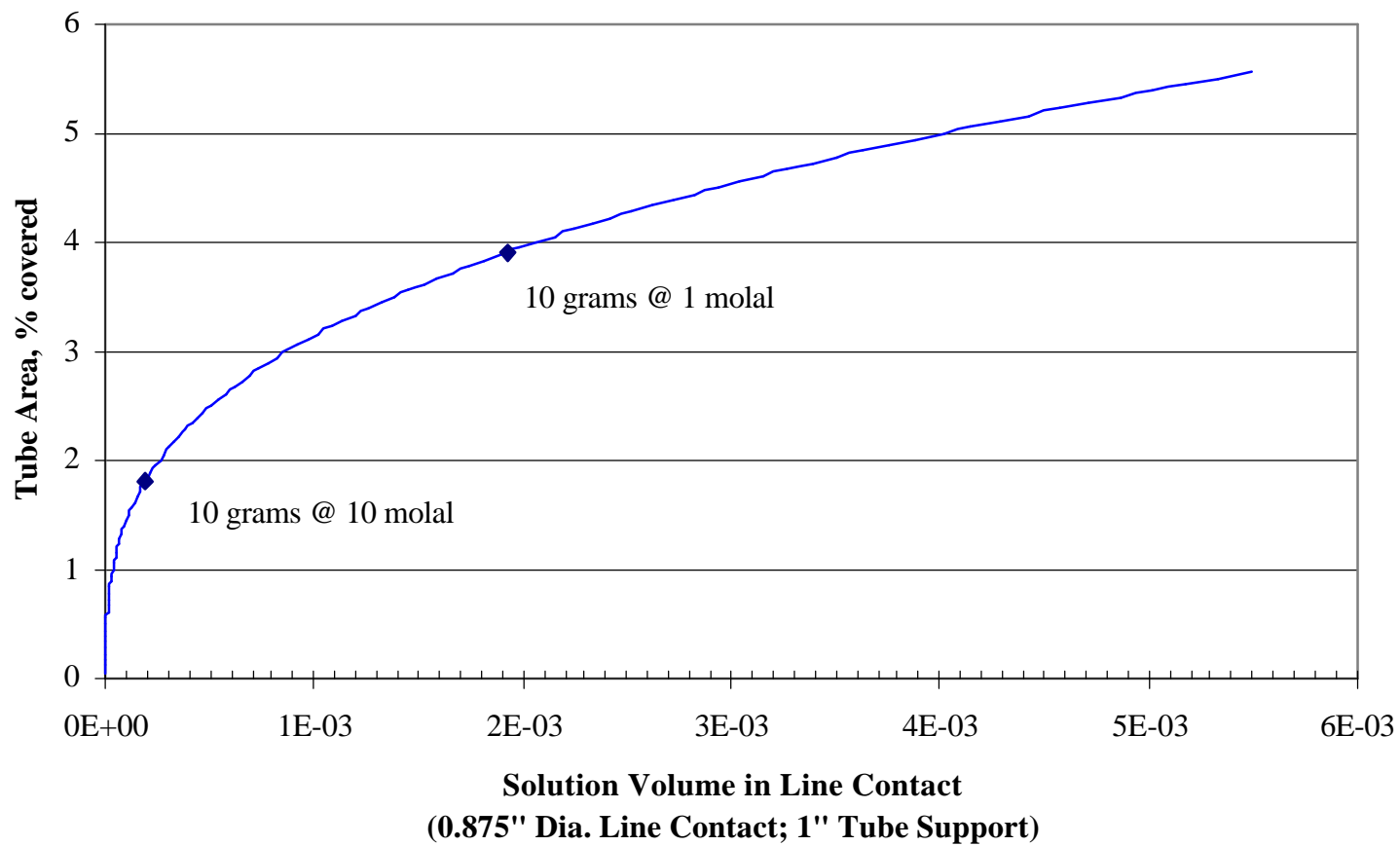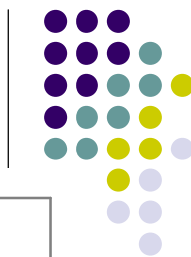
A Perspective

- Fractional hideouts of Na and Cl low in clean units

  - 1100 MWe blowdown removal per cycle at 1 ppb concentration is approximately 700 grams

  - HOR approximately 0.1 to 10 grams

  - % Hideout =1%

- Hideout rate constant of <1000 lb H_2O/h based on HOR mass balance

- Tracer studies of new units yield =1000 W_{HO} values

Summary

- Hideout return data routinely being used for:

  - Assessment of crevice chemistry

  - Identification of impurity sources

- Routine evaluations recommended in Guidelines

  - Magnitude/relation of impurity sources can change

  - Correlations with steam generator corrosion observations/tendencies believed possible

  - Results provide basis for MRC program

Status of EPRI Software Tools for Evaluating Crevice Chemistry

Tina Gaudreau

EPRIsolutions

tigaudre@epri.com

(650) 855-2819

EPRI SOLUTIONS

Software Development

- Over the last 20 years, EPRI has developed data and computer codes in support of the evaluation of crevice chemistry

- The different tools have been packaged together in a suite of software called ChemWorks

- These computer codes are windows based and many of the tools are in wide use

ChemWorks Tools for Crevice Chemistry

- MULTEQ
- CrevSim
- Hideout Return Spreadsheet
- Plant Chemistry Simulator
- SMART ChemWorks
- Integrated Exposure Calculator

MULTEQ Overview

- Interactive program to calculate composition, pH and electrochemical potential of an aqueous solution at elevated temperature

- Also designed to calculate the changing composition of the solution due to concentration processes.

MULTEQ Database

- Thermochemical library used by MULTEQ
- Text file called species.dat
- A committee reviews an approves all changes in a formal manner

MULTEQ Versions

- Currently distributed package contains MULTEQ Version 2.24 with species database #1396 (June 4, 1997)
- An update to the database (with complete documentation) is now available and labeled Version 3.0
- Version 3.0 of the program is underway and planned to be Excel based, but is not yet completed
- A Version 4.0 release of the database will be available in 2003

MULTEQ Database Versions

- Version 3 includes the following updates over the version (1396) distributed with MULTEQ 2.24
  - New Species
    - 5AP   H5AP   Piper   Hpiper   15DAP   H15DAP
    - 4AB   H4AB   Pyrrol   Hpyrrol   LiBO2
  - Updates to existing species
    - Cr+3   ETA   NaOH
    - MgOHFe+3   Cu+2
    - ZnOH   Zn(OH)2   Zn(OH)3
    - Zn(OH)4   AlOH   PbOH
    - Pb(OH)2   Pb(OH)3   MgSiO3
    - Mg5(CO3)4(OH)2.4H2O   CaSiO3Fe(BO2)2
    - ZnO   CaMg(SiO3)2   Ca2MgSi2O7
    - SiO2   PbO   PbSO4
- This version only works with MULTEQ-REDOX 2.1 or later

CrevSim

- An Excel based code
  - Track SG bulk concentrations
  - Estimate amount of impurities hiding out (based on an assumed hideout rate for each species)
  - MULTEQ embedded to determine the crevice conditions (pH) based on amount of each species hiding out and a prescribed boiling point elevation
  - Feedback loop to back-calculate hideout rates based on data retreived during hideout return
- Last updated in 1996
- Not currently in wide use

Hideout Return Spreadsheet

- Excel based program to evaluate data collected during shutdown
- Integrates amount of each species returned from crevice
- Uses a model to extract the portion of return believed to have come from crevices
- Also makes adjustments for that amount of species introduced through auxiliary feed sources
- Incorporates Molar Ratio assessment of crevice chemistry
- Output from the Hideout Return Spreadsheet is often used as input to MULTEQ for further evaluation of the potential crevice environment
- Current Version (3) released in 2001

Plant Chemistry Simulator

- This tool is a complete model of the steam cycle
- Two features built in that can help assess crevice chemistry
  - 'Internal SG Calculations'
    - Allow user to specify up to 10 locations in the SG, identified by a steam quality
    - The calculated bulk steam generator solution is then concentrated to achieve the desired quality, and the resulting concentrations and pH are output
  - 'Hideout Rate'
    - Based on a user defined hideout factor (similar to CrevSim)
    - The code can output the hideout rate (mass per time) of each species

SMART ChemWorks
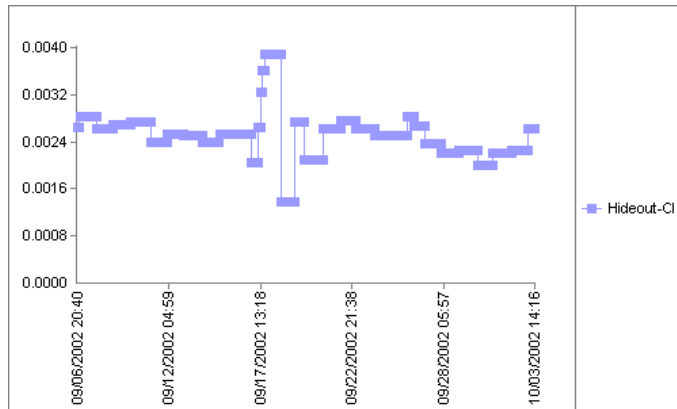
- Monitoring and diagnostic system linked directly to real-time plant data
- Plant chemistry simulator is embedded and runs automatically
- Hideout factor can be entered for each species
- Can output the hideout rate of each species as a 'virtual sensor'

525

Integrated Exposure Calculator

- Excel based program that calculates the 'integrated exposure' for a steam generator based on plant data.
- Integrated Exposure is a concept put forth in the current EPRI guidelines
- Based on the premise that the amount of impurities hiding out is proportional to the bulk concentration and time
- Allows for comparisons between acute imputiry ingress and chronic impurity ingress
- Actual Integrated Exposure is compared to reference conditions
- Version 1 was released in 2001

Future Plans

- MULTEQ Database Version 4 (2003)
    - Nickel oxide   -zinc
    - nickel ferrite   -H_2SO_4
    - DEAE   -DEA
    - DMEA   -DMAIP
    - Formate
- Excel based MULTEQ (2003+)
- Add Integrated Exposure calculation to SMART ChemWorks (2002)
- Upgrade CrevSim ?

527

Heated Crevice Seminar

Modeling and Analysis Supporting Argonne Model Boiler Facility Development

by Ken Kasza

Contributors: John Oras, Jeff Franklin, Jangyul Park, Yigang Cai, Dave Kupperman, Bill Shack

Argonne National Laboratory

October 8-11, 2002

NRC cognizant staff: Jim Davis (Program Manager) Joe Muscara (Senior Technical Advisor)

Steam Generator TIP-3

Presentation Outline

- Introduction

- Model Boiler Concept Overview

- Modeling/Analysis

  - Prototype/Boiler Crevice Region Heat Transfer and Hideout

  -Long Range Computational Needs

Introduction

- Steam generator tube ODSCC is not a well understood degradation mechanism

- Research is needed to improve predictions of potential for SCC during extended field service with Alloy 600 and 690TT

- Argonne Model Boiler Facility will study SG thermal-hydraulics and hideout chemistry for the support-plate / tube crevice region

- Studies will compliment Argonne autoclave studies of crack evolution and growth

Steam Generator TIP-3

Boiler Concept; Overview

Seven-tube boiler configuration used (longer range studies may involve a single tube boiler)

- simplified design (absence of pumped primary and secondary loops)

- primary reflux boiler chamber heated by 40Kw electrical heater used to create heat transfer across seven 12-in. long SG tubes (each with a crevice simulator)

- steam condensation occurs inside the SG tubes / boiling on the OD

- secondary-side contains a steam condenser which rejects heat to the ambient (maintains constant boiling conditions on the tube OD)

Argonne Model Boiler

Falling film vertical condenser
1.5-in., sch 160, alloy 800 pipe,
welded 2500# flanges
with fins for air cooling

Fans

Secondary: 12-in., sch 160,
316 SS pipe

Steam generator tube

12-in. RF orificed
weld neck
flange, 2500#

Crevice simulator, 3 types

Secondary water feed

Secondary
water bleed

Swagelock tube holder

Reflux primary: 12-in.,
sch 160, 316 SS pipe
Saturated steam
338°C   (640°F)
14.2 MPa (2059 psi)

7-tube support RF
orificed weld neck
blind flange, 2500#

Flanged electrical
heater (40 kW)

12-in. RF orificed
weld neck
flange, 2500#

Steam Generator TIP-3

532

Argonne Model Boiler
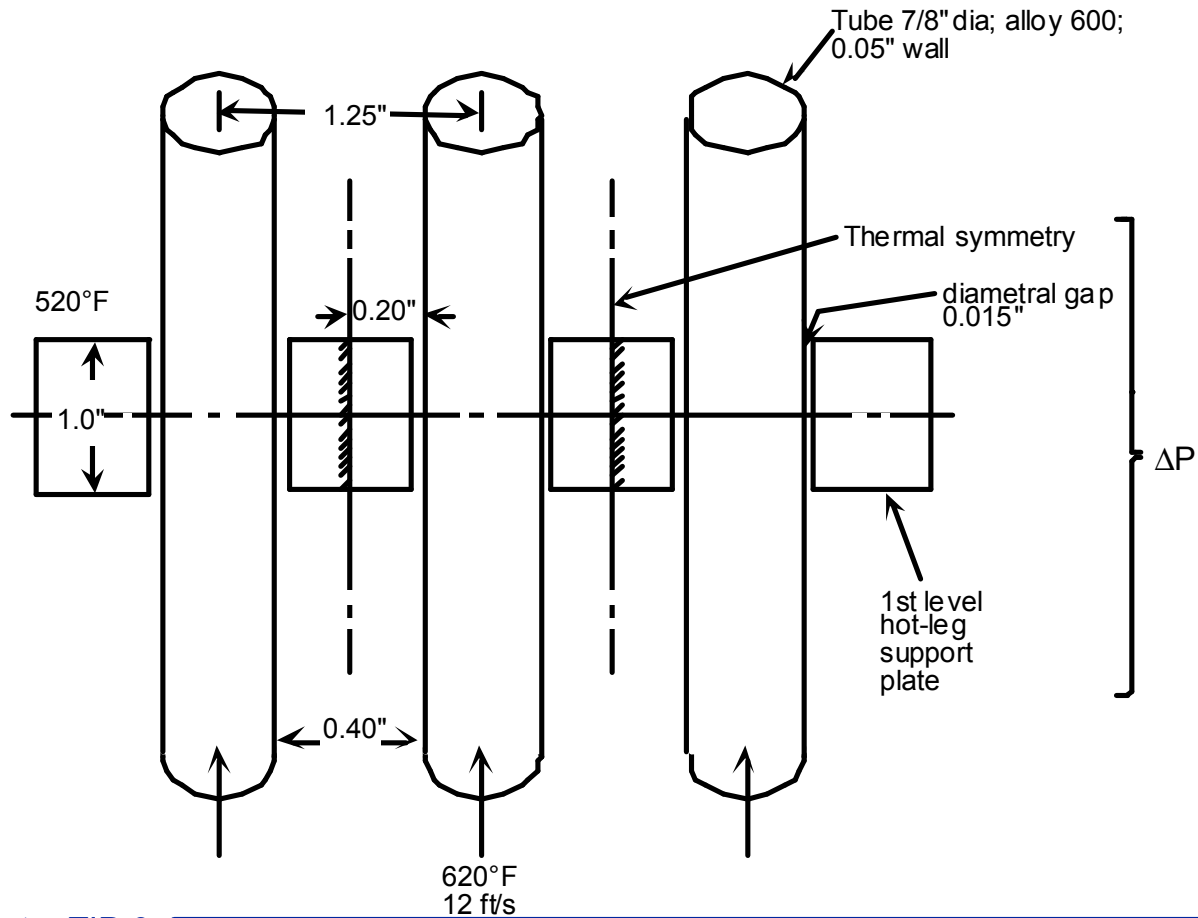# (Primary / Secondary Chambers)

Boiler Concept

- Primary side saturation temp/press controlled by controller set point on 40 Kw heater operating on bulk water temperature thermocouple

- Secondary bulk water thermocouple input to programmable speed controllers on fan(s) blowing air over the finned steam condenser pipe is used to maintain desired temp/press by controlling heat rejection to ambient from the condenser

- achieves prototypical crevice temperatures/heat fluxes and superheats using prototypical primary and secondary pressure/temperature

- SG tubes and crevice simulators are made of prototypical materials

- secondary water chemistry, thermal conditions, and crevice design can be varied to simulate other conditions of research interest or to accelerate cracking

- designed for unattended operation; run continuously for weeks

- facility meets ASME Code, Section VIII, Div 1 for a maximum allowable working pressure of 3000 psi and temperature of 680°F.

Crevice Modeling

- Thermal-hydraulics of prototype and boiler crevice regions are three dimensional

- NRC and Argonne are initiating an effort to model crevice region as a 3-D CFD problem (with fluid / thermal behavior coupled to crevice structure heat transfer)

- Initial analysis uses 1-D cylindrical model

- Analyzed heat transfer across the crevice as a function of the primary and secondary thermal-hydraulic conditions and for drilled hole crevice geometry

- T&H conditions used are those in the hot-leg at the first tube support plate (conditions for hideout are believed to be greatest at this location)

- Results for prototype and boiler crevices are compared

- Analysis guides boiler design to ensure prototypicality and aids in operation of the facility

Modeling
Prototype Drilled Hole Support-Plate/ Tube
Crevice Region

Tube 7/8" dia; alloy 600; 0.05" wall

1.25"

520°F

Thermal symmetry

0.20"

diametral gap 0.015"

1.0"

ΔP

1st level hot-leg support plate

0.40"

620°F
12 ft/s

536

Modeling
Simplified Prototype Crevice Region

T_s = 520°F sat. cond.

T_p = 620°F

V_p = 12 ft/s

Boiling

SS

Insulated (thermal symmetry)

Single phase forced convection heat transfer

SS

0.2"

1.0"

ΔP

Boiling

gap 0.015"

T_s = 520°F

Tube Alloy 600, 7/8", 0.05" wall

Modeling
Model Boiler Crevice Region

$T_S = 520°F$ sat. cond.

$T_p = 620°F$

Boiling

L

SS

Falling film conden- sation

SS

1.0"

Boiling

$T_S = 520°F$

gap 0.015"

Tube Alloy 600, 7/8", 0.05" wall
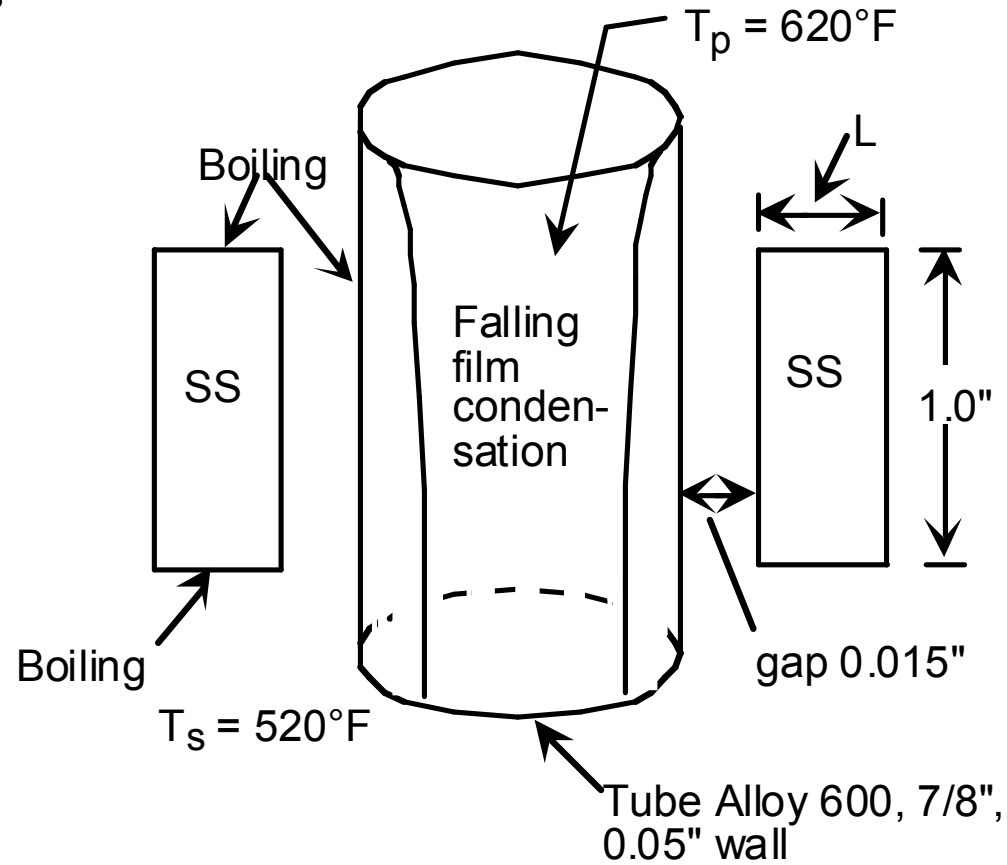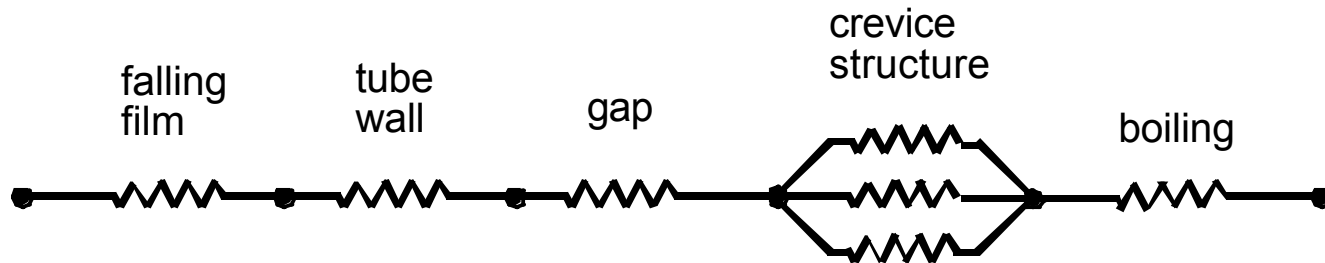
Modeling
Crevice Region 1-D Heat Transfer Electrical Circuit Analogy For The Simplified Prototype and Model Boiler Crevices
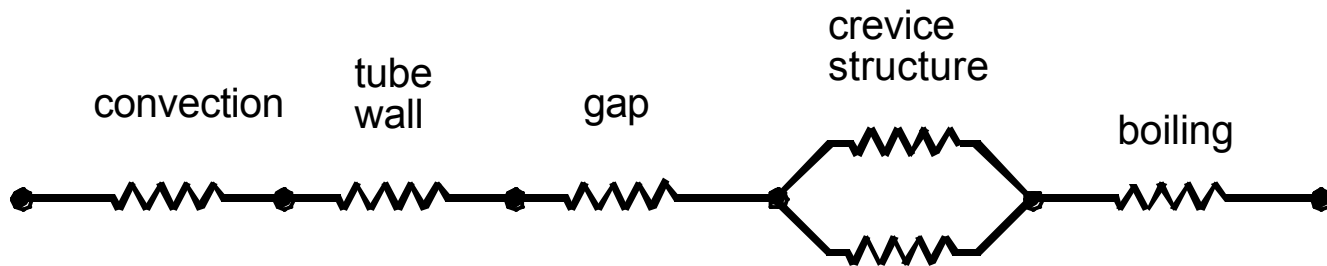
a. Simplified Prototype

b.   ANL Model Boiler

Modeling
Crevice Region

- Phenomena modeled and analyzed in comparing prototype tube/crevice behavior with that of the boiler were as follows:

  - forced convection heat transfer inside tube (prototype)

  - falling film condensation heat transfer inside tube (boiler)

  - heat conduction through the SG tube and crevice wall (prototype and boiler)

  - heat transfer through crevice gap fluid

  - boiling on the secondary (prototype and boiler)

Modeling
Crevice Region Equations

- The heat flux across the crevice/tube is given by; $q = h_a (T_p - T_s)$

- where T_p and T_s are the primary and secondary temperatures

- h_a is the overall heat transfer coefficient and represents the thermal resistance series for the problem; composed of five contributions

$$h_a = \cfrac{1}{\cfrac{d_{c_{out}}}{d_{in}}\cfrac{1}{h_v} + \cfrac{d_{c_{out}} \ln\frac{d_{out}}{d_{in}}}{2 k_w} + \cfrac{d_{c_{out}} \ln\frac{d_{c_{in}}}{d_{out}}}{2 k_c} + R + \cfrac{1}{h_b}}$$

$$R_P = \frac{R_1}{2}$$

$$R_B = \frac{R_1 R_2}{2 R_2 + R_1}$$

Modeling; Crevice Region Equations

1. model boiler falling-film condensation heat-transfer coefficient, hv, is given
   by the Roshenow correlation

$$h_v = 0.943 \left[\frac{\rho_l \left(\rho_l - \rho_v\right) g\, h'_{fg}\, k_l^3}{\mu_l L \left(T_{sv} - T_{sw}\right)} \right]^{1/4}$$

or, for the prototype, the heat transfer coefficient h for forced convection single
phase flow inside a SG tube is given by

Colburn equation from p. 260, Eq. 7-49 in Gebhart:

$$\left(\frac{h}{\rho V C_P}\right)_m \left(\frac{C_P \mu}{k}\right)_f^{2/3} = 0.023 \left(\frac{DV}{\nu_f}\right)^{-0.2}$$

Modeling; Crevice Region Equations

2. heat-transfer coefficient for the tube wall is given by

$$2\ k_w\ /\ d_{cout}$$

3. heat transfer coefficient for the crevice gap fluid, assuming all boiling is suppressed by the chemical hideout, is given by

$$2\ k_c\ /\ d_{cout}$$

4. heat transfer coefficient for the crevice wall is given by Rp and Rb

5. nucleate-pool-boiling model of Rohsenow is used to represent the heat transfer coefficient on the crevice/tube outer surfaces:

$$\frac{c_{pl}\ (T_{bw} - T_{sb})}{h_{fg}\ P_{rl}^{1.7}} = C_{sf} \left[\frac{q}{\dot{m}\ h_{fg}} \sqrt{\frac{s}{g(r_l - r_v)}} \right]^{0.33}$$

Modeling; Chemical Hideout

- bulk-water, low-concentration, low-volatility, impurities can concentrate locally

- typical locations are the crevices between tube and support plates, crevices within tubesheets, sludge piles that surround SG tubes, and porous scale deposited on tubes

- crevice temperature elevation above the bulk secondary saturation temperature occurs and is called the local superheat which is based on tube outer wall temperature

- boiling draws bulk water into the crevice and expels steam or a mixture of steam and water; some of the low-volatility impurities drawn in with bulk water remain behind to concentrate

- concentration can increase to the solubility limit and solid will precipitate which can block or alter access and escape paths for fluid or vapor

- concentration can also increase to the extent that the boiling point of the crevicel fluid is significantly increased over the boiling point of the bulk water. Crevice boiling will stop when the concentration increases to the point that the boiling point elevation equals the local superheat; "thermodynamic limit"

Modeling; Chemical Hideout

● concentration buildup can stop before the thermodynamic limit which is called "kinetically limited"

● which occurs depends on many factors: including the geometric configuration of the crevice, pathways that connect it to the bulk water, the local temperature and heat flux, constituent boiling point, and other characteristics of the fluid

● based on the thermodynamic limit the boiling point of a solution that contains impurities is related to the mole fraction of the impurities by

$$\text{Ln } X_A = \frac{\Delta H_{vap}}{R}\left(\frac{1}{T} - \frac{1}{T_o}\right)$$

Where X_A = mole fraction of water,
DH_{vap} = molar heat of vaporization of H_2O,
R = universal gas constant, 1.98717 cal/mole-K,
T_o = boiling point of pure H_2O (K), and
T = boiling point of solution (K),

Set (T_o-T) = crevice superheat

Modeling Results
Prototype / Boiler

•Argonne 1-D code calculates the temperatures of the various zones, the heat flux across the tube/crevice from the primary to the secondary, and crevice hideout for low levels of impurity in the secondary water

•Prediction results

- prototypical crevice thermal conditions are achieved in the boiler
- crevice conditions can be varied by adjusting the crevice geometry or the
          primary and secondary temperatures
- significant crevice superheats occur with potentially high levels of chemical hideout (crevice concentration factors 50,000 - 80,000 for NaOH)

Steam Generator TIP-3

Modeling Results
Prototype/Boiler
Tp = 620F; Ts = 520F or 510F

Crevice Parameters		Model Boiler Crevice			Prototype Crevice
Tp = 620 F Ts = 520 F	Crevice Wall Thickness (in.)	0.2	0.5	1.0	0.2
	Superheat (F)	76.2	77.2	77.8	87.3
	Flux (Btu/hr ft2)	11,842	7,805	4,975	11,820
Tp = 620 F Ts = 504 F	Crevice Wall Thickness (in.)	0.2			
	Superheat (F)	87.4			
	Flux (Btu/hr ft2)	13,647			

Modeling
Long Range Needs

• Current analysis of crevice region thermal behavior and hideout is 1-D

• Thermal fields and heat flux in local crevice/tube geometry strongly influence hideout

- rate of accumulation

- ultimate concentration limit

• Complex problem involving structure/fluid interactions, change of phase, and chemical species migration dependent on detailed thermal distributions in structure and the fluid all being multi-dimensional

• Different crevice designs will have an important influence on behavior of the water/steam in a particular design (as important as the primary and secondary bulk water thermal-hydraulic conditions)

• In order to ultimately be able to relate laboratory boiler and autoclave results to the field experience and the different design support plate/tube geometry's, multi-dimensional interacting CFD and crevice structural thermal behavior computer simulations are needed.

Steam Generator TIP-3

Modeling
Long Range Needs

Benchmark Computational Problem

• Drilled hole support-plate / tube crevice geometry is good benchmark computational problem

      - supports model boiler experiments/studies

      - represents a field design and is a common geometry used in past crevice studies

      - shifting the tube off-center can be used to explore conditions approaching line contact

Numerical Modeling of Steam Generator Crevice Thermal-Hydraulics

Stephen M Bajorek and Donald M. Helton
U. S. Nuclear Regulatory Commission
Office of Nuclear Regulatory Research
Washington, DC 20555-0001
Phone: (301) 415-7574
e-mail: smb4@nrc.gov

Abstract

Thermal-hydraulics and the deposition of corrosive compounds in the crevices formed by steam generator tubes and their support plates have long been recognized as complex and poorly understood phenomena. Bubble nucleation, growth and departure in confined spaces are significantly different from those which occur along an unrestricted surface. Thus, experimental data and numerical models of boiling and mass deposition processes can not be reliably applied to the steam generator crevice problem.

With advances in computing speed and refinements in analytical modeling of boiling phenomena, it is now possible to numerically simulate the fluid flow and heat transfer near a bubble growing on a surface. This paper discusses modeling possibilities and recommends an approach intended to estimate temperature, void, and flow distributions in a steam generator crevice. Two relatively simple models are described that will help characterize surface superheat in the crevice, along with a more complex model using direct numerical simulation of the flow field. The long term objectives of the numerical studies are to provide useful information for the accompanying experimental work, and to eventually predict the locations and thermal-hydraulic conditions favorable to hideout.

Introduction

The crevices formed between steam generator tubes and support plates have resulted in several unique problems that must be solved by designers and operators of pressurized water reactor (PWR) steam generators (SG). The crevices are likely responsible for crud build up and local dryout that may cause SG tube failure. Flow and heat transfer in and near the crevice is complex due to the restricted flow area and the effect it has on local vapor generation. Efforts to simulate the phenomena leading to chemical deposition in the crevice have been hampered due to a lack of basic experimental information along with the difficulties in modeling boiling and two-phase flow.

Numerical simulation of SG crevice thermal-hydraulics may be highly valuable. Estimates of local void, flows and wall superheats are useful in designing experiments to investigate crevice behavior, and analytical methods to predict long-term SG performance are of considerable practical importance.

This paper describes potential numerical approaches for modeling the SG crevice problem, and the pros and cons of each. Three options are discussed, ranging from one which is simple (but inaccurate), to a comprehensive mechanistic model that will require significant effort.

Multidimensional Conduction: The simplest approach would be to perform a 2D or 3D conduction solution to obtain the temperature distribution in the SG tube wall, the crevice gap itself and the support. Assuming no flow through the gap greatly simplifies the calculation. Two cases would be considered; one with the gap liquid filled and another with the gap filled with vapor. The main difference in the two temperature profiles would be due to the thermal conductivities of the gap fluid. Results would provide temperature distributions along both walls of the crevice and thus provide a crude estimate of wall superheats. Heat transfer coefficient boundary conditions would be applied on the inner surface of the SG tube wall and on the edges of the support plate. These could be determined using conventional correlations for flow boiling.

By ignoring flow through the crevice and assuming a high heat transfer coefficient on the SG outer wall above and below the support plate, the conduction solution will be symmetric about the support plate mid-height. The maximum wall superheat would occur at that elevation. Figure 1 shows a schematic of this approach and the expected wall superheat distribution.

There are several computer codes that could be used to perform the calculations. Structural analysis packages such as ANSYS or ABAQUS are available and have been used by the NRC staff in the past. For the simple 2D schematic shown in Figure 1, it is a relatively simple task to devise a finite difference nodalization and solve for the temperature distribution. Thus, the "pro" of this approach is its simplicity and low cost.
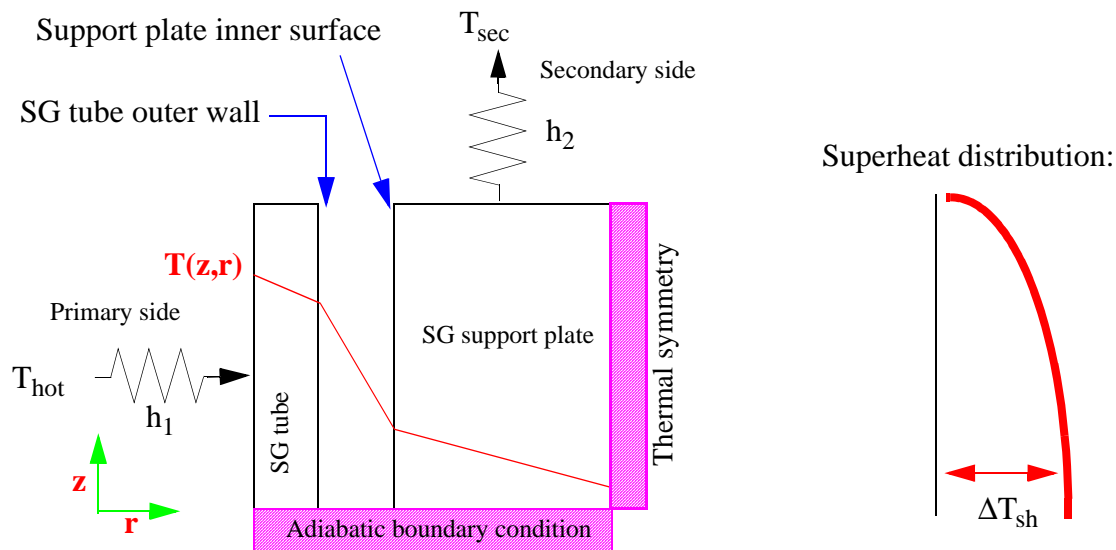

Figure 1. Schematic of Conduction Solution.

The obvious problem with this approach is that it ignores flow and phase change within the crevice. No nucleation would be predicted with this model, regardless of the wall superheat. The temperature distribution predicted would not be correct for the situations when phase change took place. Thus, the "con" of this approach is inaccuracy as bubble nucleation occurs.

Computational Fluid Dynamics: Computational fluid dynamics (CFD) has been used to investigate a wide range of complex thermal-hydraulic problems. It can provide detailed temperature, velocity, and concentration profiles in a complex geometry although the state-of-the-art is limited to single phase fluids. In this proposed CFD approach, velocity and temperature distributions without phase change would be calculated in the crevice. Temperature distributions along the crevice boundaries would be obtained. These temperature distributions would show less wall superheat than in the simple multidimensional conduction calculation because of the cooling effect of flow through the crevice. In this calculation, the crevice would be "open". That is, flow would enter from the bottom and exit out the top, dis-allowing the adiabatic boundary (symmetry) condition in the conduction approach. This would increase the size of the numerical grid. Figure 2 shows a schematic of this approach. Unlike the conduction solution, wall superheat would increase from the bottom of the crevice, as the fluid is heated.

This calculation could be done with a commercial CFD package such as FLUENT, CFX or StarCD, or with the NRC developed code, NPHASE. The NPHASE code utilizes an Euler-Euler methodology and allows mass and energy transfer between phases. Technically NPHASE could provide details on phase change in the crevice. However, implementation of nucleation and bubble growth models has not been part of NPHASE development. The NRC staff has experience in using FLUENT, but no internal experience with NPHASE.
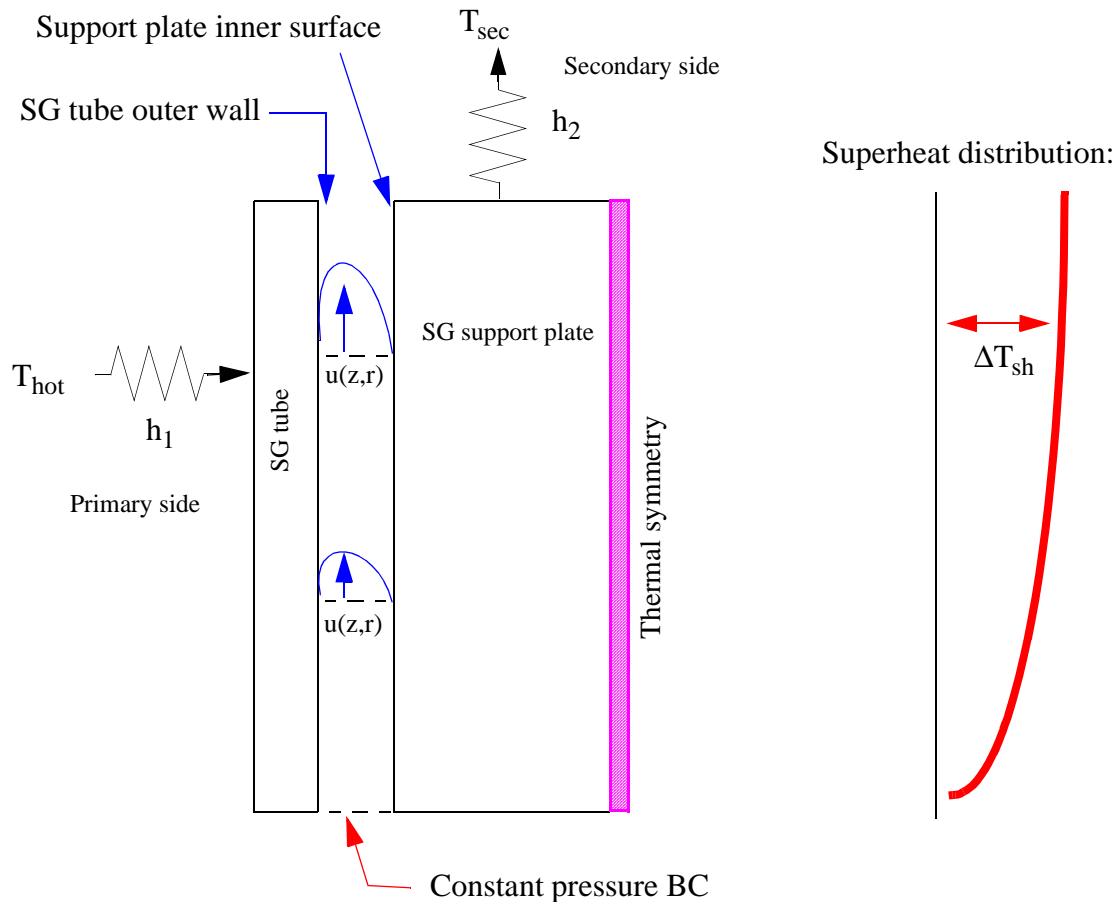

Figure 2. Schematic of CFD application to the SG heated crevice problem.

The "pro" of the CFD approach is the more detailed calculation of velocity and concentration profiles in the crevice than what might be obtained in the multidimensional conduction model approach. Commercial, or relatively mature computer code packages could be applied, which include features that would allow a wide range of crevice geometries to be examined. This is important to the SG crevice problem, as there are several types of supports that are in use.

As with the conduction approach, the "con" of the CFD approach is that the solution again ignores phase change within the crevice. Thus, application of a CFD approach to the SG heated crevice problem is not expected to yield significant insight unless there is development and implementation of models for bubble nucleation and growth.

Mechanistic Modeling: An approach that is capable of producing a reasonably accurate representation of phenomena within the crevice is mechanistic modeling of bubble growth and film formation. Because of advances in computing speed. It is now possible to solve the mass, momentum and energy equations for liquid and vapor phases simultaneously while a two-phase interface is developing. Such a solution provides not only the temperature, velocity and concentration profiles in the fluids, but also the shape of the interface. This approach is attractive, as previous experimental work has shown that localized dryout and rewetting of the crevice surfaces is important to the problem. Visualizations by Yao and Chang (1983) for example, found four different types of boiling patterns in an annular crevice. Relatively large regions of the gap were found to be occupied by the expanding bubble. Figure 3 shows some of the patterns observed by Yao and Chang. (One of the geometries considered was for a 25.4 mm high, 0.32 mm gap which is close to dimensions of interest in the SG crevice problem.) Likewise, the experiments by Tieszen et al. (1987) identified three confinement dependent flow regimes in the crevice. Each of these studies indicate that successful numerical modeling of crevice thermal-hydraulic conditions must account for two-phase interfaces.

Mechanistic modeling of bubbles and evaporating films track an interface while solving the mass, momentum, and energy equations of the liquid and vapor fields simultaneously. The approach generally divides the computational domain into micro and macro regions in which various physical processes dominate and some simplifications can be made. Dhir (2000) provides an overview of the mechanistic modeling of single and multiple bubble growth and also for film boiling. Son and Dhir (1997) provide details of modeling saturated film boiling, with Son (1996) describing the application to several multiphase problems.

In the SG crevice problem, both single bubble growth and film boiling (dryout) is expected. Because the support plate is cooler than the SG tube itself, and sufficient superheat to nucleate and/or allow local evaporation at the tube wall is expected, bubble growth initiated at the SG tube wall should dominate the gap behavior. The support plate will be cooler and may allow a liquid film to remain attached to it. Vapor formation at the SG tube will drive the flows which may be "fed" by liquid entering either the bottom or top of the crevice depending on superheat on the SG support plate surface. Because of the rapid volumetric expansion of the vapor and periodic bubble departure from the crevice, the process may be cyclic with vapor generation "flushing" the gap which later fills with liquid as the vapor departs from the crevice. Bubble growth and departure will be strongly influenced by the crevice dimensions. A bubble may initially nucleate, but because of the expected high superheats a stable vapor film may remain in the crevice and the mechanism of vapor production will be evaporation from the interface. Thus, models for interface behavior during film boiling may be applicable. Axial conduction along the SG tube may be important, and should be included in the calculations. Figure 4 shows a schematic of crevice boiling.
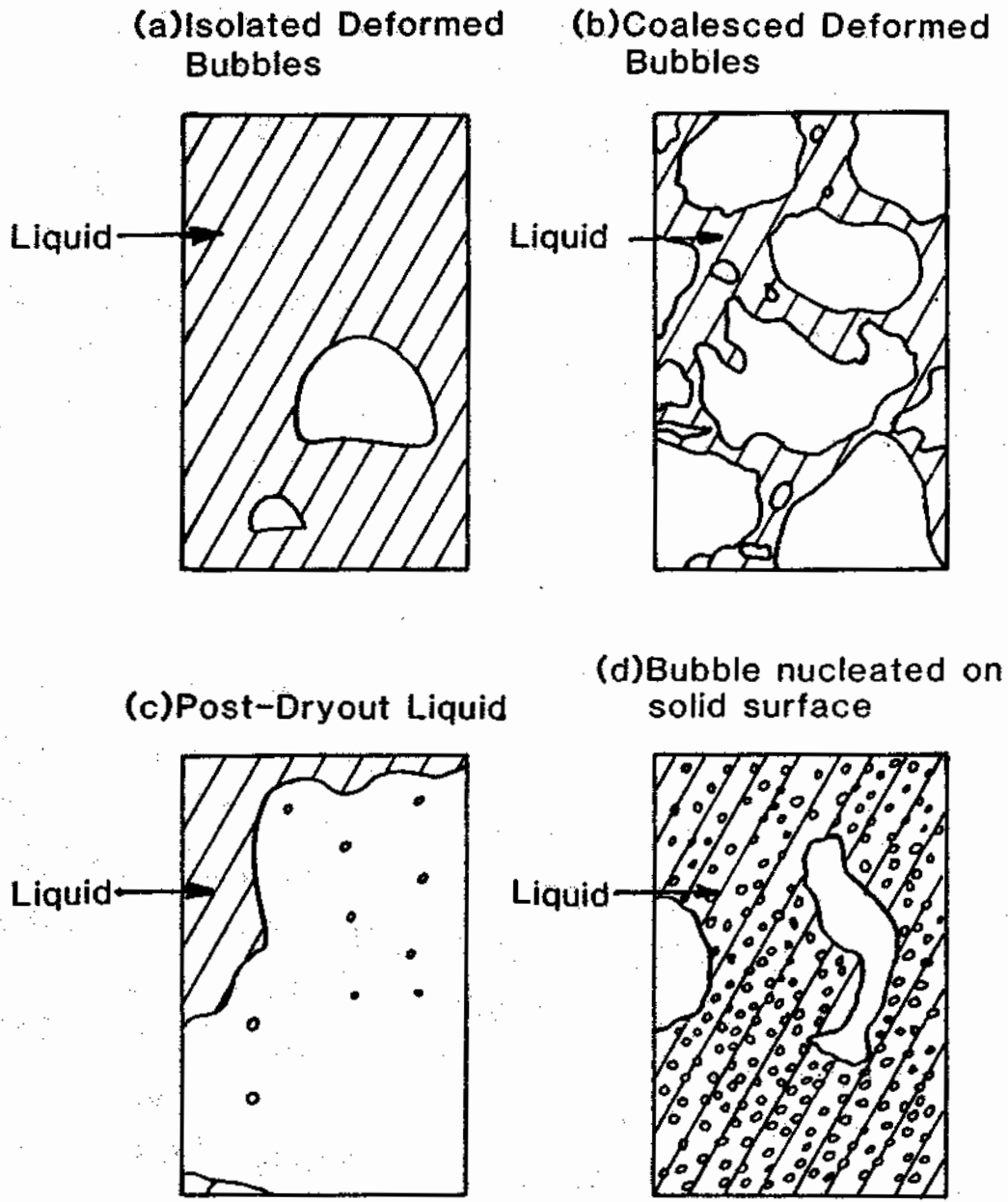
553

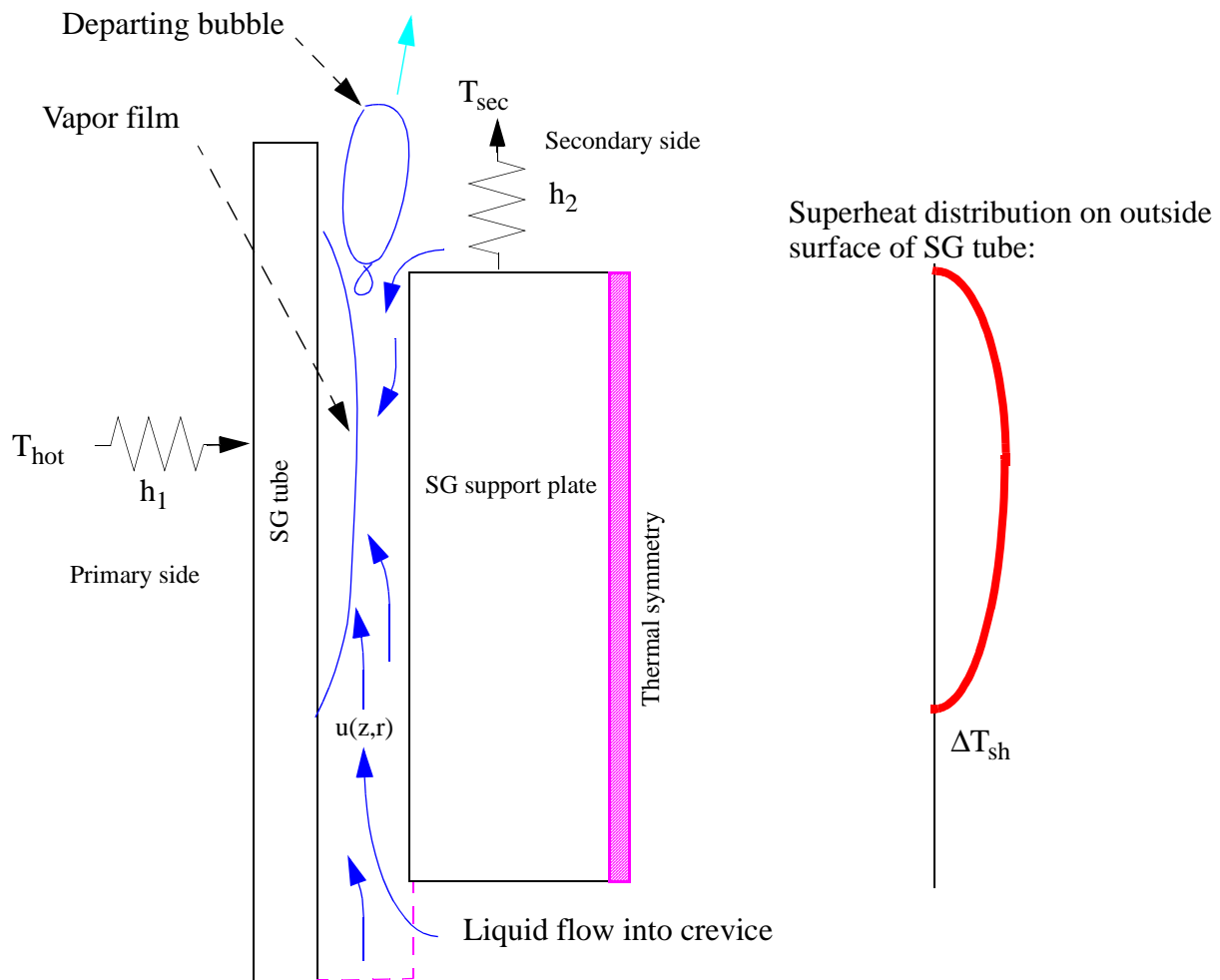Figure 3. Boiling phenomena in a confined space. From: Yao and Chang (1983).

Figure 4. Bubble growth in a SG crevice.

The "pro" of this approach is its technical validity. A mechanistic modeling of crevice phenomena would provide the most accurate representation of phenomena of importance and may result in a tool suitable for predicting conditions and geometries less prone to chemical hideout. This may be the only approach that might provide the correct physics, be extendable to similar geometries, and be capable in the long run of predicting if and where species deposition will occur.

The "con" is expense, and relatively long time frame required. Numerical calculations of this type are possible, but they are difficult. The mechanistic approach has been successful for relatively simple geometries; single bubbles, multiple bubbles growing in a uniform array, film boiling, and phase change with sublimation. However, no work has been performed with multiple solid boundaries as is the case in the SG crevice. A multi-year effort is anticipated.

Conclusions

Numerical simulation of SG crevice thermal-hydraulics is feasible, although developing an accurate model capable of predicting chemical hideout will require significant effort. Simple models (multidimensional conduction and CFD) can estimate surface temperatures with relatively little effort, but their validity is limited to single phase fluid conditions. Given the long-term effects of SG crevice phenomena on tube integrity, steam generator operation and performance, it is recommended that a multi-pronged approach be undertaken. A simple conduction model will provide crude estimates of temperatures in the crevice and surrounding structures. This may help in the design of experiments. The long term effort should include development of a mechanistic model for crevice phenomena. Development of a mechanistic model, in conjunction with a well planned experimental program should provide an important tool for dealing with the SG crevice problem.

References

Dhir, V. K., "On the Use of Numerical Simulations to Augment Our Understanding of Boiling Heat Transfer," Proc. 34th National Heat Transfer Conf,. NHTC2000-12303, Pittsburgh, PA, August 2000.

Tieszen, S., Merte, H., Arpaci, V. S., and Selamoglu, S., "Crevice Boiling in Steam Generators," J. Heat Transfer, Vol. 109, pp. 761-767, 1987.

Son, G., "Numerical Simulation of Nonlinear Taylor Instability with Application to Film Boiling and Sublimation," Ph. D. Dissertation, UCLA, 1996.

Son, G., and Dhir, V. K., "Numerical simulation of saturated film boiling on a horizontal surface," J. Heat and Mass Transfer, Vol. 119, 1997.

Yao, S. C., and Chang, Y., "Pool Boiling Heat Transfer in a Confined Space," Int. J. Heat Mass Transfer, Vol. 26, No. 6, pp. 841-848, 1983.

Heated Crevice Seminar

Application of Chemical Equilibrium Model to the Evaluation of Magnetite-Packed Crevice Chemistry

Chi Bum Bahn and Il Soon Hwang
Seoul National University

In Hyoung Rhee
Soonchunhyang University

October 7-11, 2002
Argonne Guest House, ANL

Contents

- Introduction
- SG Crevice Simulation Experiments
- Rationale & Approach
- Thermodynamic Aspects: Pourbaix Diagram
- Chemical Equilibrium Model
  - Approach
  - Species & Reactions
- Results & Discussion
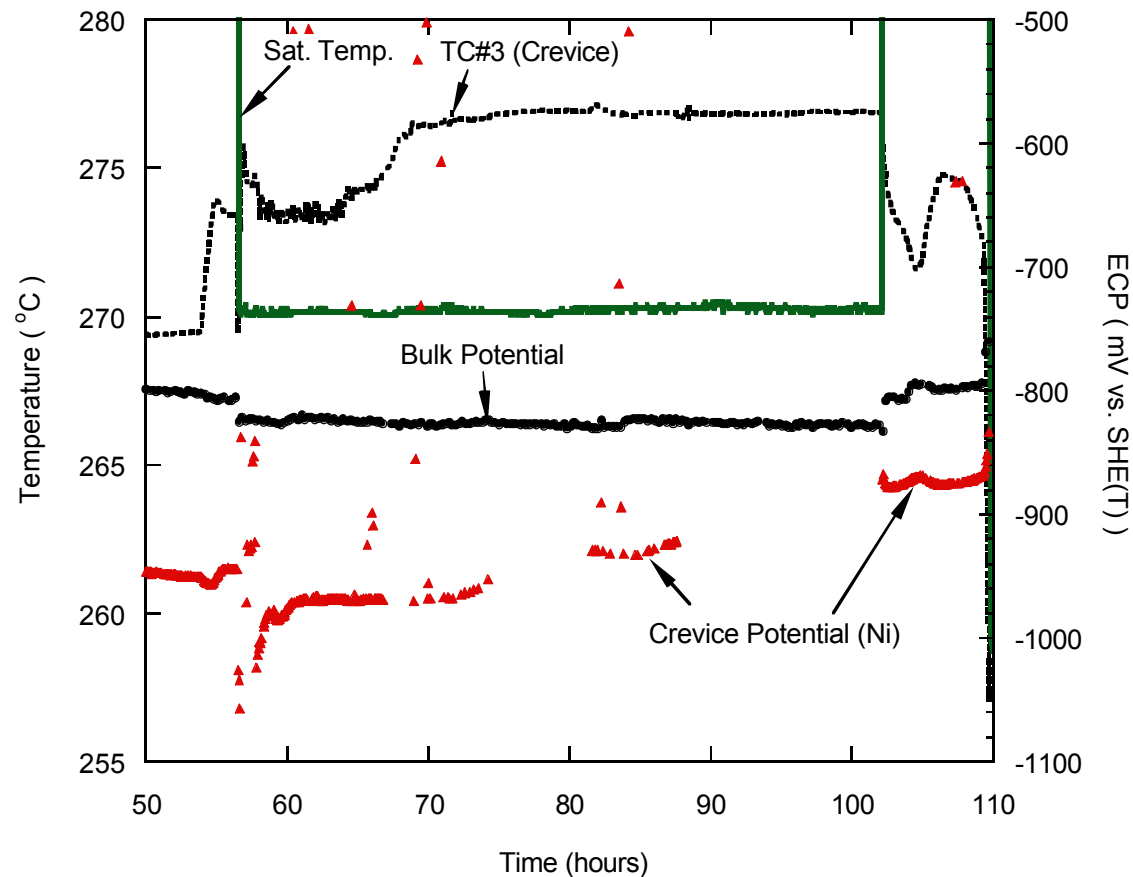- Summary & Conclusions
- Future Work

Introduction

- It is needed to develop a combined model taking into account the thermal-hydraulic and chemical phenomena.

- As a first step towards developing the combined model, a chemical equilibrium model that predicts the chemical speciation in a magnetite-packed crevice under an equilibrium state was developed.
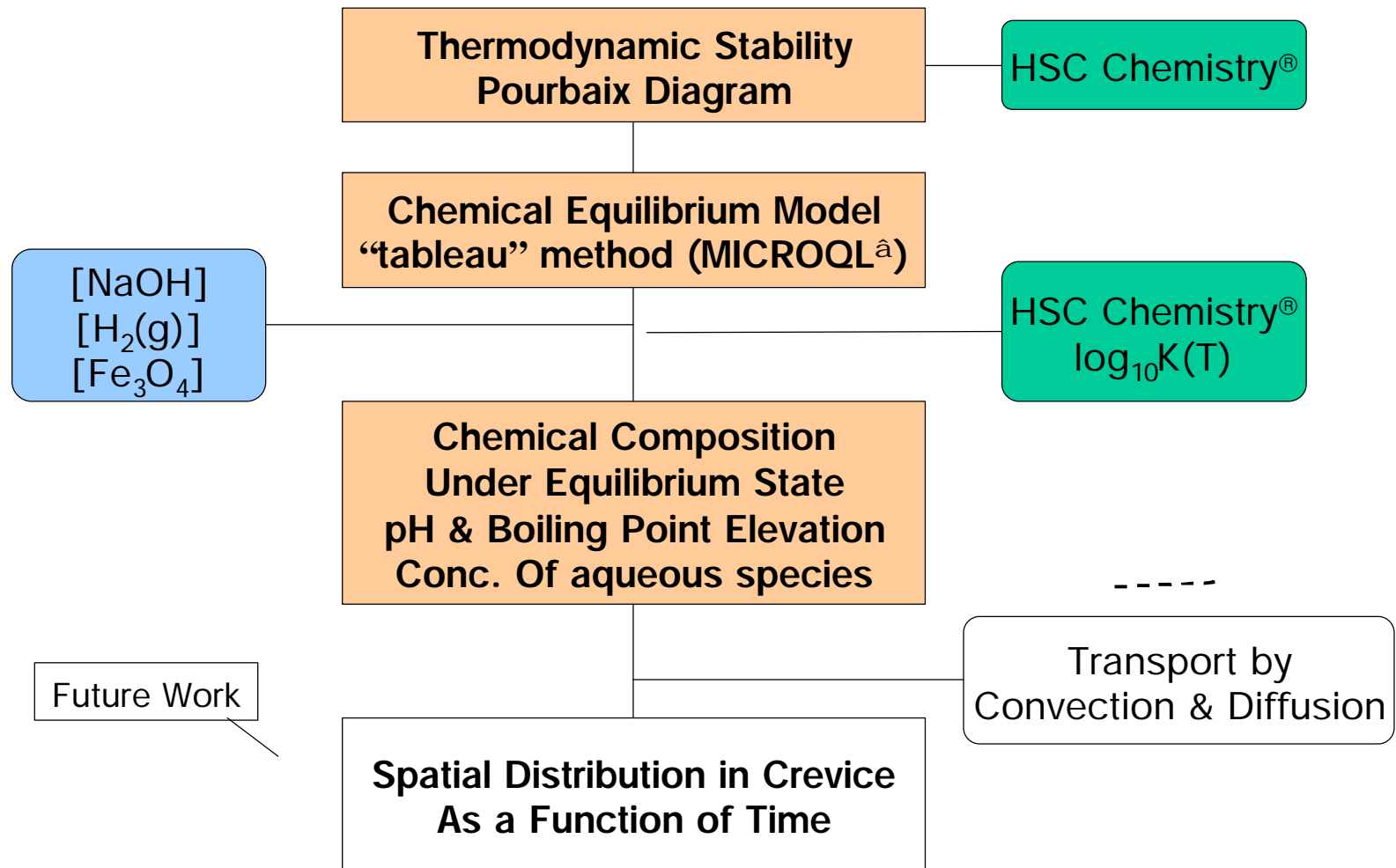
SG Crevice Simulation Experiment
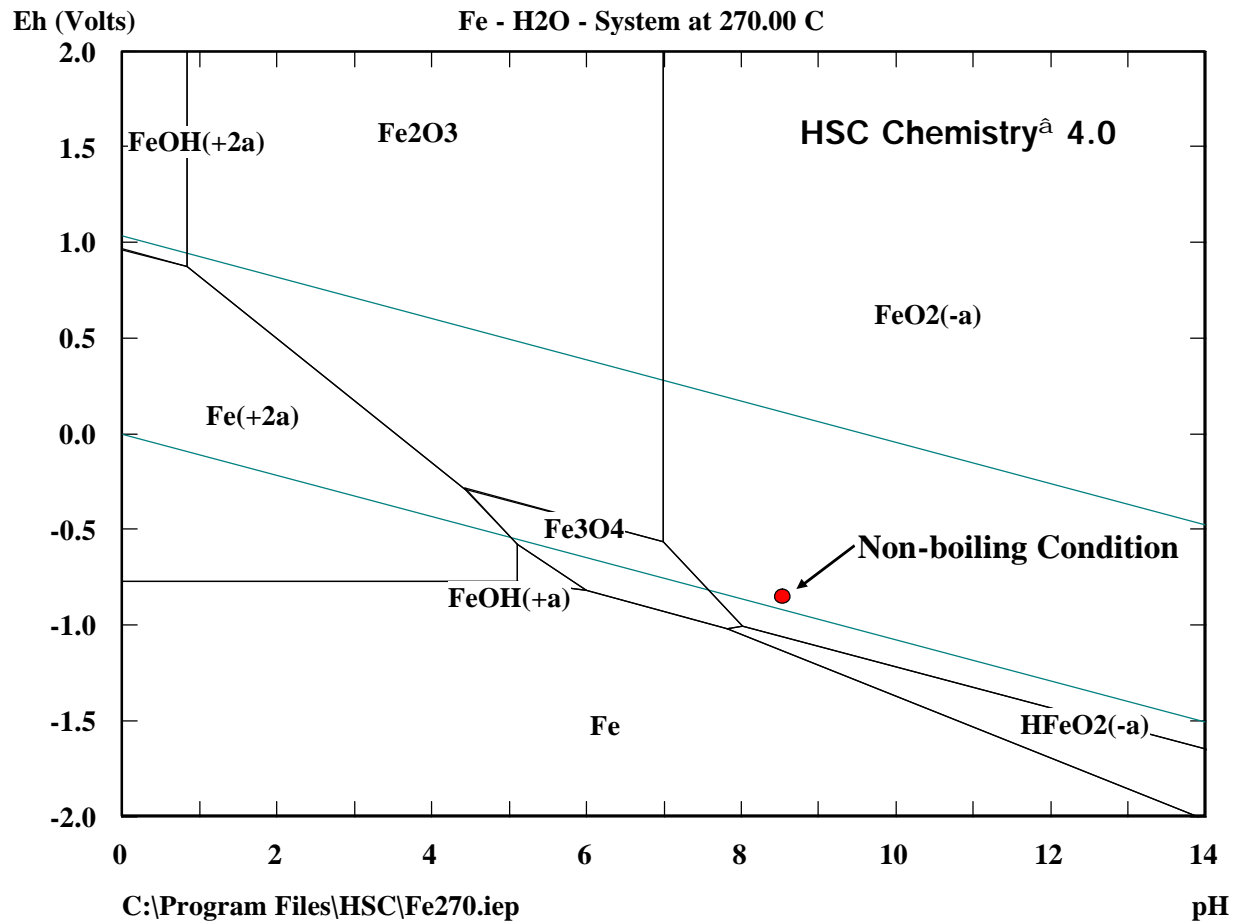## Results: Temperature & ECP

Magnetite‑Packed Crevice Condition, DT=20 ºC

Rationale & Approach

Pourbaix Diagram: Fe–H₂O System

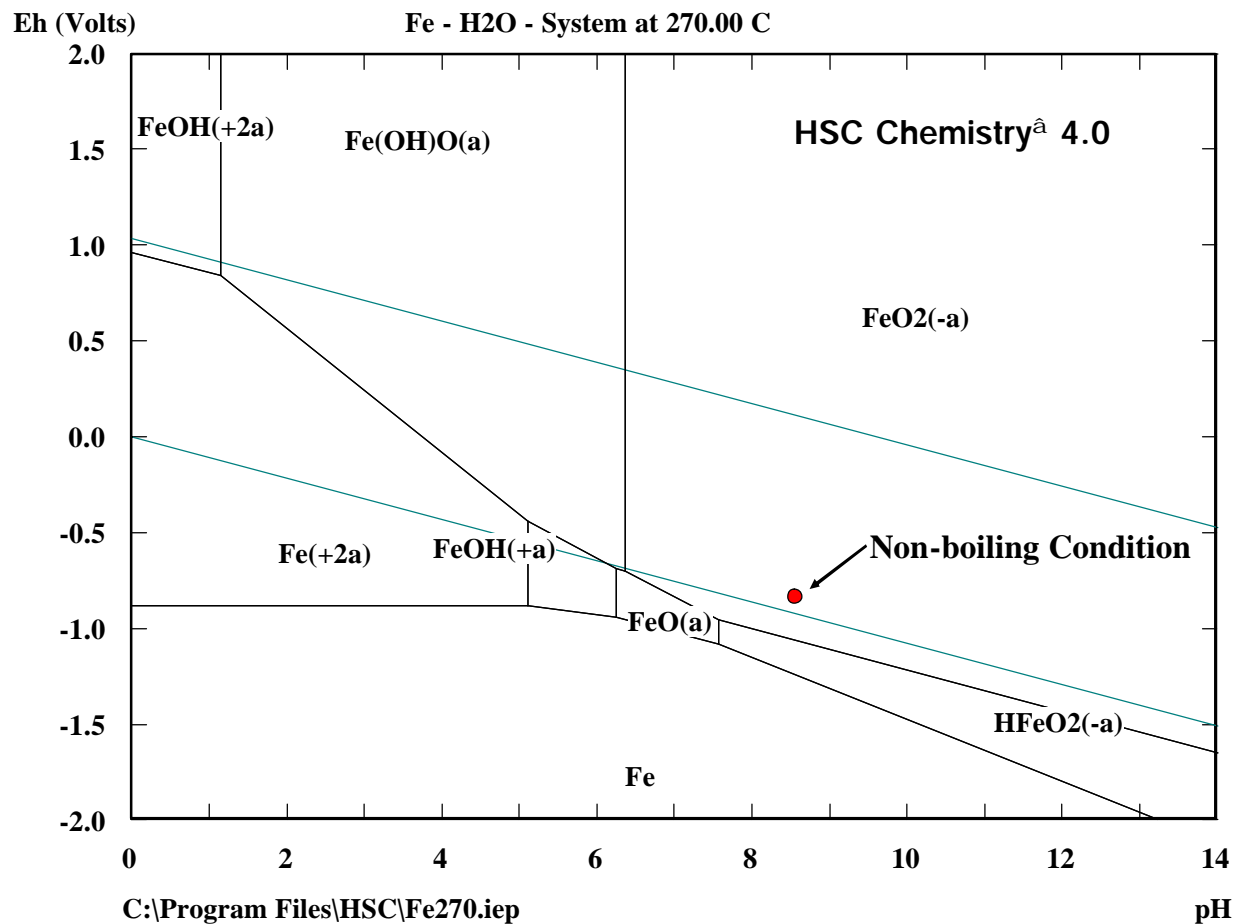Fe - H2O - System at 270.00 C

Eh (Volts)

HSC Chemistry^â 4.0

FeOH(+2a)

Fe2O3

FeO2(-a)

Fe(+2a)

Fe3O4

Non-boiling Condition

FeOH(+a)

Fe

HFeO2(-a)

C:\Program Files\HSC\Fe270.iep

pH

ELEMENTS	Molality	Pressure
Fe	1.000E-06	5.426E+01

Pourbaix Diagram: Fe–H$_2$O System

Eh (Volts)

Fe - H2O - System at 270.00 C

HSC Chemistry$^{\text{â}}$ 4.0

FeOH(+2a)

Fe(OH)O(a)

FeO2(-a)

Fe(+2a)

FeOH(+a)

Non-boiling Condition

FeO(a)

HFeO2(-a)

Fe

C:\Program Files\HSC\Fe270.iep

pH

ELEMENTS	Molality	Pressure
Fe	1.000E-08	5.426E+01

563

Pourbaix Diagram: Na–H₂O System

Eh (Volts)

Na - H2O - System at 270.00 C

HSC Chemistry^â 4.0

NaO2

Non-boiling Condition

Na(+a)

NaOH(a)

NaH

C:\Program Files\HSC\Na270.iep

pH

ELEMENTS	Molality	Pressure
Na	1.000E-06	5.426E+01

564
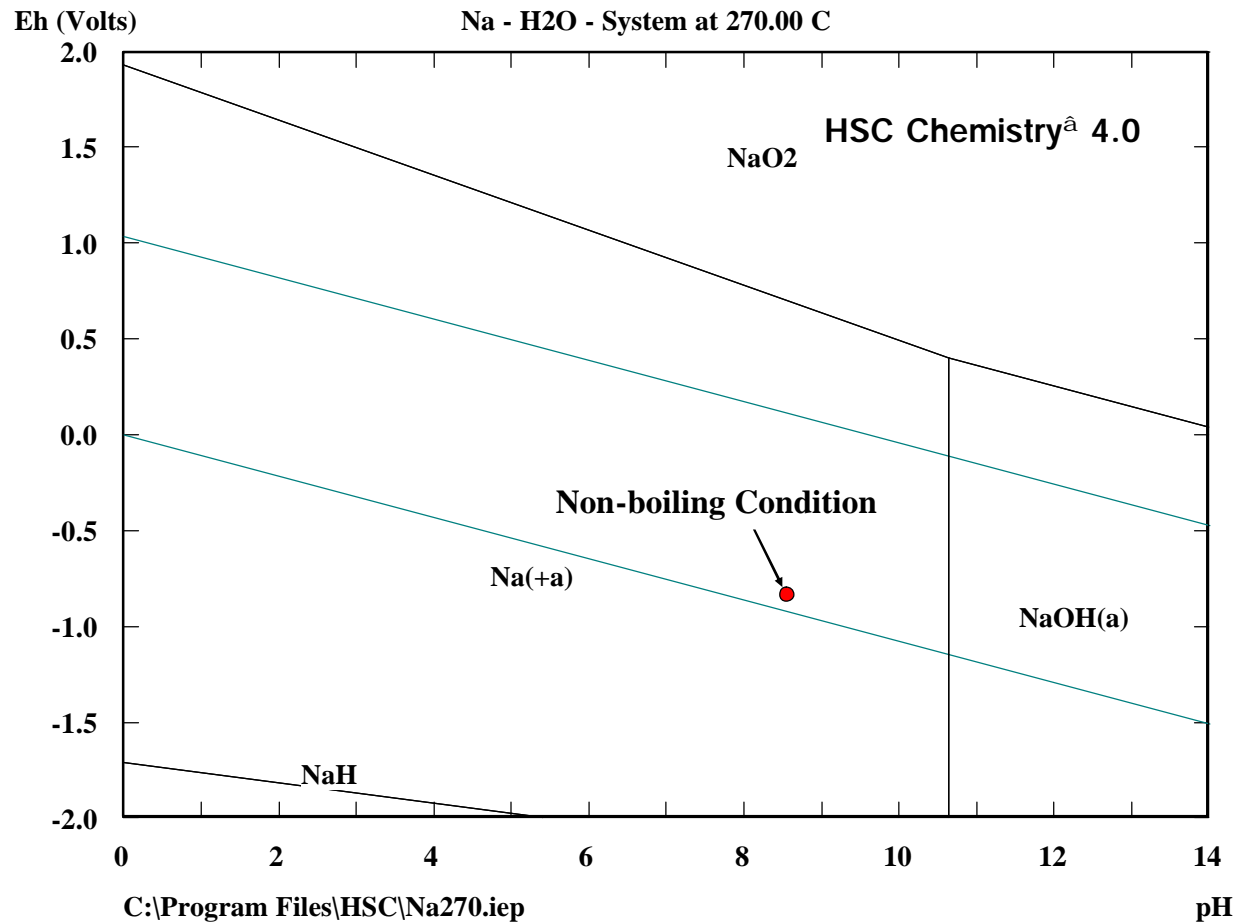
Chemical Equilibrium Model

- The equilibrium state of a closed chemical system is defined by its minimum free energy within the constraints of mass conservation.

- Two sets of equations, mole balances and the mass action laws, define a well-posed mathematical problem that can be shown to have one solution: the concentrations of the species at equilibrium.

- The "tableau" methodology is a convenient way to express the stoichiometric relations between species and components.

- MICROQL® is a chemical equilibrium program written by John Westall(1979) and essentially is a stripped down version of the program MINEQL® (Westall et al., 1976).

- Equilibrium constants of each reaction were calculated as a function of temperature by using HSC Chemistry®.

Chemical Equilibrium Model
Species & Equations

$$H^+ + OH^- = H_2O$$

$$H_2(aq) = H_2(g)$$

$$Na^+ + OH^- = NaOH(aq)$$

$$Fe^{2+} + H_2O = Fe(OH)^+ + H^+$$

$$Fe^{2+} + H_2O = FeO(aq) + 2H^+$$

$$Fe^{2+} + 2H_2O = HFeO_2^- + 3H^+$$

$$2Fe^{3+} + H_2(g) = 2Fe^{2+} + 2H^+$$

$$Fe^{3+} + H_2O = Fe(OH)^{2+} + H^+$$

$$Fe^{3+} + H_2O = FeO^+ + 2H^+$$

$$2Fe^{3+} + 2H_2O = Fe_2(OH)_2^{4+} + 2H^+$$

$$Fe^{3+} + 2H_2O = Fe(OH)O(aq) + 3H^+$$

$$Fe^{3+} + 2H_2O = FeO^{2-} + 4H^+$$

$$Fe_3O_4(s) + 6H^+ + H_2(g) = 3Fe^{2+} + 4H_2O$$

$$Fe_2O_3(s) + 4H^+ + H_2(g) = 2Fe^{2+} + 3H_2O$$
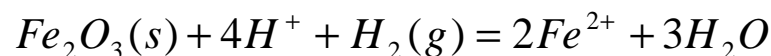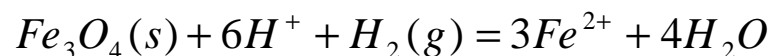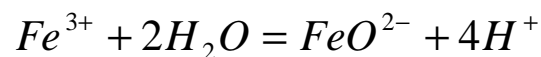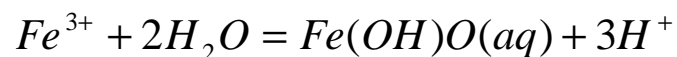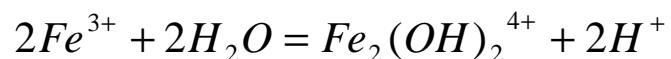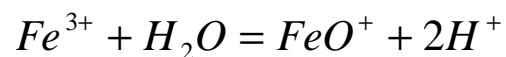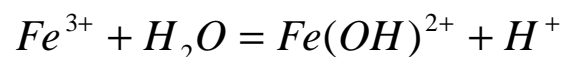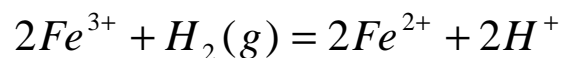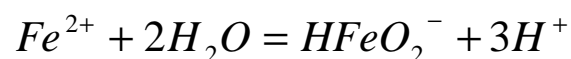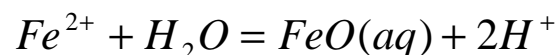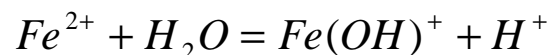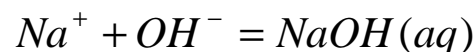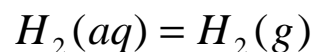
- 18 Species
  - H^+, OH^-
  - $H_2(aq)$, $H_2(g)$
  - Na^+, $NaOH(aq)$
  - Fe^{2+}, $FeOH^+$, $FeO(aq)$, $HFeO_2^-$
  - Fe^{3+}, $FeOH^{2+}$, FeO^+, $Fe_2(OH)_2^{4+}$, $Fe(OH)O(aq)$, FeO_2^-
  - $Fe_3O_4(s)$
  - $Fe_2O_3(s)$
- 14 Reactions

566

Calculation Results

- Chemical Speciation Under Non-Boiling Condition: no chemical concentration

- Crevice Chemistry Evaluation from Experimental Results
  - Estimation [NaOH] from the temperature data
  - [H_2(aq)] Calculation from the ECP data
  - pH, Concentrations of aqueous species

Results: Non-Boiling Condition

[NaOH(aq)]=0.00217 mol/kg
[H2(aq)]=0.0001 mol/kg
[Fe3O4]=10 mol/kg

568
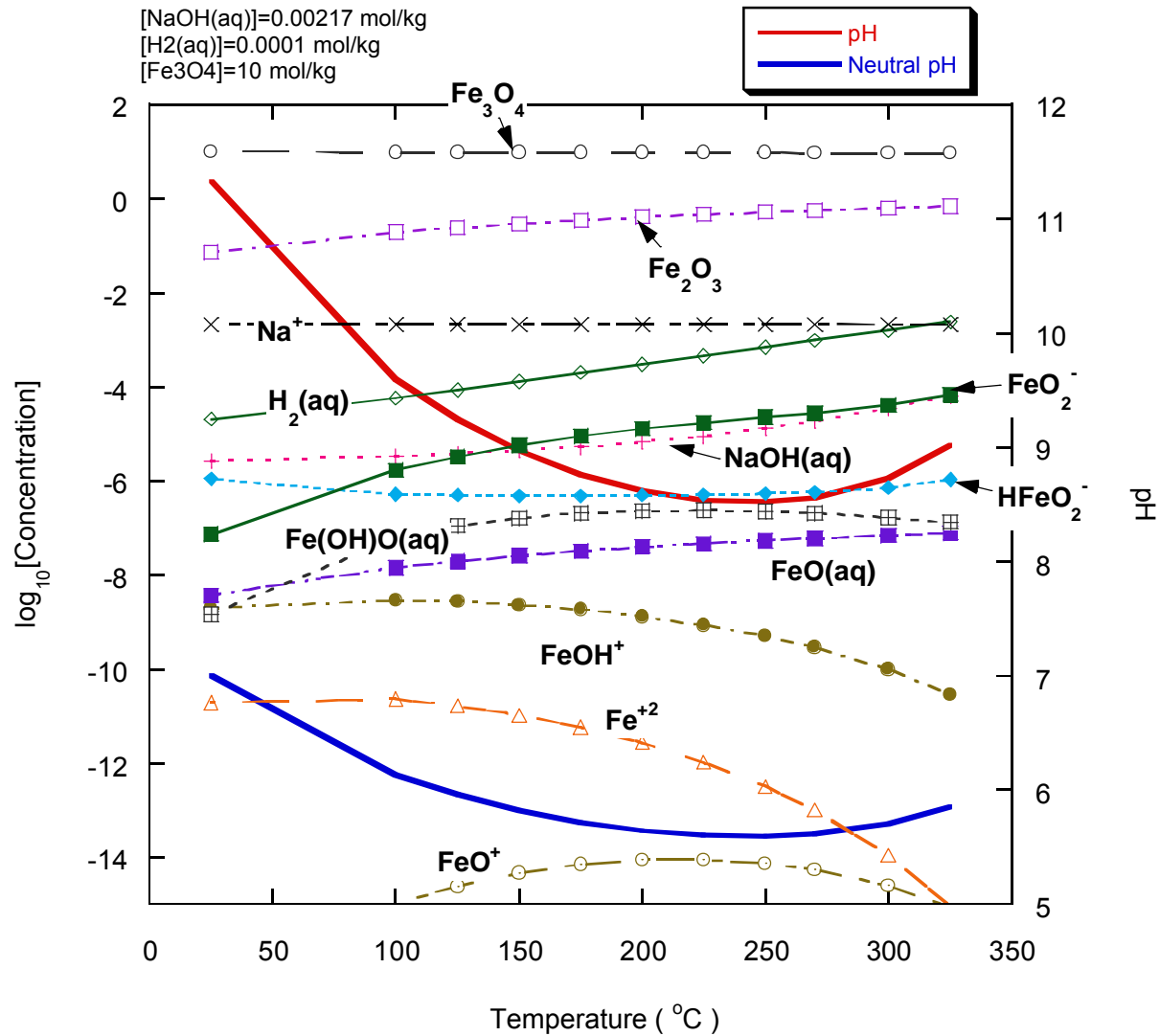
Results
Specific Time to Analyze Crevice Chemistry
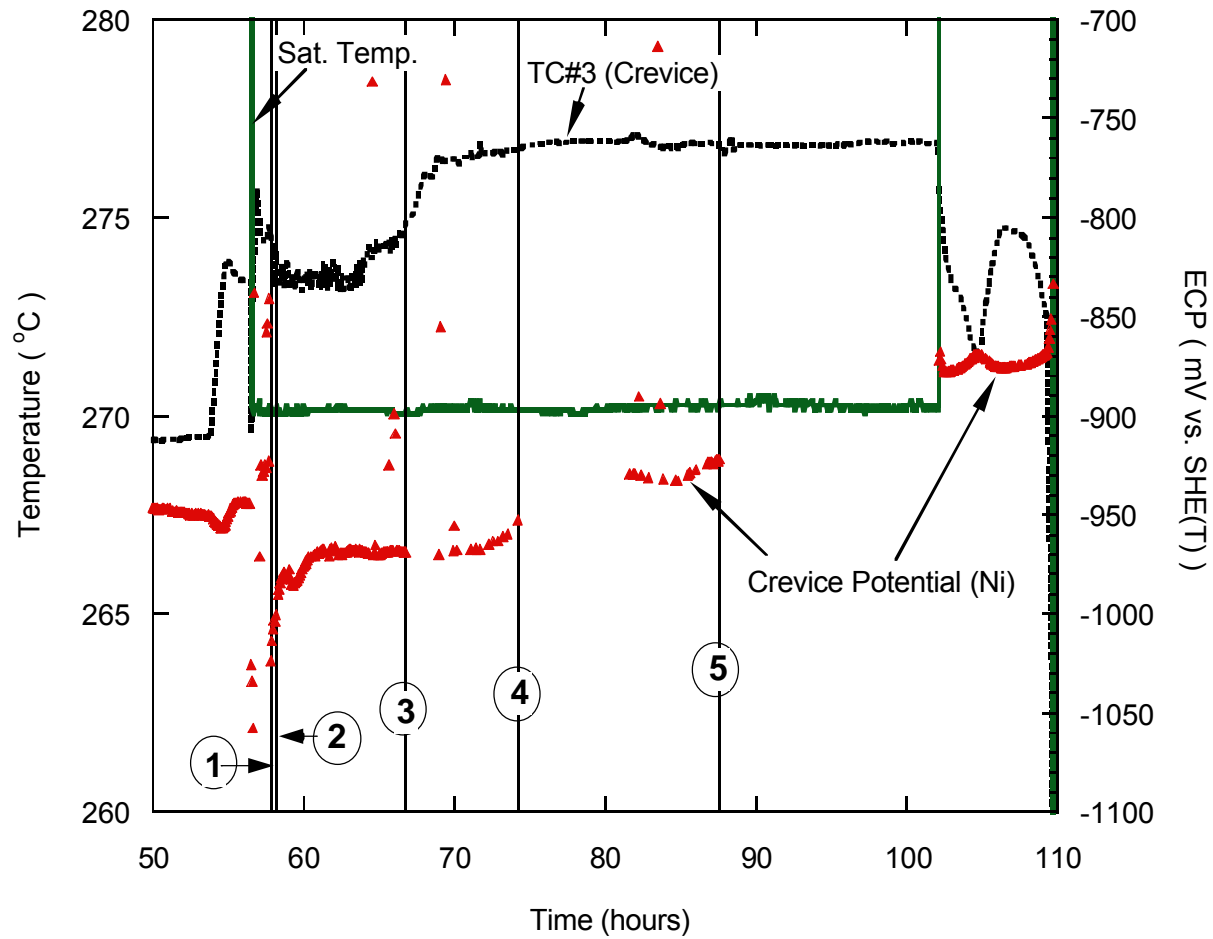
Results
pH & [H_2(aq)] Variation
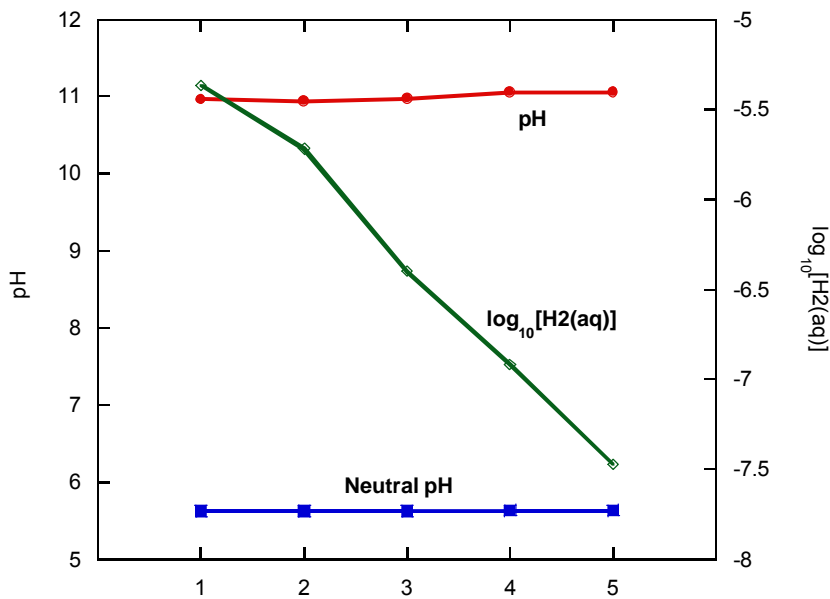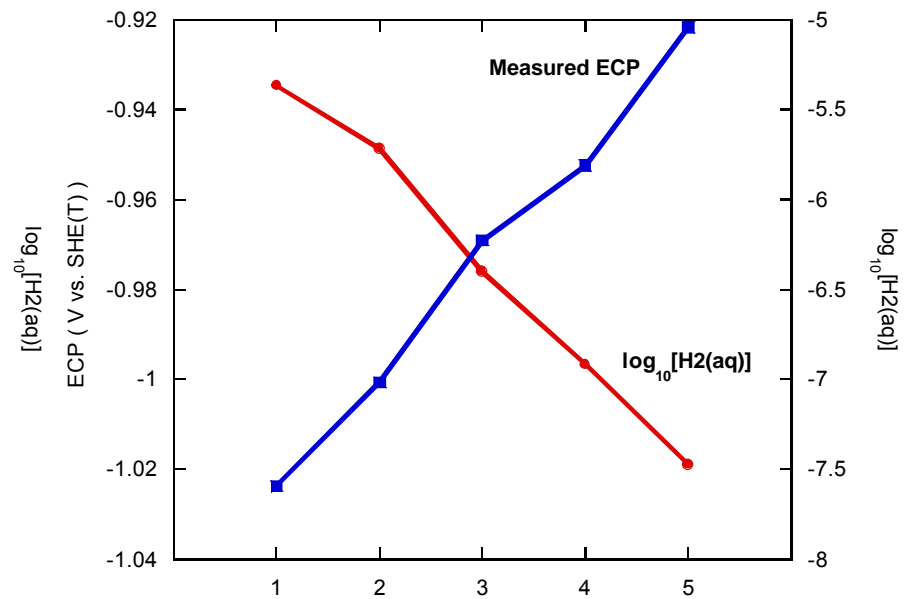
Results
Chemical Speciation
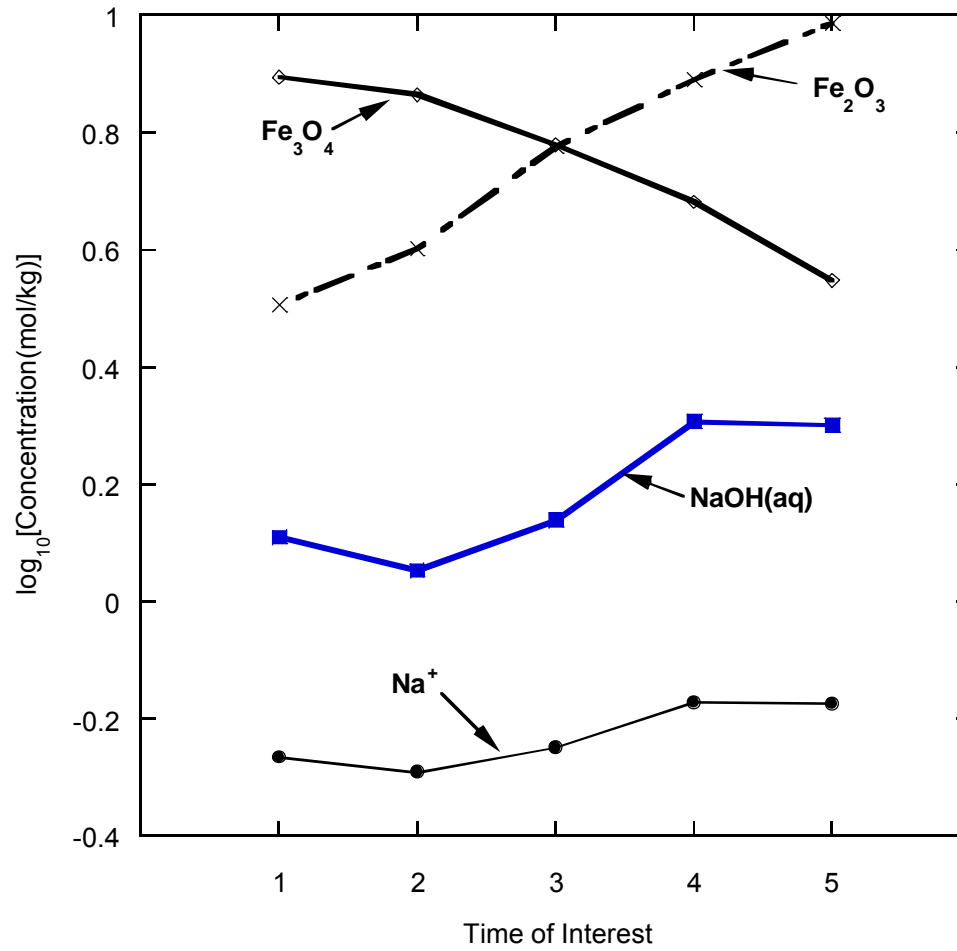
Results
Chemical Speciation
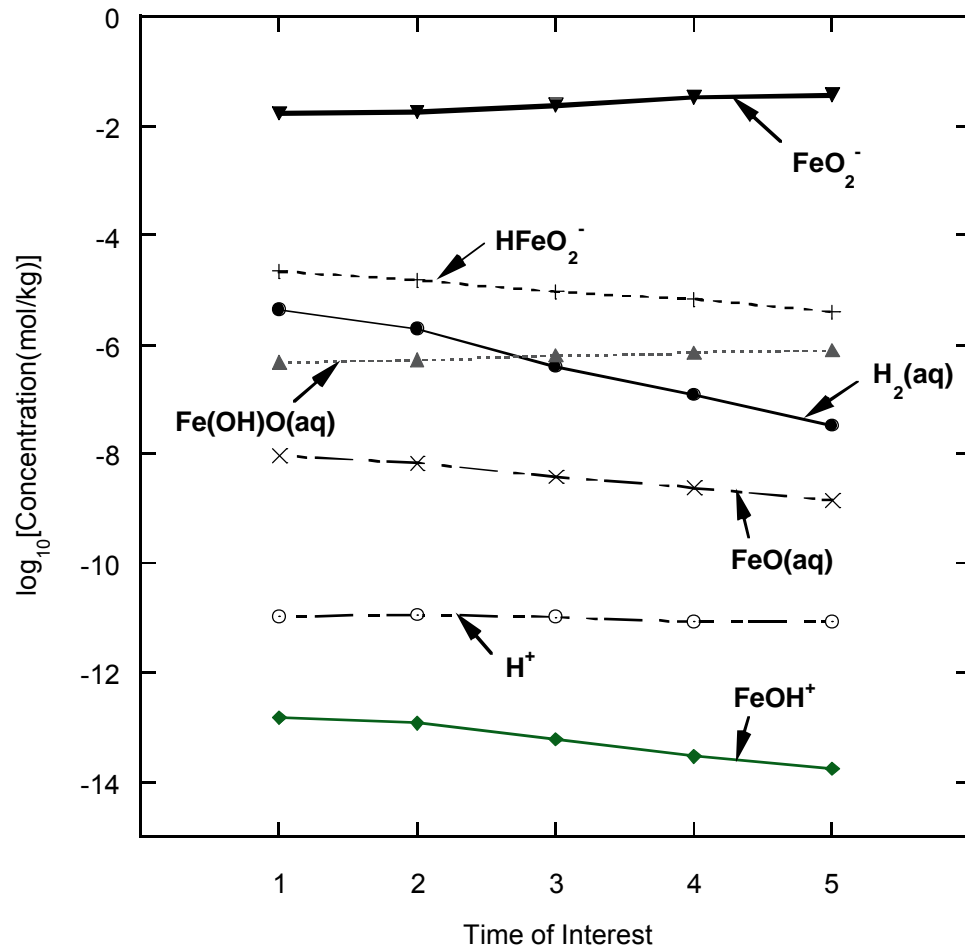
Summary & Conclusions

- Fe-H_2O stability diagrams at high temperature by using HSC Chemistry® 4.0 were constructed.

- To compute the chemical speciation under an equilibrium state in a magnetite-packed crevice environment, the "tableau" method was adopted.

- Based on the experimental results, pH, [H_2(aq)], and concentration of various species were calculated. The increase in ECP during the packed crevice test is rationalized by the decrease of dissolved hydrogen concentration by boiling process.

- Caustic crevice chemistry was developed by concentration of NaOH and it led to the dissolution of Fe_3O_4. Dominant aqueous species of iron was FeO_2^-.

- At the condition of low dissolved hydrogen, caused by crevice boiling, magnetite was transformed to hematite(Fe_2O_3) in equilibrium state.

Future Work

- Systematic consideration of the effect of volatile species, such as $H_2(aq)$ or $HCl(aq)$

- Predicting chemical distribution in a given crevice as a function of time by introducing convection and diffusion effects

The Conditions Known to Produce Crevice Corrosion by the *IR* Mechanism and Those Yet to be Investigated

H. W. Pickering
Department of Materials Science and Engineering
The Pennsylvania State University
University Park, PA 16802

ABSTRACT

Some principles of current distribution in cracks for polarization in the Tafel region that were developed in the middle of the last century by Carl Wagner are a basis for understanding crevice corrosion. Many characteristic features of crevice corrosion were also discovered at roughly the same time. The so-called *IR* mechanism of crevice corrosion that was proposed in 1985 for metals with their outer surface in the passive state is based on these principles and known characteristics. Subsequent experimentation and modeling have so far been successful in testing its applicability for describing the two broad classifications of crevice corrosion: crevice corrosion that occurs immediately and the delayed form that occurs after an induction period. Its operation in intergranular corrosion and other forms of corrosion are discussed.

INTRODUCTION

An explanation of the role of *IR* voltage and the $IR > \Delta\phi^*$ criterion of the so-called *IR* mechanism of localized corrosion, where I is the ionic current within, R is the resistance of, and $\Delta\phi^*$ is defined below in terms of the polarization curve, starts with the principles of current distribution within recesses. These principles are well known but do not appear in most corrosion books. This paper traces the development of the $IR > \Delta\phi^*$ criterion, and examines a few of its less obvious consequences. An example of the latter is that crevice corrosion is more likely to occur when the anodic and cathodic reactions are well separated. The corresponding large corrosion circuits give large R values and hence large *IR* voltages. Similarly, if the oxidant availability increases at the outer surface, e.g., due to stirring, I increases. When $IR > \Delta\phi^*$, crevice corrosion commences.

CURRENT DISTRIBUTION IN RECESSES

Tafel Region

In 1961 Carl Wagner (1) calculated the current distribution for electrodeposition on the walls of recesses in the surfaces of cathodes. The E_x profile ranged from its value at the outer surface, $E_{x=0}$, to more and more positive values as distance, x, increased into

the recess (1, 2). Thus, a part of the cathodic polarization curve existed on the cavity's walls during the plating process. Garmon and Leidheiser (3) experimentally measured the decreasing deposit thickness with increasing x under conditions of low concentration polarization and found good agreement with that predicted by the Wagner (Laplace equation) model (1). Modeling by Ateya and Pickering (4) of the HER on a crack wall, taking into account the composition gradients using the general flux equations, showed similar trends in E_x and i_x that are schematically illustrated in the cathodic curve in Fig. 1.

Wagner (5) similarly modeled metal dissolution in recesses. The rate, i_x, again decreases but E_x becomes more negative, rather than positive, with increasing distance x into the cavity for $E_{x=0}$ in the Tafel region as shown in Fig. 1 and by (1, 4)

$$E_x = E_{x=0} - IR_x \qquad (1)$$

where I is defined as positive when flowing in the $-x$ direction as during anodic

(a)

(b)
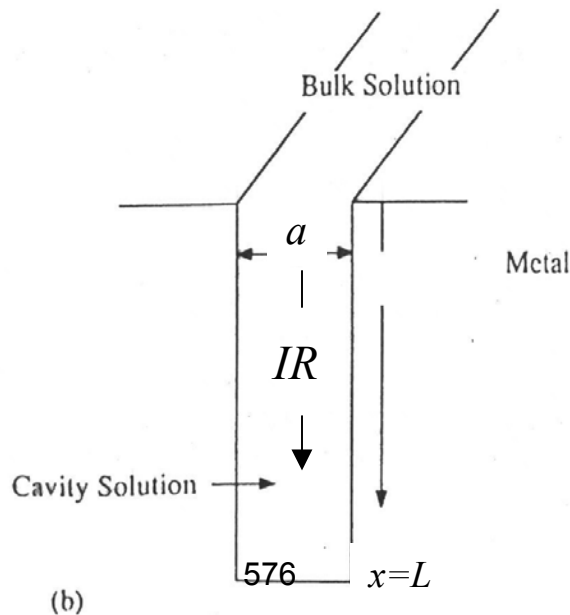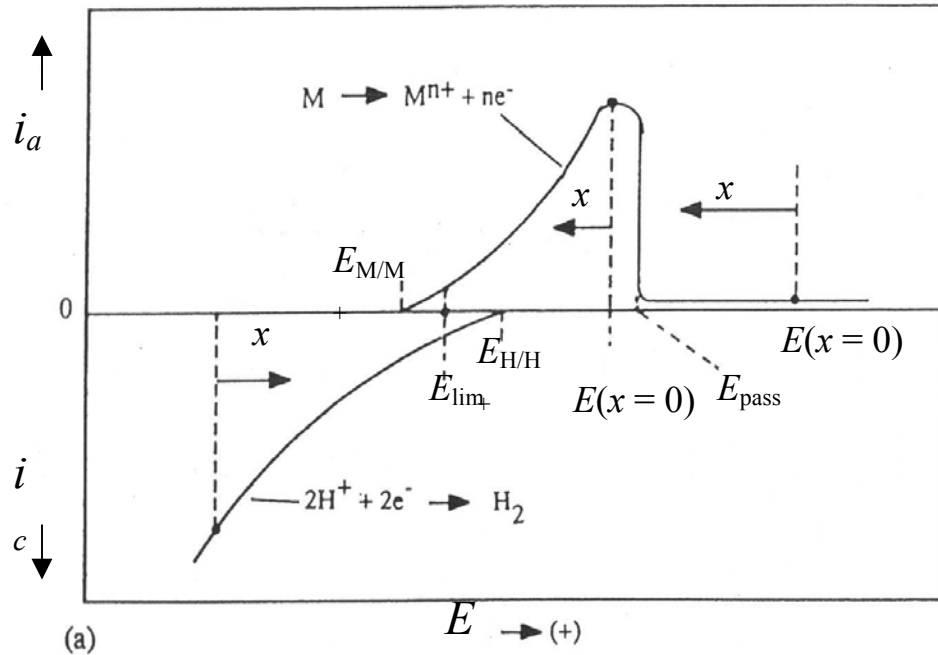
polarization, and $IR_x = \phi_x$ with $\phi_x = 0$ at $x = 0$. Thus, with a surplus of oxidant at the outer surface or using a power supply, the shape evolution of the corrosive attack on the crevice wall largely reflects this decreasing i_x with increasing distance, x, into the crevice. With $E_{x=0}$ in the active region, the highest rate of metal dissolution occurs at the x = 0 (opening) location on the wall and on the unprotected outer surface, and the E_x profile inside the crevice is given by Eq. 1. In practice, if the outer surface is painted or otherwise protected, only the crevice wall shows corrosive attack upon contact with the electrolyte. In such cases all of the crevice wall undergoes active metal dissolution, in contrast to polarization into the passive region (see below) where the *IR* mechanism explains how a part of the crevice wall nearer the opening at $x = 0$ can be in the passive state while the rest of the wall is in the active state. In both cases, the i_x distribution on the crevice wall can include an increasing HER rate with increasing x between E_{rev} of the HER and the E_{lim} value defined elsewhere (6, 7). In practice, the occurrence of the HER beyond x_{rev} can be recognized by its signature: (H_2) gas evolution from the local cell.

Passive Region

Anodic polarization of the outer surface of the electrode into the passive region gives a more complicated result with respect to the E_x and i_x distributions. The shift of E_x in the negative direction again occurs in accord with a net ionic current, I, flowing out of the crevice during anodic polarization, Eq. 1. However, initially upon polarizing from the open circuit potential, E_{oc}, in the active region into the passive region, the active current decreases to the low passive value on the outer surface and either on the entire crevice wall or only on a part of the wall closer to its opening. In the latter case the rest of the wall remains active with E_x in the active region of the polarization curve. Herbsleb and Engell (8) interpreted their measured E_x profiles inside pits as being in the active region, noting that their result was as U. F. Franck had proposed. Many investigators of that period also measured *IR* voltages of up to 10^3 mV between the inside and outside of pits and crevices (9-12). This polarization situation is also illustrated in Fig. 1 with $E_{x=0}$ in the passive region, and is presented in more detail elsewhere (13).

Fig. 1. Schematic representation of the cathodic and anodic polarization curves and their distributions on the cavity's walls (13).

Similar (Laplace) modeling for anodic polarization into the passive region by Xu and Pickering (14, 15) revealed the factors which decide between the two possibilities: passivity of all the electrode's surfaces including the walls of the cavity vs. immediate, sustained high rates of metal dissolution on the deeper part of the cavity's walls. These factors are: (i) the opening, *a*, and depth, *L*, dimensions of the cavity, (ii) applied, E_{app} (= $E_{x=0}$), potential in the passive region, (iii) the resistivity of the electrolyte, and (iv) the bulk solution's anodic polarization curve. For given factors (ii) to (iv), the onset of immediate crevice corrosion vs. no corrosion (passive wall) was shown to depend only on the aspect ratio, AR, of the crevice (14-16). The model predicts that if AR is larger than the critical aspect ratio, AR_c, crevice corrosion will occur immediately when the sample's outer surface is polarized from its E_{oc} value in the active region to a value, $E_{x=0}$, in the passive region. These modeling results are discussed more completely in later reviews (13, 17, 18). The predicted AR_c value was tested and found to be in good agreement with the experimentally determined value using two different metal/electrolyte systems, iron in acetate buffer (15) and nickel in acidic sulfate solution (16). In order to compare the model and experimental results at times beyond the immediate start of crevice corrosion,

577

experimental techniques were used which minimized changes in the composition of the crevice electrolyte so that factors (iii) and (iv) did not change appreciably during continuation of the crevice corrosion process. A similar, updated modeling of the E_x and i_x distributions and the AR_c value will soon be available (19).

Eq. 1 was adopted by Pickering and Frankenthal (9) to explain their measured E_x profiles in pits and crevices in iron during localized corrosion, and by Ateya and Pickering (4) for describing cathodic polarization inside cracks. Others of that period, although not referring to Eq. 1, attributed their measured less noble E_x values in pits and crevices during localized corrosion in titanium (12) and iron (8, 10) to *IR* voltage and salt films, respectively. Membranes covering (20, 21) and gas bubbles at the opening (22) or at the bottom (9) of pits were also suggested to account for the more negative E_x values.

In the sixties and seventies there were several reports of gas bubbles rising out of pits and crevices during localized corrosion (9, 23-28). The escaping gas was collected and analyzed during pitting in iron, titanium and aluminum and found to be hydrogen by Pickering and Frankenthal (9), Beck (27), and Bargeron and Benson (28), respectively. Other gases have also been detected emanating from pits (25, 28-30), such as CH_4, H_2S, N_2 and NO in the case of aluminum, which has been interpreted in terms of a reaction between the anion and the aluminum surface (28).

Pickering and Frankenthal (9) discovered that pit interiors were actually occupied by the gas and that the small hydrogen bubbles seen rising out of pits were fragments of this reservoir of gas. In more recent studies at Penn State, where the wall of the crevice and the tip of the Luggin capillary of the potential microprobe could be observed in-situ during the experiment, the gas bubbles which adhered to the walls of the crevice were found and to form and grow on the deeper part of the wall where the E_x value was in the region of the HER (31, 32). This observation, coupled with the earlier analysis of the collected gas bubbles as H_2 (9), provided a strong indication that the source of the gas was the HER and not escaping hydrogen that had previously entered the metal. This observation was also a strong independent confirmation of the potential microprobe measurement of the magnitude of the E_x profile. Gas was also demonstrated to fill crevices in iron during cathodic polarization (4, 33). These in-place gas reservoirs represent a significant resistance to current flow, i.e., *R* is large, since the electrolyte path is reduced in cross section to the very thin layer of electrolyte between the gas reservoir and the wall of the cavity (9). Thus, in the case of open pits in iron with the sample polarized well into the passive region, the metal dissolution current density on the pit wall, even though reduced by the bubble to below that given by the bulk solution polarization curve (9, 16, 34), can produce a very large *IR* voltage (> 1 volt was measured), whereas the calculated *IR* voltage along the *x* direction of the open pit in the absence of the gas is very much smaller (9). Formation of the H_2 bubble required that the E_x value was at least momentarily less noble than the reversible potential of the HER, e.g., as a result of an initial current spike at the moment of passive film breakdown (9).

Solid corrosion products (35), e.g., salt films, that have been suggested to form in the crevice or pit (8, 10) or as covering films (20, 21), can also produce larger *IR* voltages than would be possible in their absence for the dimensions of the cavity, in this respect having the same role as the gas reservoirs. In open pits or open crevices, gas reservoirs or other constrictions, would seemingly be required for arriving at sufficiently large *IR*

voltages. However, constrictions are not always required. Under weak oxidizing conditions the *IR* need not be large to place the bottom of the local cell in the active region (9). Also, crevices typically have very small opening dimensions, e.g., the small space between a metal washer and bolt assembly or at the interface of an organic coating whose bonding has been compromised, where the *IR* is large because *R* is large (35).

Extending the theory of mixed potentials established by Wagner and Traud (36) to local cells, one concludes that the occurrence of the HER, as well as other cathodic reactions, at the anodic sites within the crevice, leads to a reduction of the ionic current, *I*, that can flow out of the cavity. Hence, the magnitude of the *IR* voltage is also reduced, in the limit to zero in which case localized corrosion by the *IR* mechanism is not possible (6, 37). A reduction in *R* gives the same result. Thus, separation of the anodic and at least some of the cathodic reactions is necessary for the occurrence of crevice corrosion by the *IR* mechanism, as shown below in experiments where stable crevice corrosion was suddenly terminated by adding oxidant to the crevice electrolyte (37).

That the walls of pits and crevices were in the active state in those early papers on localized corrosion was indicated by various results, including the measured E_x values at the bottom of pits and crevices (8-10, 12). Herbsleb and Engell (8, 38) found that the pit walls in iron contained sulfate films just as form in the active region of its polarization curve. Others have shown facets on the walls of pits and crevices that are characteristic of the Tafel region of the anodic polarization curves of metals, e.g., in pits in nickel (39) and iron (40), and more recently in crevices in nickel (41).

At about the same time in the anodic protection industry, similar reasoning was advanced by Edeleanu and Gibson (42) and others (43, 44). These investigators analyzed the potential distribution and distance at which the passive-to-active transition occurred along a wire which was in a tube and polarized into the passive region at its one end (42). They found that passivity broke down and the protection system failed at the other end of the wire. They concluded that a possible cause was a shift of the local electrode potential into the active peak region of the polarization curve.

FORMALIZING THE *IR* VOLTAGE CONCEPT

IR > Δϕ* for the Immediate Onset of Crevice Corrosion

Using the understanding illustrated in Fig. 2 which was first presented at the NACE annual meeting in 1985 and published the next year (7), a formalism was proposed for susceptibility to localized corrosion (45, 46),

$$IR > \Delta\phi^* \tag{2}$$

$\Delta\phi^*$ is the difference between $E_{x=0}$ and E_{pass} ($E_{A/P}$ in (a) of Fig. 2), and has the magnitude given by the polarization curve existing in the cavity at the start of crevice corrosion, which is the bulk solution curve in the case of immediate crevice corrosion. The Xu-Pickering model (14, 15) correctly predicted that when the crevice's aspect ratio, *AR*, was greater than the critical aspect ratio, AR_c, Eq. 2 was met immediately (15, 16). The model also revealed that when AR > AR_c the initial location of the corrosive attack and of the

passive/active boundary, x_{pass}, on the crevice wall was at smaller x values for smaller a values, in agreement with field observations (7, 47).

$IR > \Delta\phi^*$ for Ending the Induction Period

In the case of delayed crevice corrosion, Pickering (7, 45, 46) suggested that the induction period would end and crevice corrosion would start when $IR > \Delta\phi^*$ (i.e., $IR < \Delta\phi^*$ switched to $IR > \Delta\phi^*$), e.g., when an active peak grew larger as from acidification of the crevice electrolyte or increase in temperature thereby decreasing $\Delta\phi^*$ (sketch e in Fig. 2); the passive current increases (sketch d), increasing I; or constrictions form, increasing R. Then, crevice corrosion would begin at the bottom of the crevice where $IR > \Delta\phi^*$.
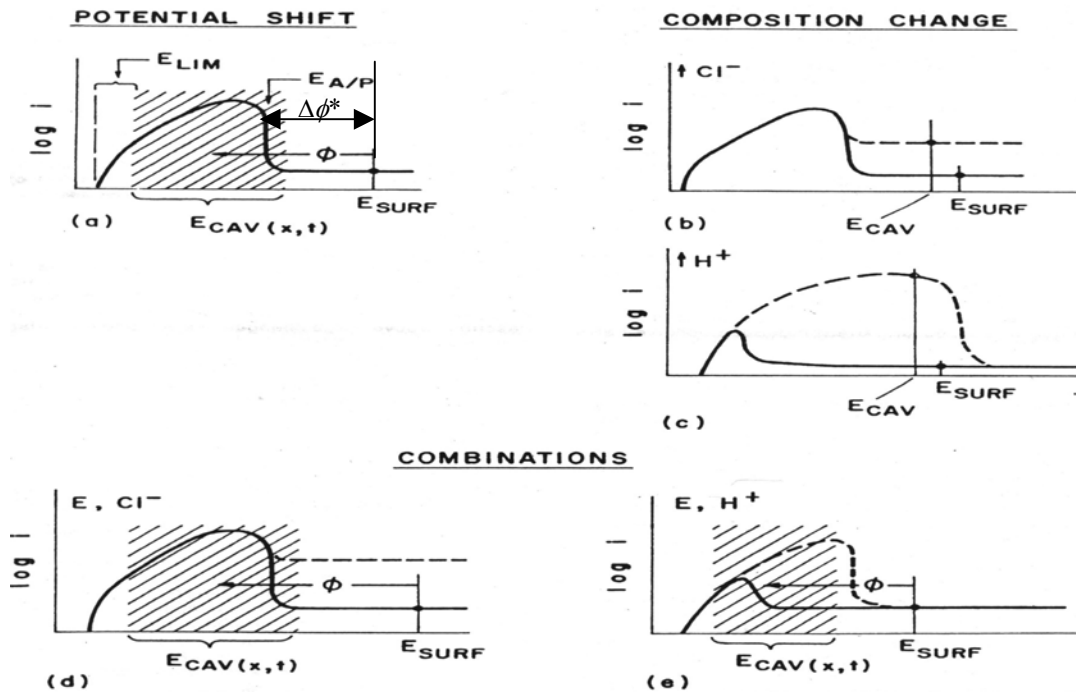

Fig. 2. Schematic representation of the IR voltage form of crevice corrosion for the two classifications: immediate onset of crevice corrosion (a), and the delayed form which requires certain changes in the polarization curve, e.g., due to a change in temperature or composition of the crevice electrolyte (d and e). Also shown is the critical solution composition mechanism where no consideration is given to the E_x distribution on the crevice wall (b and c) (7). An example of $\Delta\phi^*$ is shown in (a).

There are numerous studies in the literature where this criterion could have operated, i.e., the induction period ended and crevice corrosion started at the bottom of the crevice when the inequality in Eq. 2 was met. Some authors recognized this possibility to some extent. A recent example is the study of stainless steel in dilute NaCl solution by Brossia and Kelly (48). Although, as in most other past studies of localized corrosion it was not possible to measure E_x during the induction period, let alone the pH or chloride ion gradients, these authors reported that the corroded crevice wall was in the active state. These kinds of data (e.g., E_x as in Fig. 7 below) are needed to document whether the IR mechanism is or is not operating. Thus, many past localized corrosion

studies need to be re-examined, even though the authors may have concluded, without the benefit of such documentation, that the *IR* mechanism was not operating in their study.

PROOF-OF-CONCEPT EXPERIMENTS

Immediate Crevice Corrosion

A mechanism controversy developed some 15 years ago when Valdes (31, 49, 50) and then others (14-16, 51, 52) at Penn State presented data for crevice corrosion using a novel experimental design (31, 34, 49) and orientation (16). Prior to this time the *IR* voltage was either considered negligibly small or a quantity that developed after stabilization of the local cell process by the then generally accepted, solution-composition-change mechanism. The strategy of the Penn State experiments was to either hold the pH constant in the crevice electrolyte (31, 49, 50) or to maintain good mixing of the crevice and bulk electrolytes (16), and then measure the E_x distribution inside the crevice as crevice corrosion started and stabilized. A fine Luggin capillary mounted on a 3-dimensional, translational stage and connected to a reference electrode was used to measure the E_x distribution. In this way if crevice corrosion occurred, it would show that the *IR* voltage was the key variable for the stabilization of crevice corrosion. In addition, if crevice corrosion occurred immediately, this in itself would preclude the operation of the solution-change mechanism. The occurrence of crevice corrosion was indicated by a measured current in the mA range and by visual observation through a transparent medium constituting another wall of the crevice. Crevice corrosion was found to occur immediately and only on that part of the crevice wall that was in the active peak region of the polarization curve (15, 16, 31, 32, 34, 37, 41, 49-54). These results were a powerful statement for the operation of the *IR* mechanism in crevice corrosion. When coupled with the above mentioned computational model results, they went a long ways towards resolving the controversy between the *IR* mechanism and the change-in-solution-composition mechanism for crevice corrosion, in favor of the former.

Typical results of these investigations for spontaneously active systems with crevices whose aspect ratio was larger than the critical value are shown in Fig. 3 to 5 for a stainless steel (34). Similar results were obtained for iron (15, 16, 31, 41, 45, 46, 49-52), steel (53), and nickel (16, 41, 54). The results were clear in showing that crevice corrosion was initiated and stabilized by the above-mentioned *IR* mechanism. Firstly, the measured current was immediately in the mA range. Secondly, the corrosive attack on the crevice wall matched the E_x region of the bulk solution polarization curve. This was determined by the in-situ microprobe measurements of E_x during crevice corrosion, Fig. 3. Thirdly, the in-situ measured E_{pass} value, at the visually observable (through a transparent wall of the crevice) x_{pass} location on the crevice wall, was the same as the E_{pass} value of the 2M H_2SO_4 + 2M HCl + 1M NaCl bulk solution, i.e., was within the potential region of the passive-to-active transition of the bulk solution polarization curve. The equality of these two E_{pass} values for the duration of the crevice corrosion process indicted that there was no significant change in the polarization curve of the crevice solution from the bulk solution curve. This conclusion was supported by the in-situ measured pH value of the crevice solution and of the bulk solution (both were less than pH 0 for this system). The common features in the results for iron, steel, nickel and

stainless steel mentioned above and illustrated in Figures 3 to 5 are that all of the tested metal/electrolyte systems were spontaneously active systems and all of the crevices initially had aspect ratios, AR, that were larger than their respective critical aspect ratios, AR_c. These are, in fact, the requirements for the immediate onset of crevice corrosion by the *IR* mechanism (14-18).

Termination/Reinitiation of Crevice Corrosion.

In principle, a decrease in *I* or *R* and/or an increase in $\Delta\phi^*$ could invert Eq. 2, causing immediate termination of crevice corrosion. In recent experiments oxygen saturated bulk solution was added to the crevice electrolyte, effectively moving the cathodic reaction close to the anodic sites on the crevice wall. This caused $E_{x=L}$ and *I* to abruptly and simultaneously rise to near the outer surface, $E_{x=0}$ value and decrease to the passive value, respectively, terminating the crevice corrosion process, Fig. 6. Sudden reinitiation of crevice corrosion on the passive wall by change of the composition of the crevice solution, e.g., increasing the chloride ion concentration (increasing i_{pass}), was also experimentally demonstrated (37).
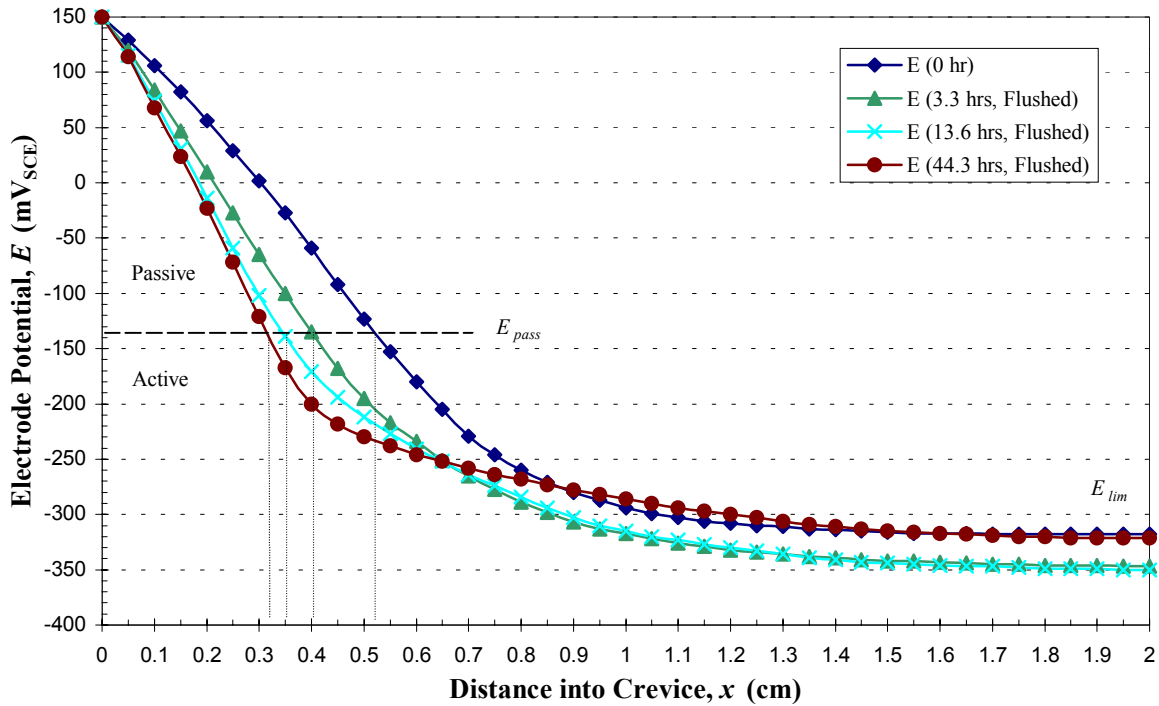
Fig. 3. In-situ microprobe measurements of E_x during crevice corrosion of T-2205 duplex stainless steel in strongly acidic chloride solution showing that E_x has shifted over 300 mV in the negative direction into the active peak region of its polarization curve, thereby stabilizing the crevice corrosion process (34).

$x=0$

x_e

x_{pass}

x_{lim}

5 mm

$x = L$

Fig. 4. The crevice wall of the sample in Fig.3 showing the corrosive attack below the x_{pass} boundary. This photograph was recorded in-situ at 14 hours (x_{pass} = 0.34 cm) (34).

$x = 0$

x_{pass}

$x = L$

5 mm

Fig. 5. Cross-sectional photograph after completion of the experiment in Fig. 3 showing the corrosive attack below the x_{pass} location on the crevice wall (34)

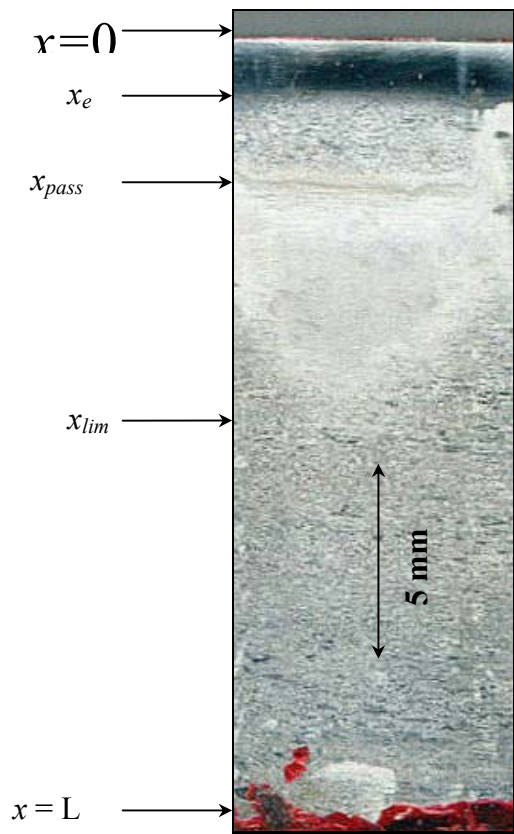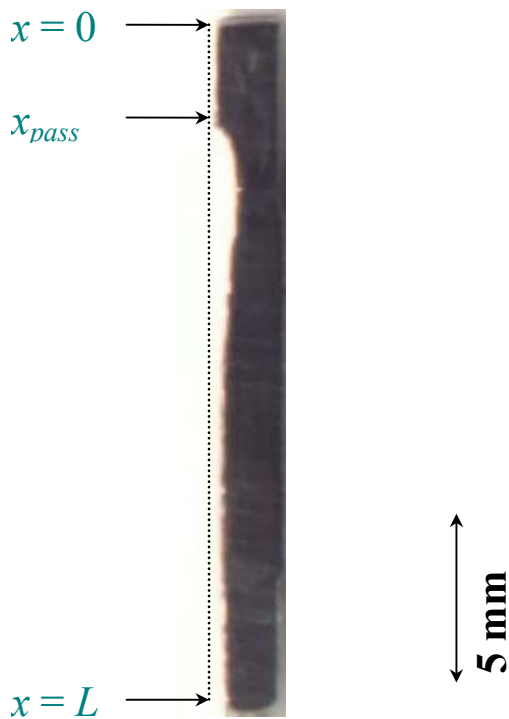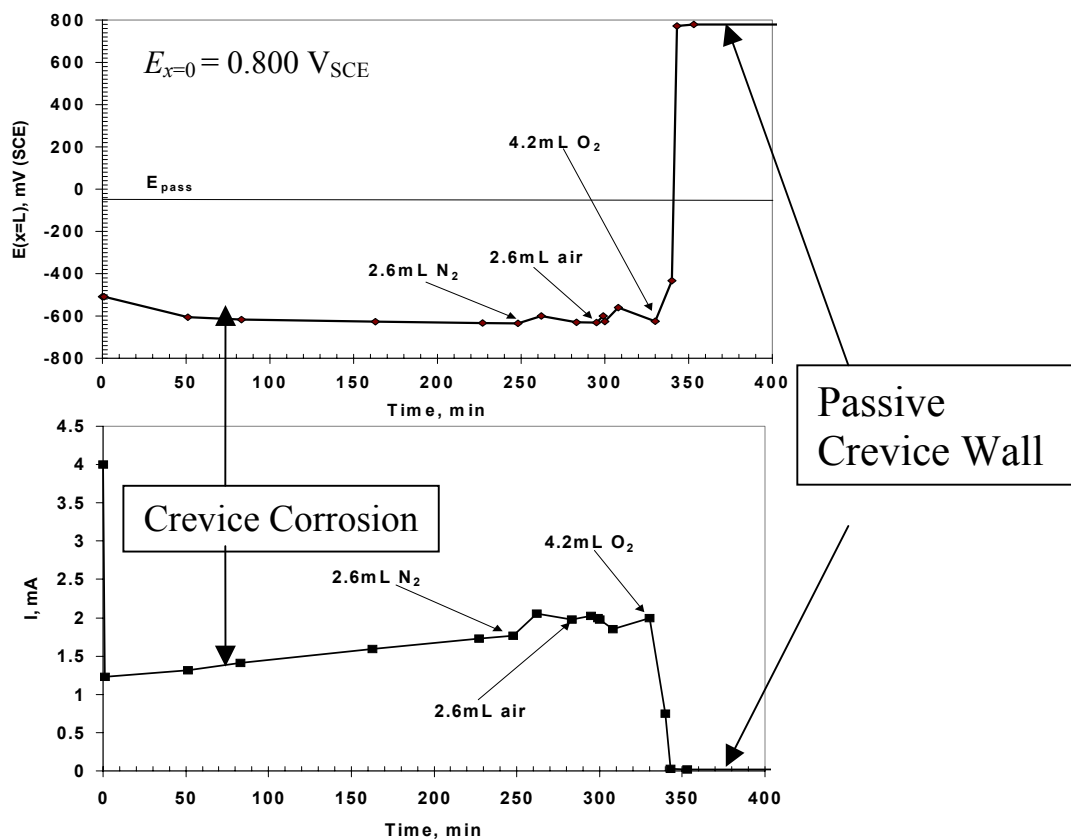Fig. 6. Upon adding O_2 to the crevice electrolyte at 328 min., termination of crevice corrosion occurred, as indicated by the steep (a) ascent of $E_{x=L}$ = -600 mV$_{SCE}$ from the active region to near the outer surface $E_{x=0}$ = 800 mV$_{SCE}$ value in the passive region and (b) decrease of the mA ionic current, I, to that for the passive current. Fe/0.5 M Na$_2$SO$_4$ - 0.1 mM NaCl. See source for other details (37).

Delayed Crevice Corrosion

If initially the condition in Eq.2 (or AR > AR$_c$) is not met resulting in passivation of the entire crevice wall, there are the above-mentioned changes in the system that could occur during an induction period that would allow this condition eventually to be met (7, 14-16, 45, 46). The moment $IR < \Delta\phi^*$ switches to $IR > \Delta\phi^*$ (or AR < AR$_c$ switches to AR > AR$_c$) the induction period would end and crevice corrosion would commence. These changes include one or more of the following (14-16): (i) the corrosion, E_{corr}, or applied potential, E_{app}, becomes less noble ($\Delta\phi^*$ decreases), (ii) the composition of the stagnant crevice electrolyte changes in such a way that it tends to increase the size of the active peak ($\Delta\phi^*$ decreases), passive current increases (I increases) and/or solution resistivity increases (R increases), and/or (iii) there is a decrease in the effective cross sectional area of the electrolyte volume in the crevice due to gaseous or solid corrosion product formation (R increases). All of these variables and respective given directions of change tend to promote the inequality in Eq. 2 and to decrease the value of AR$_c$.

584

The first experimental data that were consistent with this *IR* explanation of the end of the induction period and start of crevice corrosion that is illustrated in Fig. 2, were obtained over a decade ago and are shown in Fig. 7 (52). A fine Luggin capillary microprobe was used to measure the electrode potential half way into the crevice as a function of time during the induction period. Fig. 7 shows that the electrode potential inside the crevice abruptly shifted in the less noble direction by over one volt just as the induction period was ending and crevice corrosion was starting at approximately 13.5 hours for this iron sample in buffered alkaline (pH 10) solution. The start of crevice corrosion was shown by the simultaneous increase in the measured current at 13.5 hours in Fig. 7. These data indicate that the *IR* voltage framework of crevice corrosion illustrated in Fig. 2 was the explanation of the end of the induction period and start of crevice corrosion. Close examination of Fig. 7 shows *I* increasing and *E* decreasing slightly with time from the start of the induction period, in accord with Eq. 1. This slight increase in *I* over most of the induction period represents a gradual increase in i_{pass}, as illustrated in sketch (d) of Fig. 2. It is also conceivable that in this experiment the active peak was increasing in size during the induction period as the buffer became less effective inside the crevice, sketch (e), thereby decreasing $\Delta\phi^*$. The latter could have been resolved at the time by in-situ pH measurements of the crevice electrolyte during the induction period. Thus, the increase in *I* and any decrease in $\Delta\phi^*$ seemingly led to the end of the induction period and start of crevice corrosion at 14 hours when $IR < \Delta\phi^*$ switched to $IR > \Delta\phi^*$. This framework of crevice corrosion has also been used by Shaw, et. al. (55), and considered by Lillard, et. al. (56, 57), for describing the end of the induction period and onset of localized corrosion in alloy 625, a corrosion resistant commercial nickel base alloy. DeJong and Kelly (58) have presented evidence of its operation in nickel.

Recent experiments of the type in Fig. 7 for a spontaneously passive system included the in-situ measurement of the pH (59). This unbuffered system was found to change to a spontaneously active system through formation and growth of an active peak as the pH decreased from its initial pH 9 value. At the end of the 7 minute induction period and start of crevice corrosion, the measured pH inside the crevice was pH 4. At this time the electrode potential at the bottom of the crevice, $E_{x=L}$, decreased and *I* increased steeply in the simultaneous manner already shown in Fig. 7 (59).

OTHER CORROSION FORMS SUBJECT TO THE $IR > \Delta\phi^*$ CRITERION

Pit Initiation

Early discussions of *IR*-induced pit initiation focused on how the system could provide the necessarily large *IR* voltage when the pit was early in its growth or, indeed, at its very inception. The results described in the early Pickering-Frankenthal papers (9, 40, 60) led these authors to suggest a mechanism of pit nucleation which was based on the *IR* voltage and bubble formation within the pit electrolyte: When local breakdown of the passive film occurs, the initial current spike due to metal dissolution, though quickly subsiding as polarization occurs, could momentarily produce a large *IR* voltage (9). Its momentary presence within the small cavity in the passive film and into the incipient pit, could produce an $E_{x=L}$ value at the pit bottom that would promote H_2 gas formation and
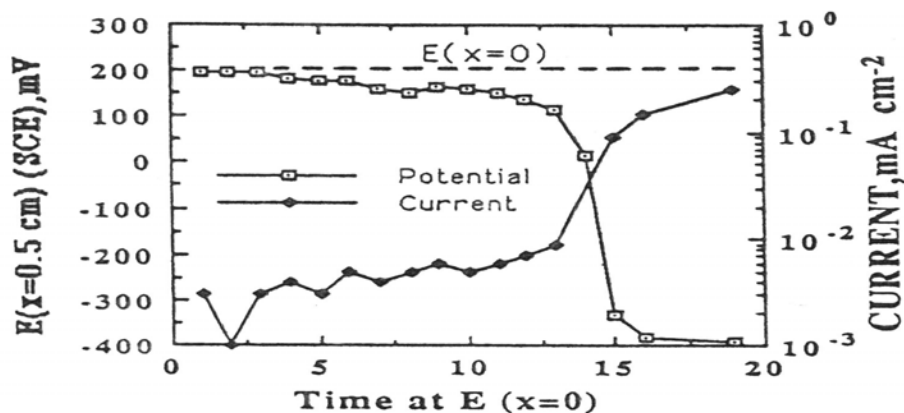
Fig. 7. E_x and I data showing the onset of crevice corrosion after a 14 hour induction period. The large IR voltage shown by the several hundred mV shift of E_x at the end of the induction period and simultaneous start of crevice corrosion indicates operation of the IR voltage form of crevice corrosion (52).

its inclusion within the pit, thereby stabilizing the large IR voltage and the pitting process itself. Later, it was proposed that a repetitive process of pit initiation and repassivation at the same incipient (metastable) pit sites could eventually produce a cavity shape with a large enough aspect ratio so as to exceed the system's critical aspect ratio, AR_c (15). These first and second generation proposals are based on the IR mechanism, the latter of which incorporates metastable pits which eventually become stable pits.

Lace-Like Pattern During Pit Growth

Pit growth often continues until the pit consumes all of the metal in its growth direction. Sometimes the growth also occurs backwards towards the surface on which the pit originated. Upon penetrating the original surface the metal around the new hole passivates, and the process repeats eventually forming a lace-like pattern of holes around the original pit opening (9). Streicher (61) and others (40, 62) had already shown a similar pattern of small pit-like holes around the original, usually larger pit opening. Frankenthal and Pickering (40) observed that the original pit opening at the center of the pattern usually formed at an inclusion in their austenitic stainless steel samples, and that . the outer circle of the concentrically growing holes represented the extent of growth of a single large pit underneath the lace-like cover. They proposed that the steep E_x profiles found for their open (uncovered) pits in iron (9) also existed in these covered pits, while also invoking the enhancement of chloride ion accumulation for these covered pits (40). In a series of SEM stereo-micrographs they found that the outer surface between the holes of the lace-like cover remained smooth (from the original metallographic polish of the surface), whereas the underneath surface of the lace-like cover was rough. Similar observations were made by Streicher (61) and Rosenfeld and Danilow (62). Hence, it was concluded that the pattern formed by dissolution and breakthrough of the surface was caused by active metal dissolution from inside the growing large pit that supported the lace-like cover (40). Later, researchers at Penn State elaborated on this IR mechanism for the lace-like pattern based on its appearance in iron (15, 31) and nickel (16) samples and their above mentioned proof-of-concept experiments for the IR mechanism.

586

Grain Boundary Corrosion and Cracking (IGSCC)

Bennett and Pickering (63) noticed in their studies of grain boundary corrosion of sensitized austenitic stainless steel that the resulting grain boundary grooves were wider and uneven in width, sometimes by as much as one or two orders of magnitude, than the predicted chromium depleted-zone width. This result was also apparent in micrographs in papers by Briant (64) and Streicher (65). The predicted value of the grain boundary chromium depleted-zone width was based on the chromium depletion theory of grain boundary corrosion discovered by Strauss, et. al., (66) and Bain, et.al., (67) for austenitic stainless steel and by Baumel (68) and others (69, 70) for ferritic stainless steel. Thus, bulk austenitic stainless steel with its normal (>18 %) chromium content was seemingly under going high rates of anodic dissolution, a result not explained by the chromium depletion theory. Bennett and Pickering (63) concluded that a secondary corrosion process occurred that attacked the bulk 18 % Cr austenitic stainless steel while the chromium depleted alloy along the grain boundary was being anodically dissolved via the chromium depletion mechanism.

More recently, Zamanzadeh et. al., (71) concluded the same based on an investigation of a stainless steel tube which failed in acid service from intergranular corrosion and stress corrosion crack (IGSCC) propagation. In a laboratory investigation of this phenomenon in a sensitized ferritic stainless steel, Kelly, et. al., (72) showed that the second intergranular corrosion mechanism was crevice-like in nature. They concluded, based on evidence of a large IR voltage inside the groove and the absence of acidification or chloride ion build up within the corrosive solution inside the grain boundary groove, that the above described $IR > \Delta\phi*$ criterion eventually became operative and caused the significantly increased grain boundary corrosion of the bulk 18 % Cr ferritic stainless steel. Thus, the $IR > \Delta\phi*$ criterion and IR mechanism of localized corrosion became established as a secondary mechanism of intergranular corrosion at the moment the aspect ratio of the grain boundary groove (which increases with time during operation of the chromium depletion mechanism) just exceeded the critical aspect ratio, AR_c, of the system (which typically decreases with time as stagnation (e.g., acidification) of the grain boundary groove occurs) (13). This moment is when the $IR < \Delta\phi*$ condition switches to the $IR > \Delta\phi*$ criterion of Eq. 2 at the base ($x = L$) of the grain boundary groove or tip of an insipient crack initiation event.

The required high tensile stresses for crack initiation could exist at the base of the groove which functions as a stress raiser. This state-of-stress/electrochemistry condition at the base of the grain boundary groove at the moment the $IR > \Delta\phi*$ is met, can be visualized as the trigger for the initiation of a stress corrosion crack (IGSCC) propagation (73).

Porous Sintered Electrodes

Powder metallurgical structures of metal/electrolyte systems exhibiting active/passive behavior can be susceptible to the $IR > \Delta\phi*$ form of localized corrosion. An example is sintered iron in aqueous ammoniacal solution (74, 75). The anodic polarization behavior of sintered iron powder was similar to that of bulk iron in ammoniacal solution, showing active, passive and oxygen evolution regions. A very high current density observed with the outer surface polarized into the passive region for some sintered specimens and sintering conditions, was attributable to active dissolution of the metal pore walls within the pore structure, analogous and equivalent to conditions during crevice corrosion by the $IR > \Delta\phi*$ mechanism. This phenomenon can also be the explanation of the more negative

measured corrosion potential of a powder metallurgy sample than its wrought bulk equivalent composition (76).

CONCLUSIONS

1. Carl Wagner, a half century ago, provided the theoretical foundation for *IR*-induced current and potential distributions in cavities during polarization into the Tafel region. This theory can be directly used to explain crevice corrosion and the shape evolution of the corrosive penetration on the crevice wall of coated metals when the outer surface potential, $E_{x=0}$, is in the active region. An extension of these concepts, supported by mathematical modeling, provide a similar underpinning for the *IR* mechanism of localized corrosion in the case of polarization in the passive region.

2. The *IR* mechanism for polarization into the passive region, defined by the $IR > \Delta\phi^*$ condition, has been established in cases of immediate crevice corrosion. When crevice corrosion occurs immediately it means that the crevice's aspect ratio is initially larger than the critical aspect ratio that applies for the particular metal/electrolyte system, temperature and existing or applied electrode potential at the outer surface, i.e., AR > AR_c initially holds for the bulk, ambient electrolyte and applied $E_{x=0}$ value in the passive region. The value of AR_c can be obtained from the Xu-Pickering model (14, 15) or from experiment.

3. Adding oxidant to the crevice solution, can cause sudden termination of crevice corrosion by inverting the inequality $IR > \Delta\phi^*$ via a decrease in I (or inverting AR > AR_c via an increase in AR_c). These results show the need for separation of the anodic and cathodic reactions, provide an improved understanding of the role of oxygen depletion in the crevice's electrolyte and provide a further proof of the operation of the *IR* mechanism.

4. The in-situ observations of H_2 gas formation confirms the magnitude of the measured E_x profiles and that its source is the HER rather than the escape of hydrogen from the metal.

5. Based on a few results to date, the *IR* mechanism controls the length of the induction period, i.e., both the electrode potential at the bottom of the crevice, $E_{x=L}$, and the ionic current, *I*, flowing out of the crevice simultaneously assumed values characteristic of *IR*-induced crevice corrosion at the end of the induction period. This was furthered supported by the in-situ measured pH at the end of the induction period, which had decreased to pH 4, characteristic of an active peak in the polarization curve in this otherwise spontaneously passive system.

6. The *IR* mechanism has been proposed to account for pit initiation, transition from metastable to stable pitting, pit growth, formation of the lace-like structure, corrosion in the pores of sintered metals, and secondary grain boundary corrosion of sensitized stainless steel based on some corroborating experimental evidence.

The author reports in this review the work of several graduate students and visiting scholars: Albert Valdes, Kyehyun Cho, Eric Nystrom, Maria Sawford, Jamal Al-Khamis, Aboubakr Abdullah, Ryan Wolfe, Tae Youn Won, Ahmed Al-Zahrani, Dr. Yuan Xu, Dr. Badr Ateya, and Dr. Mohammed Abdulsalam.

REFERENCES

1.   C. Wagner, Plating, **48**, 997 (1961).
2.   C. Wagner, J. Electrochem. Soc., **98**, 116 (1951).
3.   L. B. Garmon and J. H. Leidheiser, Plating, **48**, 1003 (1961).
4.   B. G. Ateya and H. W. Pickering, J. Electrochem. Soc., **122**, 1018 (1975).
5.   C. Wagner, J. Electrochem. Soc., **101**, 225 (1954).
6.   H. W. Pickering, in *Corrosion and Corrosion Protection*, R.P. Frankenthal and F. Mansfeld, Editors. 1981, The Electrochemical Society: Pennington, NJ. p. 85.
7.   H. W. Pickering, Corrosion, **42**, 125 (1986).
8.   G. Herbsleb and H. J. Engell, Z. Elektrochem., **65**, 881 (1961).
9.   H. W. Pickering and R. P. Frankenthal, J. Electrochem. Soc., **119**, 1297 (1972).
10.   G. Herbsleb, Werkstoffe Korrosion, **17**, 649 (1966).
11.   I. L. Rosenfeld and K. Marshakov, Corrosion, **20**, 115t (1964).
12.   C. M. Chen, F. H. Beck, and M. G. Fontana, Corrosion, **27**, 234 (1971).
13.   H. W. Pickering, Materials Science and Engineering, **A198**, 213 (1995).
14.   Y. Xu and H. W. Pickering, J. Electrochem. Soc., **140**, 658 (1993).
15.   Y. Xu, M. Wang, and H. W. Pickering, J. Electrochem. Soc., **140**, 1448 (1993).
16.   M. Wang, H. W. Pickering, and Y. Xu, J. Electrochem. Soc., **142**, 2986 (1995).
17.   H. W. Pickering, in *Research Topical Symposium: Localized Corrosion*, G.S. Frankel and J.R. Scully, Editors. 2001, NACE International: Houston, TX. p. 103.
18.   B. G. Ateya and H. W. Pickering, in *Passivity of Metals and Semiconductors*, M.B. Ives, J.L. Luo, and J.R. Rodda, Editors. 2001, Electrochemical Society: Pennington, NJ. p. 710
19.   M. Vankeerberghen, M. I. Abdulsalam, H. W. Pickering, and J. Deconinck, submitted to the J. Electrochem. Soc., (to be Published).
20.   I. L. Rosenfeld and I. S. Danilov, Corros. Sci., **7**, 129 (1967).
21.   U. F. Frank, Werkstoffe Korrosion, **11**, 401 (1960).
22.   G. Masing and D. Altenpohl, Z. Metallk., **43**, 433 (1952).
23.   H. P. Leckie and A. W. Loginow, Corrosion, **24**, 291 (1968).
24.   H. Kaesche, Z. Physik.Chem., N.F., **26**, 138 (1960).
25.   H. Kaesche, Z. Physik.Chem., N.F., **34**, 87 (1962).
26.   P. Forchammer and H. J. Engell, Werkstoffe Korrosion, **20**, 1 (1969).
27.   T. Beck, J. Electrochem. Soc., **120**, 1317 (1971).
28.   C. B. Bargeron and R. C. Bensen, J. Electrochem. Soc., **127**, 2528 (1980).
29.   S. B. de Wexler and J. R. Galvele, J. Electrrochem. Soc., **121**, 1271 (1974).
30.   A. A. Adams, K. E. Engle, and R. T. Foley, J. Electrochem. Soc., **119**, 1692 (1972).
31.   A. Valdes and H. W. Pickering, in *Advances in Localized Corrosion*, H. Isaacs, U. Bertocci, J. Kruger, and S. Smialowska, Editors. 1990, National Association of Corrosion Engineers: Houston, Texas. p. 393.
32.   K. Cho, M. I. Abdulsalam, and H. W. Pickering, J. Electrochem. Soc., **145**, 1862 (1998).

33. D. Harris and H. W. Pickering, in *Effect of Hydrogen on the Behavior of Materials*, A.W. Thompson, I.M. Bernstein, and A.J.W. ed., Editors. 1976, Metallurgical Soc. of AIME: Warrendale, PA. p. 229.
34. J. N. Al-Khamis and H. W. Pickering, J. Electrochem. Soc., **148**, B314 (2001).
35. B. G. Ateya and H. W. Pickering, in *Hydrogen in Metals*, A.W. Thompson and I.M. Bernstein, Editors. 1974, ASM: Metals Park, Ohio. p. 206.
36. C. Wagner and W. Traud, Z. Elecktrochem., **44**, 391 (1938).
37. M. K. Sawford, B. G. Ateya, A. M. Abdullah, and H. W. Pickering, J. Electrochem. Soc., **149**, B198 (2002).
38. G. Herbsleb and H. J. Engell, Werkstoffe Korrosion, **17**, 365 (1966).
39. I. Garz, H. Worch, and W. Schatt, Corros. Sci., **9**, 71 (1969).
40. R. P. Frankenthal and H. W. Pickering, J. Electrochem. Soc., **119**, 1304 (1972).
41. M. I. Abdulsalam and H. W. Pickering, J. Electrochem. Soc., **145**, 2276 (1998).
42. C. Edeleanu and J. G. Gibson, Chemistry and Industry, **30**, (1961).
43. J. W. D. France and J. N. D. Greene, Corrosion, **24**, 247 (1968).
44. M. N. Fokin and V. A. Timonin, Doklady Akademii Nauk, SSSR, **164**, 150 (1965).
45. H. W. Pickering, Corros. Sci., **29**, 325 (1989).
46. H. W. Pickering, in *Advances in Localized Corrosion*, H. Isaacs, U. Bertocci, J. Kruger, and S. Smialowska, Editors. 1990, National Association of Corrosion Engineers: Houston, Texas. p. 77.
47. M. G. Fontana and N. D. Greene, Corrosion Engineering. second ed. 1978, New York: McGraw-Hill. 465.
48. C. S. Brossia and R. G. Kelly, Corros. Sci., **40**, 1851 (1998).
49. A. Valdes and H. W. Pickering, in *Environmental Degradation of Engineering Materials III*, M.R. Louthan, R.P. McNitt, and R.D. Sisson, Editors. 1987, Penn State University: University Park, PA. p. 655.
50. A. Valdes and H. W. Pickering, in *II Congress Iberoamericano de Corrosion y-Protection*. 1986, National Association of Corrosion Engineers and The Latin American Association for Corrosion: Maracaibo, Venzuela. p. 357.
51. K. Cho and H. W. Pickering, J. Electrochem. Soc., **138**, L56 (1991).
52. K. Cho and H. W. Pickering, J. Electrochem. Soc., **137**, 3313 (1990).
53. E. A. Nystrom, J. B. Lee, A. A. Sagues, and H. W. Pickering, J. Electrochem. Soc., **141**, 358 (1994).
54. M. I. Abdulsalam and H. W. Pickering, Corros. Sci., **41**, 351 (1999).
55. B. A. Shaw, J. P. Moran, and P. O. Gartland, Corros. Sci., **32**, 707 (1991).
56. R. S. Lillard, M. P. Juninski, and J. R. Scully, Corrosion, **50**, 251 (1994).
57. R. S. Lillard and J. R. Scully, J. Electrochem. Soc., **141**, 3006 (1994).
58. L. A. DeJong and R. G. Kelly, in *Critical Factors in Localized Corrosion III*, R.G. Kelly, G.S. Frankel, P.M. Natishan, and R.C. Newman, Editors. 1998, Electrochemical Society: Pennington, NJ. p. 678.
59. A. M. Al-Zahrani, in Materials Science and Engineering. 2002, University Park, PA: Pennsylvania State University.
60. H. W. Pickering and R. P. Frankenthal. *Mechanism of Pit and Crevice Propagation on Iron and Stainless Steel*. in *International Conference of Localized Corrosion*. 1971. Williamsburg, VA: National Association of Corrosion Engineers.
61. M. A. Streicher, J. Electrochem. Soc., **103**, 375 (1956).
62. I. L. Rosenfeld and I. S. Danilow, Z. Physik.Chem., **226**, 257 (1964).

63. B. W. Bennett and H. W. Pickering, Metallurgical Trans. A, **18A**, 1117 (1987).
64. C. L. Briant, Corrosion, **36**, 497 (1980).
65. M. A. Streicher, J. Electrochem. Soc., **106**, 161 (1959).
66. B. Strauss, H. Schottky, and J. Hinnuber, Z, anorg allgem. Chem., **188**, 309 (1930).
67. E. C. Bain, R. H. Aborn, and J. J. Rutherford, Trans. Am. Soc. Steel Treating, **21**, 481 (1933).
68. A. Baumel, Arch. Eisenhuttenwes., **34**, 135 (1963).
69. A. P. Bond, Trans. TMS-AIME, **245**, 2127 (1969).
70. R. P. Frankenthal and H. W. Pickering, J. Electrochem. Soc., **120**, 23 (1973).
71. M. Zamanzadeh, R. N. Iyer, W. K. Kelly, and H. W. Pickering, in *International Symposium for Testing and Failure Analysis*. 1988, ASM International: Metals Park, OH. p. 425.
72. W. K. Kelly, R. N. Iyer, and H. W. Pickering, J. Electrochem. Soc., **140**, 3134 (1993).
73. H. W. Pickering and J. N. Al-Khamis, in *Chemistry and Electrochemistry of Stress Corrosion Cracking: A Symposium Honoring the Contributions of R. W. Staehle`*, R.H. Jones, Editor. 2001, TMS (The Minerals, Metals and Materials Society): Warrendale, PA. p. 319.
74. H. S. Kim, Y. T. Kho, H. W. Pickering, and K. Osseo-Asare, Metallurgical Trans. B, **22B**, 323 (1991).
75. H. S. Kim, Y. T. Kho, H. W. Pickering, and K. Osseo-Asare, J. Electrochem. Soc., **138**, 1599 (1991).
76. B. A. Shaw, *Short Course on Corrosion*. 2002, Penn State University: University Park, PA.